Insights into the role of additives as anticaking agents for sodium chloride

Proefschrift

ter verkrijging van de graad van doctor
aan de Radboud Universiteit Nijmegen
op gezag van de rector magnificus prof.dr. J.H.J.M. van Krieken ,
volgens besluit van het college van decanen
in het openbaar te verdedigen op
vrijdag 16 februari 2018
om 10:30 uur precies

door

Eleanor Rose Townsend

geboren op 23 april 1991
te Ipswich, Verenigd Koninkrijk

Promotoren:	Prof. dr. Elias Vlieg	
Copromotoren:	Dr. Willem J. P. van Enckevort	
	Dr. ir. Jan A. M. Meijer	AkzoNobel Chemicals, Deventer
Manuscriptcommissie:	Prof. dr. Daniela A. Wilson	
	Prof. dr. Daniel Bonn	Universiteit van Amsterdam
	Dr. Wim L. Noorduin	AMOLF

Insights into the role of additives as anticaking agents for sodium chloride
Thesis, Radboud University Nijmegen
Illustrated; with bibliographic information and Dutch summary
Cover design: Floor van Schayik

Insights into the role of additives as anticaking agents for sodium chloride

Doctoral Thesis

to obtain the degree of doctor
from Radboud Universiteit Nijmegen
on the authority of the Rector Magnificus prof.dr. J.H.J.M. van Krieken,
according to the decision of the Council of Deans
to be defended in public on
Friday, February 16, 2018
at 10:30 hours

by

Eleanor Rose Townsend

Born on April 23, 1991
in Ipswich, United Kingdom

Supervisor:	Prof. dr. Elias Vlieg	
Co-supervisors:	Dr. Willem J. P. van Enckevort	
	Dr. ir. Jan A. M. Meijer	AkzoNobel Chemicals, Deventer
Manuscript commission:	Prof. dr. Daniela A. Wilson	
	Prof. dr. Daniel Bonn	Universiteit van Amsterdam
	Dr. Wim L. Noorduin	AMOLF

Insights into the role of additives as anticaking agents for sodium chloride
Thesis, Radboud University Nijmegen
Illustrated; with bibliographic information and Dutch summary
Cover design: Floor van Schayik

Contents

Contents

Introduction

This chapter exists for the purpose of introducing several subjects and topics which are extremely relevant to the understanding of this thesis. We begin in the a historical manner, discussing the evolution of the use of crystals, leading further onto broad topic of crystal growth, the role of impurities and the functions and properties of sodium chloride. The chapter ends with an outline of what will be discussed in this thesis.

History of Crystals

Matter exists in three separate states; solid, liquid and gas which all display very different levels of atomic mobility. Crystals fall into the former category, a solid in which molecular motion is confined to small oscillations between neighbouring atoms. Crystalline solids consist of long range ordered atoms fixed into a specific pattern called a crystal lattice. This high degree of internal regularity corresponds to a minimum in enthalpy and entropy, which is a fundamental characteristic of the crystalline state. The strictly fixed positions of the internal atoms often lead then to a macroscopic crystal with clearly defined facets. The observation of the presence of these facets on solids were the beginning of crystallography as we know it, which started as an observational science linked to the study of minerals. Indeed, the beautiful shapes that were encountered in naturally occurring crystals attracted attention even from the earliest times, from the Ancient Sumerians who used crystals as a healing medium; to the Ancient Egyptians who used them as jewellery and for protection. For these purposes, crystals are still used to the present day. Many properties of crystals were also attributed by the Ancient Greeks, who are responsible for the name deriving from the Greek $\kappa\rho\upsilon\sigma\tau\alpha\lambda\lambda o\sigma$ (*krustallos*) from the words "ice" and "rock crystal". The first mathematical description of crystals came from the German scientist Johannes Kepler, who wrote "The six-cornered snowflake" in 1611, inspired by his observations of snowflakes and their perfect symmetry. In this paper, he gave much thought to the idea of close packing of spheres and how this related to crystallographic structure. [1] [2]

Figure 1: *De Niue Sexangula* **(1611)** with an example of the 6 fold symmetry displayed in a snowflake (reproduced from www.snowcrystals.com).

Kepler's vision of crystals as stackings of particles also inspired the 1784 mineralogical theory of Rene-Just Hauy, *"Essai d'un Theorie sur la Structure des Cristaux"*

which forms the basis of all crystallographic structure understanding today. However, modern structural crystallography was further improved into the nineteenth century, with the 1830 publication by Johann Hessel which, building on the work of Hauy, described that from all the crystalline morphological instances, they can all be categorised into one of thirty two types of symmetry in Euclidean space. These were thus known as point-groups. Furthermore, contributions from Auguste Bravais, Evgraf S. Federov and Arthur Schoenflies led to the current knowledge that the combination of 14 Bravais lattices and 32 point groups can combine to form 230 space groups which describe fully the arrangement of atoms and molecules inside a crystal. This fundamental theory was confirmed by Max von Laue (after the discovery of X-rays by Wilhelm Rontgen in 1895), who discovered the diffraction of X-rays by crystals, which earned him a Nobel Prize in 1914. This became the basis of the pioneering work by William Henry Bragg and Lawrence Bragg, which forms a relationship between the atomic structure of a crystal and its X-ray diffraction pattern. This work, which earned a Nobel prize in 1915, underpins the entire X-ray crystallography field that we know today.

Crystal Growth

In the process of crystallisation, there are two main events: nucleation and crystal growth. After the nucleation of the main seed, the crystal grows by addition of new growth units to specific positions on the lattice, to create the ordered 3D pattern that we expect from a perfect crystal. These processes are driven by both thermodynamic and chemical conditions in the solution, such as supersaturation and temperature. There are two broad categories of crystal growth: cooling crystallisation and evaporative crystallisation. In the case of sodium chloride, we only concentrate on evaporative crystallisation, as the solubility is almost independent of temperature. The time over which this crystal growth takes, can have a large impact on the resulting quality of the crystal, as well as its size. A "perfect" crystal would take an extremely long time to grow, whereas an imperfect crystal can grow faster due to the presence of crystalline defects which offer necessary growth points. Crystals grown on geological time scales, can evolve to huge sizes, such as those discovered in the Naica mine in Mexico in 2000. These giant crystals have formed over 500,000 years from selenite ($CaSO_4$ dihydrate) and have been found to measure up to 12 metres in length.

Nowadays, the control of crystal growth is extremely pertinent, due to the use of crystals in pharmaceuticals or other industrial products. For example, the morphology of crystals strongly influences end-product quality and functionality, as well as

Figure 2: Selenite crystals grown in the Naica mine, Mexico. Image courtesy of Alexander van Driessche, Wikimedia.

downstream processing.[3] Needle-like crystals are known to be widely undesirable in most cases, as they can block industrial equipment and also clump together, as they have a large surface area. This can also occur for crystals of other habits such as NaCl. In the production of sodium chloride, this clumping tendency or caking can also cause many problems, from a storage and transport point of view.

Caking of crystalline powders

The caking of crystalline powders is a phenomenon which describes the aggregation of solid material particles into large agglomerations due to various external conditions. The caking of crystals leads to a great deal of negative impact on the resultant product quality in an industrial setting, influencing both the flowability and the storageability of the product. There are a variety of mechanisms of which have been reported to influence caking[4], with humidity, temperature and crystal size and shape all contributing to the effect. According to Rumpf[5] and Chen et al.[6], there are a wide variety of mechanisms of how caking can occur, one of which is crystal bridge formation. It has been observed that the caking of sodium chloride occurs through this mechanism, with solid bridges of sodium chloride forming between neighbouring crystallites in the powder. As NaCl is hygroscopic, during times of high humidity, atmospheric water is attracted to the crystals, causing partial dissolution. On recrystallisation in dryer periods, the solid redistributes and forms strong connecting bridges between individual crystallites. These bridges are termed “crystal bridges” and are described in Figure 3.

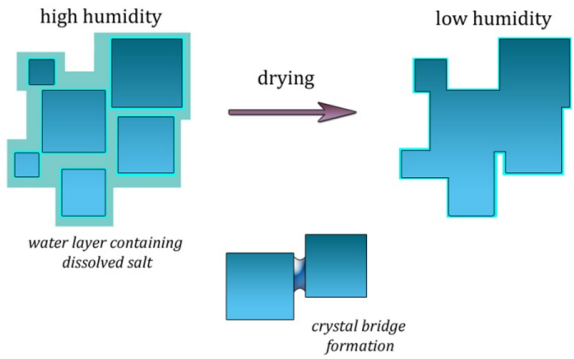

Figure 3: Schematic diagram describing the formation of crystal bridges in NaCl.

This phenomenon leads to the necessity of applying additives to the raw salt, blocking growth and thus to prevent this tendency towards lump formation and to inhibit the effects of humidity on the crystals.

The role of impurities and additives

An impurity in a solution was described by Buckley as "another type of particle in a solution present at crystallisation...which is not sufficiently related to be isomorphous with the parent or host lattice". [7] The crucial difference however, between an impurity and an additive, is that the former is unintentionally added and the latter is intentional. Perhaps the earliest and best known example of an additive having an effect on the growth of crystals, is that of Rome de l'Isle in 1783 [8], who described the formation of octahedral sodium chloride crystals in the presence of urea. Additives are now often specifically applied to crystallisation systems to obtain specific crystal shapes, which can be beneficial from a production point of view. This industry has come to the point where there are tailor made additives added to systems designed to interact stereospecifically with crystal surfaces during growth and dissolution. [9]

Cabrera and Vermilyea described in their 1958 publication [10], a mechanism based on strongly bound impurity molecules on the surface of the host crystal, in the case of low impurity concentration. This is relevant to this thesis and centres around the phenomenon of "step blocking". If a step meets an impurity at the surface, it stops and tries to grow around the blockage, causing a deformation of the step. If there are multiple impurity particles bound to the surface, at a distance separation of equal to or less than the size of a two-dimensional critical nucleus at the surface of the

host material at the corresponding supersaturation, then the step will be completely blocked.

It is also possible to have an impurity, which has an effect on the growth of the host crystal, without being so strongly bound. In this case, according to Chernov [11] [12], these impurities occupy a part of the active growth centres of the host crystal, leading to a blocking of the growth. Both of these mechanisms can be directly associated with the interactions of additives in contact with sodium chloride crystals.

Sodium Chloride

Sodium chloride has been an important compound for thousands of years, and is an excellent example of a crystal. The colloquial name for sodium chloride, "salt", comes from the Latin *salarium*, when people were actually paid using this valuable material. Salt had a variety of uses for these ancient people, most importantly to preserve and flavour food and therefore had extensive value.

Nowadays, sodium chloride, apart from food flavouring and preservative, is also widely used in many industrial processes. The majority of the salt produced in the Netherlands (up to 75%) is currently used in the chloralkali process (*acc.* AkzoNobel), to produce sodium hydroxide and chlorine gas; but it is also used in the manufacture of sodium bicarbonate, hydrochloric acid, hydrogen and many other chemicals. There is also a market for road salt, as the application of sodium chloride to frozen surfaces, lowers the freezing point of the water and thus increases road safety. Sodium chloride is also involved in many natural biological processes, such as an electrolyte in brain cell activity and as a component in bodily fluids.

Sodium chloride has a face centred cubic crystal structure, which is also known as the "halite" or "rock salt" crystal structure. The lattice consists of sodium ions, each of which is surrounded by six chlorine atoms, creating an octahedral surrounding around the central sodium/chlorine atom. Due to its ionic property, it has a high melting point of 801°C and is highly soluble in polar solvents such as water. Grown from a pure aqueous solution, the NaCl crystals exhibit a cubic morphology bound by {100} faces.

As previously mentioned, sodium chloride was one of the first crystalline compounds for which additives were shown to have a modification effect, with Rome de l'Isle reporting visible {111} facets in the presence of urea in the growth solution. [8] Later work showed the same effectivity with various chloride compounds such as $CrCl_3$, $CdCl_2$, $ZnCl_2$ and $MnCl_2$. [13] [14] A more detailed investigation of the change in observed habit for sodium chloride in the presence of these various positive ions (Pb^{2+},

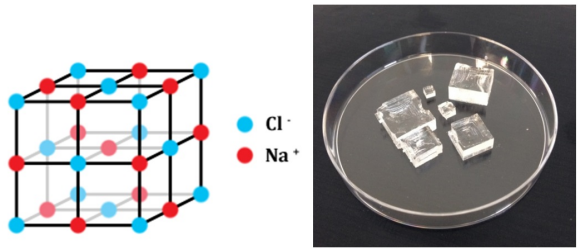

Figure 4: The crystal lattice of sodium chloride and solution grown NaCl crystals exhibiting the expected cubic morphology.

Mn^{2+}, Cd^{2+}, Mg^{2+}) was performed by Bienfait et al., showing the development of {111} facets from {100} with increasing concentration of impurity.[15]

As also previously mentioned, sodium chloride is widely used in a variety of industrial processes but has the somewhat challenging tendency to cake. There are a variety of ways to overcome this caking tendency, including humidity control and drying of the salt. However, in an industrial setting, retaining the dryness of multiple tons of salt during storage (Figure 5) and transport is impossible. Therefore, additives are used in small amounts to disrupt the formation of crystal bridges and retain a smoothly free-flowing product. These additives are termed "anticaking agents".

Anticaking agents

Anticaking agents are compounds which are added to powdered materials to prevent particle agglomeration and to keep the product smooth and free flowing. In the food industry, these additives can have various purposes, such as to absorb water (in the case of sodium aluminosilicate) or to coat particles (stearic acid and polydimethylsiloxane). It is also possible to use such additives to block growth of recrystallising hygroscopic compounds, such as in the case of sodium chloride.

For NaCl, the most widely used anticaking agents currently are sodium ferrocyanide and potassium ferrocyanide. These compounds are used in all types of salt, from food grade to road salt to electrolysis salt, all at extremely low concentrations of as low as a few ppm.[16] [17] These additives have an octahedral molecular structure, with a central Fe^{2+} atom surrounded by six cyanide ligands. Bode et al.[18] found, using the technique of surface X-ray diffraction, that the ferrocyanide ion adsorbs onto the NaCl {100} surface, replacing one sodium atom and five surrounding chlorine ions. This then blocks the further growth of the crystal, as the only way to continue growth

Figure 5: Salt pile in storage at AkzoNobel, Delfzijl.

is by desorbing the ferrocyanide ion or leaving an energetically unfavourable sodium vacancy. It is an extremely effective anticaking agent, having an anticaking effect at as low as 2.5 ppm with relation to the salt.

In current industrial use, however, the use of ferrocyanide as an anticaking agent for NaCl has been showing some issues. As previously mentioned, the majority of salt produced in the Netherlands is used in the chloralkali process to produce sodium hydroxide and chlorine gas. This is performed through electrolysis of aqueous NaCl in a membrane system. However, the stability of the ferrocyanide anticaking agent present on this salt poses a problem, in that it decomposes to iron hydroxide ($Fe(OH)_3$) which accumulates on the membranes blocking the flow through the system and increasing the voltage due to resistance increase. This also contributes to the production of explosive nitrogen trichloride gas.

These drawbacks lead AkzoNobel to the conclusion that a new anticaking agent was necessary, one which was readily degradable during electrolysis and also had favourable properties from an environmental point of view. In 2000, a patent was filed [19], further investigated in [20], both describing the use of a carbohydrate based metal complex in the place of ferrocyanide. This compound consists of different stereoisomers of tartaric acid complexed with Fe^{3+}, and is commonly known as iron meso-tartrate (Fe-mTA). The proposed structure is shown in Figure 6. It is effective as an anticaking agent for NaCl at low concentrations in the pH range 4-5, and as it is a weaker complex than ferrocyanide, it can more easily be removed from the aqueous NaCl solution prior to electrolysis. These tartrates are obtained as ecological side products from the wine

making industry. The drawback to this compound is that it readily degrades under conditions of light or heat and is extremely dependent on the pH for it to have the desired anticaking effect.

Some previous work investigating the complex of Fe-mTA was carried out by Bode et al.[21] which detailed a proposed molecular structure in solution based on a combination of experimental work and molecular modelling. They propose a binuclear Fe^{3+} structure, complexed with two bridging meso-tartrate ligands and two water molecules, giving an octahedral surrounding of the Fe^{3+} ions. When these water molecules are removed, it is suggested that this leaves a flat charged area which matches the NaCl {100} surface, which allows bonding. However, what is not discussed in this paper, is why the compound used on NaCl in production is a mixture of meso, L and D tartaric acids with Fe^{3+} instead of solely meso tartaric acid, and why this mixture is more effective than the pure Fe-mTA.

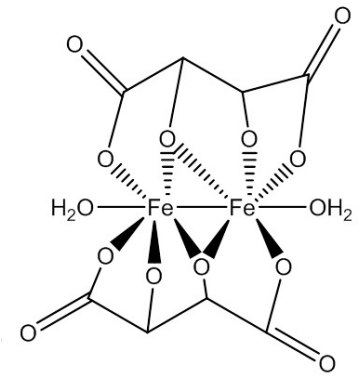

Figure 6: Proposed structure of the iron meso-tartrate complex.

It is evident then from the literature, that an effective anticaking agent for sodium chloride does not have a specific molecular structure, but instead displays either a charged area compatible with the NaCl {100} surface or a structure similar to the size and configuration of sodium or chloride ions in NaCl with a matching charge. The presence of iron in the complexes can be a hindrance, due to the aforementioned reasons, therefore it is extremely interesting to investigate the possibilities of other anticaking agents with different components or functional groups, which may still display the desired anticaking effect.

Applied Techniques

In order to do a comprehensive study on the effects that various additives have on the crystallisation of a model crystal, like NaCl, a broad range of techniques must be employed to investigate the influence of these compounds on both the surface and the bulk crystal.

Much of the earliest work on crystal growth was performed using basic optical microscopy to macroscopically observe the growth process. Much of the work in this thesis actually also consists of simple experiments, mirroring those which could have been performed centuries ago. However, the reproducibility of these results is much enhanced, as we have temperature and humidity controlled climate chambers to regulate the environment in which the crystals can grow. The resulting crystals were observed ex-situ using high quality optical microscopes, or observed nucleating and growing in-situ using temperature regulated growth cells coupled with an optical microscope.

Besides these relatively simple optical techniques, two more specialised techniques were also employed to observe microscopically what was happening on the crystalline surface. These were Scanning Electron Microscopy (SEM) and Atomic Force Microscopy (AFM). These both proved extremely useful, to observe crystal growth patterns at high magnifications, which would otherwise be impossible with optical microscopy.

The technique of Surface X-Ray Diffraction was utilised in the final chapter of this thesis, to determine the structure of the surface layer of a crystalline material and its liquid-solid interfaces. [22] [23]

Atomic Force Microscopy

Atomic Force Microscopy (AFM) is a technique in which a surface is scanned, resulting in a near atomic scale image of its structure. AFM was developed to improve on the technique of STM in that it can be used to investigate both conductors and insulators on an atomic scale. [24]

The microscope functions to map the surface by scanning over the surface using a cantilever with a sharp tip. The force is not directly measured, but can be calculated by the deviation of the tip, while knowing the stiffness of the lever. This follows Hooke's Law: $F=-kx$, where F is the force, k is the the stiffness of the lever and x is the deviation. This deviation is measured using a laser, which is reflected onto a photo-sensitive quadrant diode which can map the position. This output can be mapped as a topographical image as shown in Figure 7.

AFM can be operated in various modes, but in this investigation we employed only

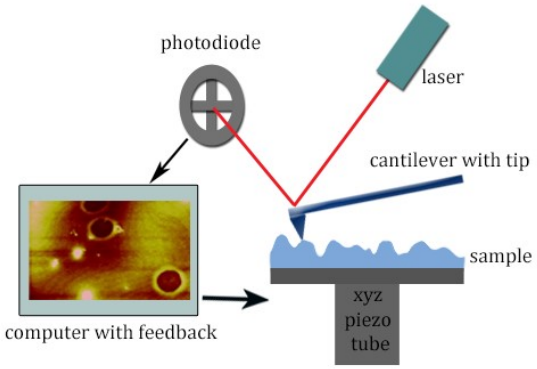

Figure 7: Schematic diagram showing the function of an Atomic Force Microscope.

contact/constant force mode. In this the force between the tip and sample surface is kept constant, by varying the height, x, of the tip. Recording this variation of height as a function of position gives the topographical map. This mode, which involves a high lateral force, works well for sodium chloride with strongly bound surface additives, but can cause issues with sample degradation or movement of loosely attached objects on less robust samples.

Surface X-Ray Diffraction

Surface X-ray diffraction is a specific type of X-ray diffraction which can be used for structure determination of surfaces and interfaces.[25] This method is similar to other types of X-ray diffraction, in principle, but instead of being concerned with the diffraction pattern observed from the bulk crystal as in the case of powder or single crystal X-ray diffraction, one is only interested in the diffraction from the top few layers of atoms at the surface. We gain information about the surface structure from diffraction rods (explained below), which give surface sensitivity. The experiments are performed at low incidence angles to promote a more favourable signal to noise ratio. However, in turn, this results in very weak diffraction intensity, leading to the necessity of using a synchrotron X-ray source to perform experiments.

Diffraction from a bulk crystal leads to intense signal at defined points in reciprocal space following Bragg's Law, called Bragg peaks. This is due to the fact that in crystals there is periodicity in the x, y and z directions, leading to defined points in reciprocal space. In comparison, for a thin surface layer, there is only periodicity in

two dimensions and none in the z direction. This leads to the occurrence of diffraction rods, which after recording, can give valuable information about the surface structure. The combination of Bragg bulk peaks and diffraction rods give crystal truncation rods[26], which are observed in our experiments and displayed in Figure 8.

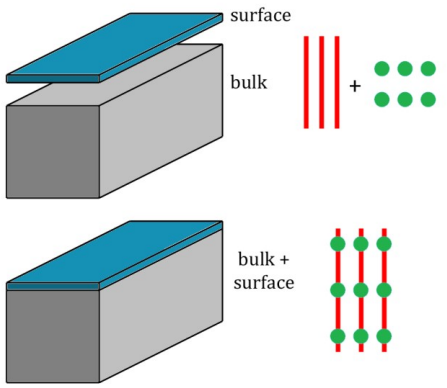

Figure 8: Diffraction from a 2D surface layer results in rods in reciprocal space. When combined with a 3D bulk crystal, the combination results in crystal truncation rods.

From the results, we can determine information about the out-of-plane and the in-plane ordering of the molecules at the surface. The specular rod, (00), is a special case, in that it is only sensitive to out-of-plane ordering on the surface and so can give information about liquid layers which are only ordered in this direction. We can also gain information about the in-plane ordering on the surface from examining differences in the non-specular rods. From this, we can determine if there has been any surface reconstruction. A major advantage of this method is that it can be used in-situ, for example in this thesis for a crystal surface in contact with its saturated solution.

This thesis

The research presented in this thesis has the overall goal of determining ways to diminish the caking of crystalline materials using various additives. The general mechanism of action of these additives at a fundamental level on our sodium chloride model crystalline system is a very relevant research question, as, if we can determine the mechanism of action of one additive, we can then design new generations of anticaking agents with improved properties. As the reported anticaking agents for NaCl have all increasingly varied structures, the determination of a general mechanism is extremely relevant.

The second and third chapters of the thesis discuss the development and understanding of a new screening technique for sodium chloride, creeping. Creeping is the evaporation driven extension of crystallites outside the solution boundary of a liquid on a solid non-porous substrate. The relationship between caking and creeping was established and confirmed using powder flow analysis experiments coupled with simple creeping experiments. The second chapter explores further why these specific additives cause creeping in sodium chloride, comparing experimental results with a theoretical model. Here, we concluded that the presence of an anticaking agent on the crystal surface contributes to a lowering of surface energy, which in turn disrupts the surface growth, leading to increasing morphological instability and enhanced branching.

The fourth chapter concerns our initial hypothesis, that polymers could make excellent anticaking agents for NaCl as they have multiple points along the molecule where bonding is possible, leading to a more strongly bonded additive. It was concluded that while the polymers do bond strongly to the surface, some are shown to form surface macroclusters which act as a glue, leading to enhanced caking. However, it was also concluded that one polymer, polyacrylamide has a much-enhanced habit modification effect on NaCl, than its corresponding monomer, formamide. This leads to the conclusion that the amide functional group is important in this whole investigation and that multiple bonding sites can indeed help.

The fifth chapter then discusses the phenomenon observed when using a branched amide as an additive, of which at high concentrations, ultrathin needle growth is observed. The origin of these needles is discussed in depth, coupling experimental observations with a theoretical model. This morphology, apparently violating the $4\bar{3}m$ point group symmetry, has been explained using a model, based on tip formation by initial morphological instability followed by time dependent adsorption of additive

molecules blocking the growth of the needle side faces. The latter suppresses side branch formation, which normally occurs for dendrite growth.

The sixth chapter focuses on why it seems to be necessary to have three amide branches present on an amide molecule to have an anticaking effect on NaCl. We showed that there is no anticaking activity when two and singular branched compounds are used and also not for multiple branched compounds, such as polyacrylamide. We theorise that this could be due to the steric hindrance of the smaller and larger compounds, whereas the three-branched variant can bend into a specific conformation which can bind perfectly to the flat surface of the NaCl. It is also possible that this variant binds specifically to a growing NaCl step, thus validating the necessity for a larger compound which has the ability to bend.

Finally, the seventh chapter discusses the interaction between lead chloride and sodium chloride {100}. Lead chloride is a previously reported habit modifier and growth blocker for sodium chloride but up until now, the exact mechanism at an atomic scale was unknown. Using surface x-ray diffraction, we found that lead adsorbs to the NaCl surface replacing a sodium ion, which cannot be incorporated into the bulk as there is a charge mismatch of which it is energetically unfavourable to compensate for. This thus slows the growth of NaCl {100}.

Chapter 1

Creeping: An efficient way to determine the anticaking ability of additives for sodium chloride

Eleanor R. Townsend, Floris Swennenhuis, Willem J.P. van Enckevort, Jan A.M. Meijer, Elias Vlieg

*CrystEngComm, **2016**, 18, 6176-6183*

Abstract

This article investigates the relationship between additive induced creeping and anticaking activity in sodium chloride. Through a series of creeping experiments and powder flow analysis, we establish a clear correlation between the amount of creeping and the anticaking effect of an additive. Habit modification is found not to be a sufficient condition for an anticaking agent. The correlation is explained by the fact that both creeping and anticaking require blocking of crystal growth.

1.1 Introduction

Sodium chloride is an important industrial material, used in a wide variety of applications such as winter road maintenance, production of chemicals and as a food preservative. However, a production issue arises, in that sodium chloride has the tendency to cake and thus forms large agglomerates of material, through a crystal bridging process.[7] [27] Such solid bridges are formed by partial dissolution of the crystallites and subsequent regrowth in contact areas under conditions of varying humidity.

In order to prevent caking, additives are applied to the salt, termed "anticaking agents". Currently, the most widely used anticaking agent for sodium chloride is ferrocyanide, $(Fe(CN)_6)^{4-}$ (FCN). It is extremely effective in small amounts and is stable.[17] However, there is a drawback associated with the use of this additive, which is the fact that it degrades the membranes used during the electrolysis process, which is used to produce chlorine gas and sodium hydroxide. It is therefore of great industrial interest to investigate the potential of new-generation anticaking agents which do not have this same drawback.

It is, however, difficult to predict the effectivity of a compound as an anticaking agent, because the mechanism of their action on the sodium chloride surface is not always known. In the case of ferrocyanide, it is known that anticaking proceeds through "step blocking" on the surface, which hinders the formation of the previously mentioned crystal bridges between individual salt crystals.[28] Bode et al. have shown that the ferrocyanide ion replaces five chlorine atoms and one sodium atom at the surface of sodium chloride, thus preventing the propagation of steps.[18] However, other known anticaking agents have vastly different structures to ferrocyanide, therefore prediction of a compounds' anticaking effectivity is difficult.

The investigation can be performed using a screening process, but this is time consuming due to the lengthy crystal growth times and caking measurements. We explore here the usefulness of a much faster approach, using the technique of creeping. Creeping can be defined as the evaporation driven extension of crystals from the solution boundary on solid non-porous substrates.[29] [30] It is well-known that sodium chloride has the tendency to creep and the effect is very pronounced in the presence of ferrocyanide (see Figure 1).[29] [30] Similar salt evaporation patterns have been observed by Shahidzadeh et al.[31]. This observation suggests that additives which promote creeping also exhibit anticaking activity.

The aim of this paper is to verify the relationship between additive induced creeping effects and anticaking activity for NaCl. For this, we examined the "creepability" of sodium chloride treated with a range of additives, both known and unknown anticaking agents, habit modifiers and even a pro-caking agent.[32] These included ferrocyanide, metal-carbohydrate complexes[20], branched amides[33][34] and branched amide-metal complexes. The above experiments were carried out by in-situ microscopic observation of creeping patterns extending from the rim of solution droplets on top of a glass substrate. These creeping experiments were complemented by powder flow analysis (PFA) experiments to determine the actual anticaking ability of the additives.

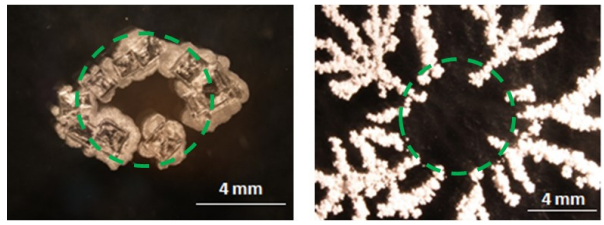

Figure 1.1: (a) Creeping pattern of NaCl from saturated brine, (b) Creeping pattern of NaCl from saturated brine using 1% FCN additive (original droplet boundaries indicated).

1.2 Methods

1.2.1 Additives used

The additives used in this investigation are mostly of organic or metal-organic origin. As a reference, we use the well-established anticaking agent, FCN, $(Fe(CN)_6)^{4-}$. Another currently used anticaking agent from Akzo Nobel, iron meso-tartrate (Fe(III)-mTA)[35] was also tested. This compound consists of a mixture of iron(III) chloride and meso, L and D tartaric acids fixed at a specific pH, as set out by Akzo Nobel guidelines. A related compound is iron(III) citrate (Fe-citrate), which has been previously mentioned in the literature as an anticaking agent regarding sodium chloride.[35]

Other organic compounds which were tested were two branched amides, nitrilotriacetamide (NTAA) and methylglycinediacetamide (MGDA). Their structures are shown in Figure 2. NTAA has been previously shown in the literature[33] [34] [36], to have an effect on the crystallisation of sodium chloride. As the effective anticaking agents, Fe-mTA and Fe-citrate, are compounds consisting of metals complexed with organic molecules, the branched amides were also tested in conjunction with metal ions, Fe^{2+} and Cu^{2+}. These metal ions were supplied from $FeCl_2$ and $CuCl_2$.

Finally, two habit modifiers, polyacrylamide (PAA) and formamide, were tested. Both of these additives have habit modification effects on NaCl[32] but no proven anticaking ability. The various additives and their concentrations used in the different experiments are summarized in Table 1. The amide metal combination experiments were carried out using molar ratios instead of % (w/w) to ensure equal amounts of each component. The common concentration of anticaking agent was set at 1% (w/w) for the creeping experiments, to ensure fair testing between the differing compounds. The only exception here was in the case of formamide, in which a minimum of 20% (w/w) is required in the brine solution to have a habit modification effect.[37]

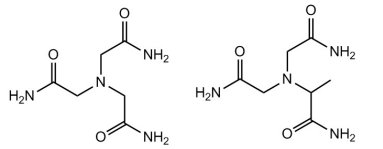

Figure 1.2: Structures of nitrilotriacetamide (NTAA) and methylglycine diacetamide (MGDA).

Compound/ Additive	**Source purity**	**pH**	**Concentration**[a]	**Concentration**[b]
NaCl (Sanal P®)	>99%	-	-	-
FCN	99%	N/A	1% (w/w)	2.5x10^{-4} % (w/w)
Fe-mTA	*AN*	4.2 [35]	1% (w/w)	0.02 % (w/w)
Fe-citrate	*AN*	6.7 [35]	1% (w/w)	0.02 % (w/w)
Fe-citrate	*AN*	0.8	1% (w/w)	0.02 % (w/w)
MGDA	*AN*	N/A	1% (w/w)	0.02 % (w/w)
NTAA	*AN*	N/A	1% (w/w)	0.02 % (w/w)
MGDA + metal	*AN*	N/A	0.01M MGDA + 0.01M Fe^{2+}/Cu^{2+}	2x10^{-3} mol kg^{-1} MGDA + 2x10^{-3} mol kg^{-1} Fe^{2+}/Cu^{2+}
NTAA + metal	*AN*	N/A	0.01M NTAA + 0.01M Fe^{2+}/Cu^{2+}	2x10^{-3} mol kg^{-1} NTAA + 2x10^{-3} mol kg^{-1} Fe^{2+}/Cu^{2+}
PAA	99%	N/A	1% (w/w)	0.02 % (w/w)
Formamide	>99%	N/A	20% (w/w)	0.5 % (w/w)

Table 1.1: The additives and their concentrations used in the different experiments. (AN = as per AkzoNobel guidelines) [a]: in creeping experiment (w.r.t. solution), [b]: in powder flow analysis (w.r.t salt)

1.2.2 Creeping Experiments

Saturated solutions of sodium chloride (solubility: 359 g L^{-1} water) were prepared at ambient temperature (20-25°C). The chosen compound was then added to this brine solution to make a 1% (w/w) solution in relation to the solution. Small droplets of each solution (approximately 0.1 ml) were then applied to the centre of a glass microscope slide using a syringe fitted to a Pall GHP Acrodisc 0.45μm filter and the slide was then placed inside a closed cell with a saturated aqueous $MgCl_2$ solution in order to keep the humidity constant (≈33%). The contact angles of the droplets with the glass substrate are 60 ±10°, as measured using an optical projection set-up. The evolution of the droplet drying pattern was viewed through the cell's glass window using a Leica Wild M10 stereo-optical microscope and photos were taken periodically using a Nikon digital camera system (Digital Sight DS-L1). The time frame of these experiments was in the range of 1-2 hours and were performed in duplicate to ensure reproducibility. The creeping patterns are quite diverse, but as a measure of creeping we will simply

use the amount of crystal extension radiating from the outer peripheries of the original droplet.

1.2.3 Concentration variance in creeping experiments

To determine the amount of additive required to have an effect, series of creeping experiments were performed with the same additive but at different concentrations in the solution. This was performed using iron citrate, Fe-mTA, MGDA and NTAA. This was carried out as it is suspected that there is a correlation between the concentration of additive and the creeping pattern observed. Based on these trial runs, we came to an optimal concentration of the different additives of 1% (w/w) with respect to the solution, which, except for formamide, was further used in the actual creeping experiments (Table 1).

1.2.4 Powder Flow Analysis (PFA)

Caking tests were performed following a standardized measurement employed by Akzo Nobel.[38] The measurements were performed in quadruplicate using a Powder Flow Analyzer rheometer to determine the caking strength of the sodium chloride when treated with additive solutions. 50 g batches of high-purity Akzo Nobel Sanal P®salt were placed into separate plastic bags and treated with 2% (w/w) moisture. The moisture consisted of a solution of 1% (w/w) additive in MilliQ water. This yields an additive concentration of 0.02% (w/w) with respect to the salt; different concentrations are used for the formamide and the NTAA/MGDA+ metal complexes as given in Table 1. The treated salt batches were then placed in separate plastic containers of 50 mm diameter and preconditioned by compressing with 1 kg weight and purging with dry air for 2 hours. The strength of the cake of the samples was then measured using the rheometer (type TA-XT21, Stable Micro Systems), which is a screw-like moving blade which enters the salt cake and continuously measures the vertical force imposed by the salt. The measurement unit is CE20, which is the relative caking energy in N.mm required to enter a cake of 20 mm. All results were compared to a standard blank test and the standard ferrocyanide test, of which the concentration is fixed at 2.5 x 10^{-4} % (w/w) with respect to the salt. These experiments were carried out at ambient temperature.

1.3 Results

1.3.1 Creeping Experiments

1.3.1.1 Carbohydrate-metal complexes

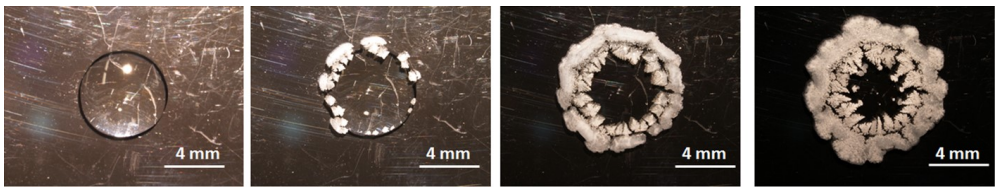

Figure 1.3: Creeping pattern of saturated brine containing 1% (w/w) mTA.

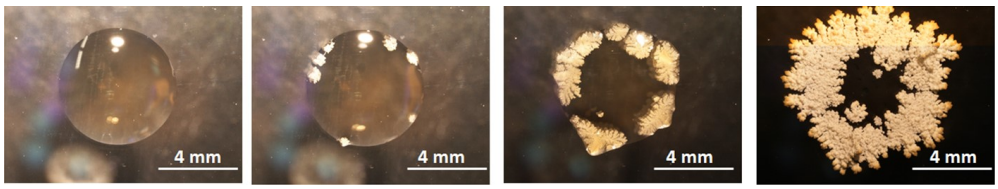

Figure 1.4: Creeping pattern of saturated brine containing 1% (w/w) Fe-citrate at pH 6.7.

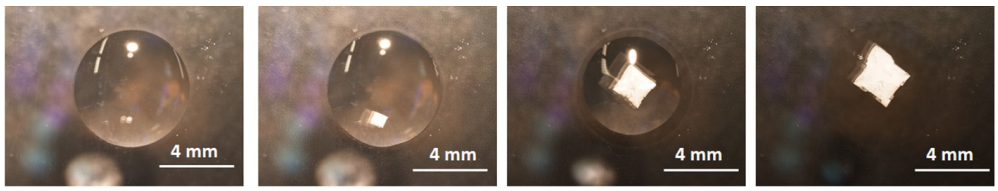

Figure 1.5: Creeping pattern of saturated brine containing 1% (w/w) Fe-citrate at pH 0.8.

Fe-mTA Figure 3 shows the propagation of the creeping pattern of an evaporating brine solution treated with 1% (w/w) Fe-mTA. It is evident that the pattern differs much from that of the control (Fig. 1(a)), as there is no evidence of cubic crystallites, rather fine branched crystallites without preferential orientation are observed to be radiating from the droplet.

Fe-citrate Figure 4 images the evolution of the creeping pattern of sodium chloride solution with 1% (w/w) Fe-citrate at pH 6.7. There are multiple nucleation points around the edge of the droplet. This is followed by destabilization of these cubic nuclei, leading to dendritic growth. This dendritic growth first fills the periphery of the droplet and then crystal growth extends outwards, forming a ring of branched crystallites with no preferred orientation. This result indicates that the addition of 1% Fe-citrate to a brine solution at pH 6.7 has an effect on the crystal growth of sodium chloride, which deviates from the preferred cubic form.

It has been previously reported, that the activity of Fe-mTA is limited to a narrow pH range of 4 - 5.[35] It was therefore of interest to investigate the sensitivity of Fe-citrate to pH. Figure 5 images the evolution of the growth pattern of sodium chloride with again the addition of 1% Fe-citrate, but with an extreme pH of 0.8. This pH was set using a dilute solution of HCl. It shows a marked difference to that observed in Figure 5, with only one large crystal with cubic morphology forming at the centre of the droplet. It can also be said that the addition of this additive at this low pH does not destabilise the crystals and inhibits nucleation, as there is only one large crystal, rather than a number of smaller ones as observed in the control test. This result therefore indicates that Fe-citrate does not induce creeping of the sodium chloride at pH 0.8 and seems to act as a nucleation inhibitor. At this extreme low pH, it is possible that the Fe-citrate complex has dissociated leaving free citric acid in the solution and therefore does not have the same anticaking effect as observed at pH 6.7.

1.3.1.2 Amide containing additives

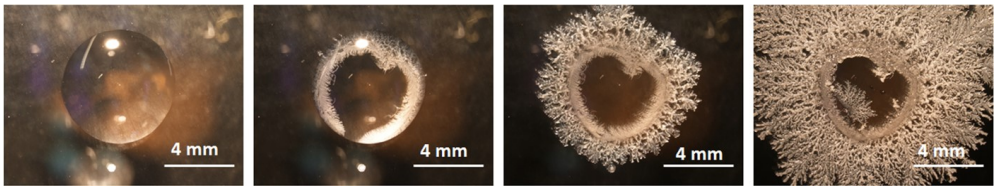

Figure 1.6: Creeping pattern of saturated brine containing 1% (w/w) NTAA.

NTAA Figure 6 describes the evolution of the creeping pattern of a brine solution containing 1% (w/w) NTAA. The pattern differs markedly to that of the control, as it develops in two separate stages. The first shows the initial formation of needle-shaped crystallites, which grow inward and surround the peripheries of the droplet, much like

that seen in the case of Fe-mTA in Figure 2. The second stage consists of the extension of the branched crystallites from the edges of the droplet, extending outwards over the glass substrate. There is little evidence of inward crystallite growth after the initial stage. There is no indication of macroscopic cubic crystal growth as observed in the control test.

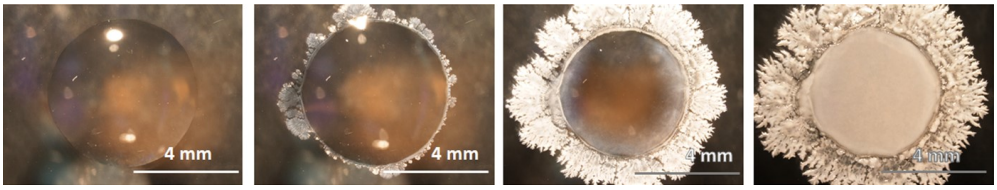

Figure 1.7: Creeping pattern of saturated brine containing 1% (w/w) MGDA.

MGDA Figure 7 describes the creeping pattern of brine treated with 1% (w/w) MGDA solution. Again, this creeping pattern develops through two stages, as observed for that of 1% (w/w) NTAA. Macroscopically visible crystallites form first, to surround the periphery of the droplet. After the surrounding is complete, branched crystallites begin to extend outward over the glass substrate similar as observed in Figure 7. However, microscopic needle crystallites also begin to fill the centre of the droplet, differing from that of the NTAA, where no crystal growth was observed in this area. These microscopic crystallites are shown in a SEM micrograph in Figure 8. Once again, there is no evidence of macroscopic cubic crystal growth as observed in the control.

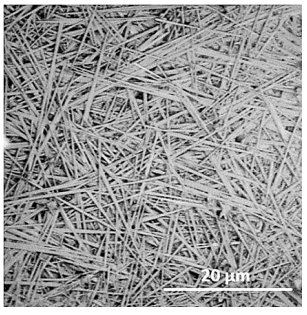

Figure 1.8: SEM micrograph of microscopic needle crystallites in the centre of the creeping pattern of brine with 1% (w/w) MGDA.

Amide-metal complexes It is known that several carbohydrate-metal complexes work well as anticaking agents for NaCl (i.e. Fe-mTA, Fe-citrate). As the branched amides in Section 1.3.1.2 also show strong anticaking activity for sodium chloride, it was interesting to investigate if the addition of a metal to the amide solutions would enhance their anticaking activity by forming a unique complex. Evidence for the formation of this complex can be seen through the colour change of a copper chloride solution from blue to green on addition of a colourless branched amide solution.

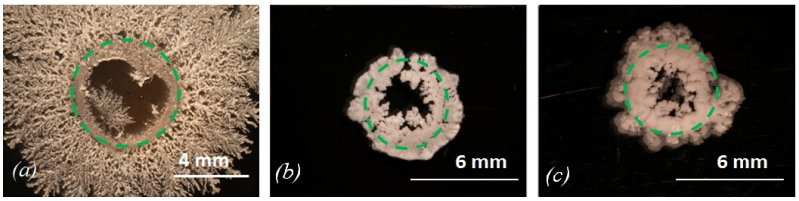

Figure 1.9: Creeping patterns of saturated brine containing (a) NTAA, (b) 1:1 NTAA: Cu^{2+}, (c) 1:1 NTAA:Fe^{2+}.

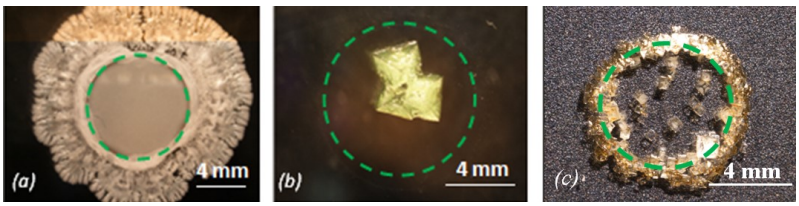

Figure 1.10: Creeping patterns of saturated brine containing (a) MGDA, (b) 1:1 MGDA: Cu^{2+}, (c) 1:1 MGDA:Fe^{2+}.

Figure 9 shows the effect of Fe^{2+} and Cu^{2+} on the creeping pattern of brine containing 1% NTAA. It is evident from these pictures that the spread of the crystallites over the substrate is hindered by the addition of the metal. However, the pattern is still markedly different to that of the control and the crystallites are in branched needle forms rather than the expected cubic. A small amount of creeping can be recognised. Figure 10 shows the contrast between the creeping pattern of brine with 1% MGDA only and those with the addition of Cu^{2+} and Fe^{2+}. It is evident from these results that the addition of the metal cancels out entirely the creeping effect of the MGDA molecule, as only cubic crystals were observed in the growth patterns containing the metal ions. No creeping occurs at all here, with the combination of MGDA and Cu^{2+} even displaying signs of nucleation inhibition.

1.3.1.3 Additives with habit modification properties

There are a large number of additives known to modify the habit of sodium chloride. For example, it was reported by Rome de l'Isle in 1783 [8] that addition of urea to brine solution leads to the development of {111} facets on the sodium chloride crystals. However, we here investigate if habit modifiers for sodium chloride are not necessarily anticaking agents in the industrial setting in which we use them.

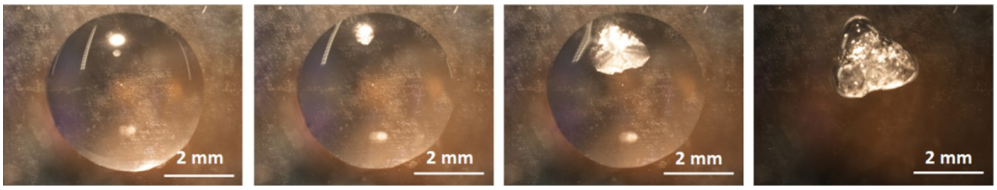

Figure 1.11: Growth pattern of saturated brine containing 1% (w/w) PAA.

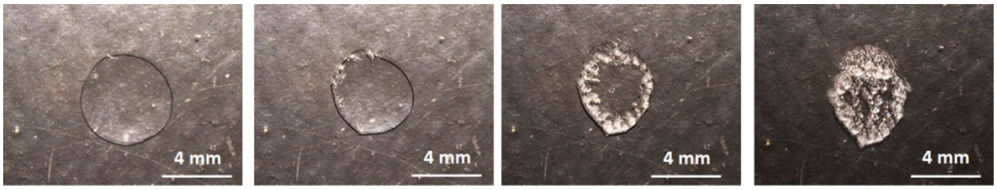

Figure 1.12: Growth pattern of saturated brine containing 20% (w/w) formamide.

Figure 11 shows the development of the growth pattern of PAA, which is a reported habit modifier for NaCl. [32] The pattern shows no evidence of branched crystallite formation by creeping, rather a stabilization of the central large crystal with evidence of {111} facet development. The formation of one large crystal instead of many smaller ones as in the control agrees with the literature, which stated that PAA acts as a nucleation inhibitor for NaCl.
Another well-known habit modifier for NaCl is formamide, which causes a morphological change in NaCl, leading to the development of {111} faceted octahedral crystals. The growth pattern from a droplet of brine containing 20% (w/w) formamide is shown in Figure 12. This large amount of additive in comparison to the other experiments was used due the fact that no habit modification effect is observed until a concentration of 20% (w/w) in brine solution. There is again no evidence of creeping, i.e. no extension of the crystallites from the original droplet boundary.

1.3.2 Powder Flow Analysis

In the following section, the technique of PFA was used to determine the actual anti-caking abilities of each additive.

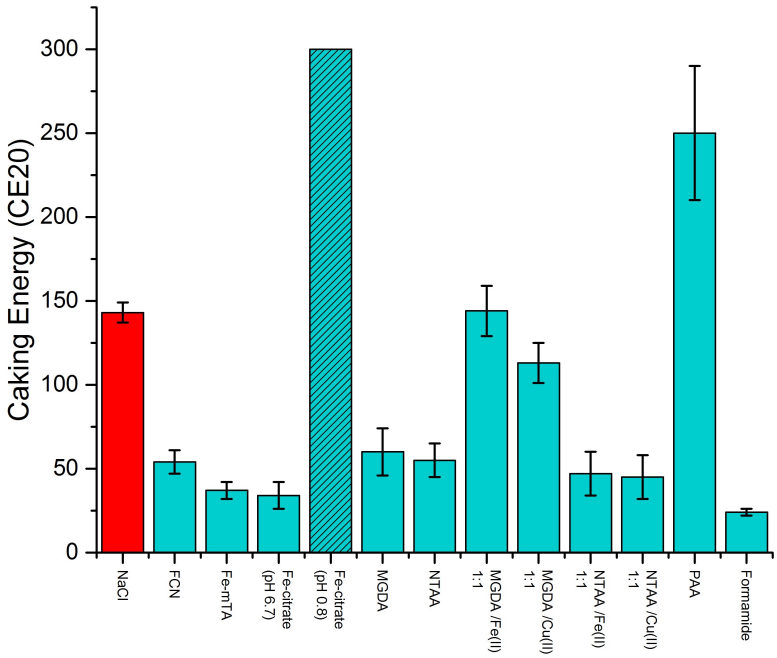

Figure 1.13: PFA test results of NaCl caking with varying additives, compared to control and FCN. Overloaded measurements are shown shaded in grey.

1.3.2.1 Carbohydrate-metal complex additives

Fe-mTA and Fe-citrate Figure 13 describes the measured caking energy for salt treated with Fe-mTA and Fe-citrate in comparison to the control and FCN cases. At 0.02% (w/w), it is evident that Fe-mTA has an anticaking effect on NaCl, as the caking energy is a factor of three smaller than the measured value for the control. The caking energy found for salt treated with 0.02% (w/w) Fe-citrate at pH 6.7 was approximately a factor of four less than the value found for the control sample. It was also found that the caking energy necessary to break the caked salt treated with Fe-

citrate at pH 0.8 exceeded the maximum caking energy measurable on the equipment, so more than double the energy required for the breaking of the control sample.

1.3.2.2 Amide containing additives

The PFA tests of salt treated with 0.02% (w/w) NTAA show a threefold decrease in the caking energy in comparison to that of the control and an almost identical value to that of the FCN treated salt (see Figure 13). The PFA tests also show that using 0.02% MGDA as an additive decreases the caking energy by approximately threefold in comparison to the control and is at approximately the same value as that of FCN.

1.3.2.3 Amide-metal complexes

Presented also in Figure 13, are the values for the caking energy when using an amide-metal complex as the additive. It is evident that the activity of the NTAA is not affected by the addition of the metal ion but it is the case for MGDA. The caking energy for MGDA in conjunction with the metal ion, was in the same range of the control, indicating that it displays no anticaking activity at all. This could be due to the formation of a complex between the MGDA and the metal, which changes the steric structure of the amide, leaving it unable to bind to the surface of the sodium chloride, as in the case of the free amide. It should be noted here that the NTAA-metal complexes show slight creeping, which shows the correlation observed between that and the anticaking activity of these compounds in contrast to the MGDA complexes.

1.3.2.4 Additives with habit modification properties

The corresponding PFA testing (Figure 13) proves that PAA does not act as an anti-caking agent, rather being a "pro-caking" agent. The caking energy value is approximately 1.5 times larger than that of the control. In the case of formamide, the caking energy found for 0.5% (w/w) additive on the salt was found to be surprisingly low in comparison to the control and FCN (Figure 14). This is directly in contrast with the idea that an additive which does not cause creeping also does not have an anticaking effect. However, it was observed during the measurement, that the salt cakes did not fully dry over the 2 hour drying time allowed per sample. This can also be seen in the final image of the growth pattern in Figure 11, that there is still liquid present on the sample. It should be realised that the vapour pressure of formamide at 20°C (6 Pa[39]) is orders of magnitude lower than that of water (2330 Pa) so it hardly evaporates and instead stays on the surface of the NaCl. It is also hygroscopic. Because of these reasons, we conclude that it acts as a lubricant instead of a genuine anticaking agent. In order to confirm that there has been no growth modification to the salt crystals,

but instead a layer of solvent surrounding them, SEM imagery was taken of the salt crystals used in the PFA measurements (Figure 14). They show that there is no {111} facet growth and also very little difference from a control sample.

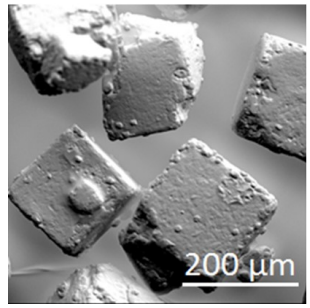

Figure 1.14: Scanning electron microscopy image of salt crystals treated with 0.5% (w/w) formamide after PFA experiment.

1.4 Discussion

Table 2 and Figure 15 summarise the results of our creeping and PFA experiments. A clear relation exists between the extension of creeping and anticaking activity, i.e. the effective anticaking agents for NaCl display distinct creeping patterns in the droplet experiments. The two habit modifying additives show no creeping and the PAA shows no anticaking effect. The exception to the rule is formamide, which displays a low caking energy when added to salt at 0.5% (w/w). However, as already concluded above, that this results from a lubrication effect rather than an actual growth modification effect as with true anticaking agents.

Compound/ Additive	**Amount of creep (mm)**	**Caking energy (CE20)**
NaCl (Sanal P)	0	143 (±6)
FCN	4.1	54 (±7)
Fe-mTA	3.3	37 (±5)
Fe-citrate, pH 6.7	2.2	34 (±8)
Fe-citrate, pH 0.8	0	258
MGDA	1.5	60 (±14)
NTAA	5.3	55 (±10)
MGDA + Fe^{2+}	0	144 (±15)
MGDA + Cu^{2+}	0	113 (±12)
NTAA + Fe^{2+}	0	47 (±13)
NTAA + Cu^{2+}	0	45 (±13)
PAA	0	250 (±40)
Formamide	0	24 (±2)

Table 1.2: Summary of values for amount of creeping and for caking energy of each compound/additive

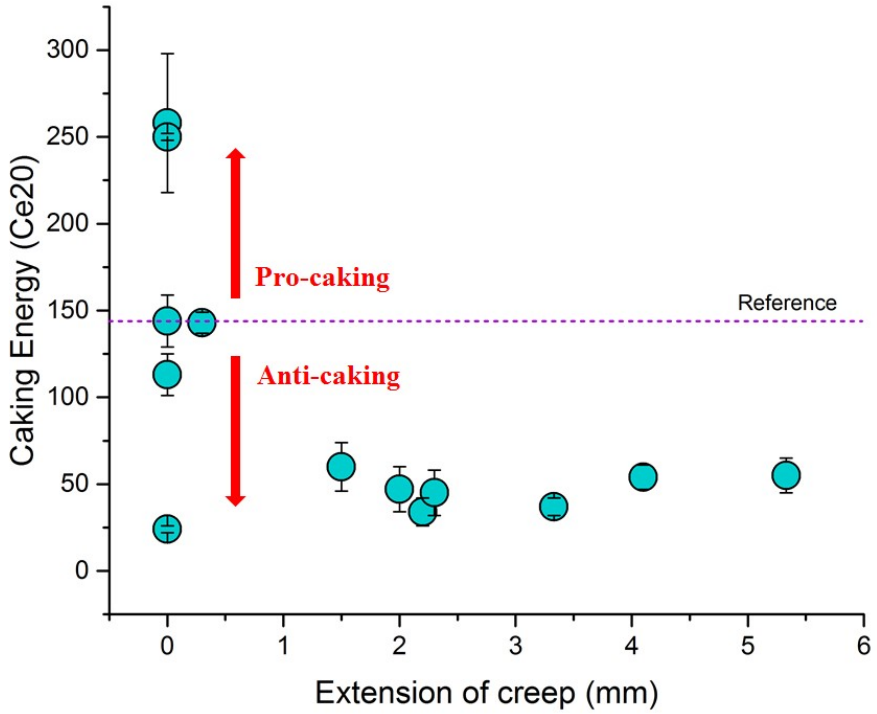

Figure 1.15: The correlation between caking energy and extension of creep induced by the different additives in this study.

We can understand the correlation between creeping and anti-caking by looking into the mechanism of creeping.

The occurrence of creeping patterns requires [30]: i) a not too high environmental humidity to allow solvent evaporation, ii) the correct wetting conditions (for instance, by using a glass substrate), iii) a repeated formation of micro-crystallites without orientational order by 3D nucleation. Condition iii) requires a low crystallite surface free energy, promoting the formation of 3D nuclei as well as a strong blocking of growth, slowing down further growth of the crystallites. Namely, 3D nucleation is largely determined by the free energy of a critical 3D nucleus and thus by its surface free energy, whereas the growth of the nuclei is inhibited by adsorption of the additive molecules "protecting" the surface from further growth. Lowering the surface energy is a result of the adsorption of the additive molecules, following the Gibbs adsorption isotherm. [40] This leads to adsorption enhanced roughening (similar to "chemical roughening" [41])

as can be recognized from the non-faceted crystallites, imaged by scanning electron microscopy.[42] This layer of additive molecules inhibits crystal growth, which is essential for a good anticaking agent. In this way, a connection between creeping and anticaking is made.

Furthermore, upon addition of the additives in lower quantities, the NaCl surfaces tend to roughen on a micro to nano-scale as a consequence of additive adsorption[28]; this reduces the contact area between the adjacent crystallites and thus also reduces the amount of caking.

1.5 Conclusions

We found a relation between the occurrence of anticaking activity on NaCl by several additives, such as FCN, Fe-mTA, Fe-citrate, NTAA, MGDA and NTAA + Cu^{2+}/Fe^{2+} and the occurrence of creeping. No creeping was found for MGDA + Cu^{2+}/Fe^{2+}, Fe-citrate at low pH and polyacrylamide, which also show no anticaking effect. Therefore, we can conclude that monitoring creeping provides a simple and convenient test for finding new possible anticaking agents for NaCl and other crystalline powder compounds.
The only inconsistency was found for when using formamide, but this is caused by a lubrication effect as the formamide did not fully dry at the high amounts at which it was used in this experiment. We can therefore also conclude that habit modifiers are not necessarily good anticaking agents for NaCl. The relationship between branched creeping and anticaking is explained by the hampering of crystal growth by the additives adsorbed onto the crystal surfaces.

Chapter 2

The mechanism of additive enhanced creeping of sodium chloride crystals

Eleanor R. Townsend, Willem J.P. van Enckevort, Jan A.M. Meijer, Elias Vlieg

Crystal Growth and Design, ***2017****, 17, 3107-3115*

Abstract

This article investigates the mechanism behind the creeping of sodium chloride induced by additives. Here, an experimental approach is complemented with theoretical considerations to describe how creeping patterns of brine evolve and how the introduction of additives into the solution affects the morphology of the resultant crystals. We have found that these additives cause kinetic roughening and morphological instability due mainly to the reduction of surface free energy. There was also a marked increase in 3D nucleation of the NaCl crystals and thus, branching.

2.1 Introduction

Creeping is a phenomenon observed for many crystalline compounds growing from solution which results in the extension of crystallites across a solid substrate, usually in an unwanted fashion. [7] [30] [34] [43] For example, the creeping tendency is well known for sodium chloride and can be largely enhanced by the addition of appropriate additives to the solution. We have shown previously, that this tendency can be exploited to our advantage, namely to determine whether an additive is a good anticaking agent for sodium chloride. [44] This is particularly pertinent as caking is one of the main problems encountered during the production, storage and transport of sodium chloride. When an effective anticaking agent is added to a brine solution, the creeping effect is enhanced and resulting crystallites often show different shapes. [30] Additive enhanced creeping has also been exploited to conserve stonework and statues by reducing damage caused by salt crystallisation. [29] [45] [46] [47]

Creeping can be defined as the evaporation-driven extension of crystals on solid, nonporous substrates beginning from the solution rim. [30] In our study, we concentrate on primary (mural) creeping, i.e. the direct growth of the crystals on the surface of the substrate. No attention will be given to secondary (efflorescent) creeping, which is creeping upon previously deposited crystals. [29] [30] The features observed are branched patterns radiating from the central solution source. As classified by Brener et al. [48], there are two different crystal morphologies which can be observed in branched crystal patterns, namely seaweed and dendritic forms. Seaweed crystal patterns have no pronounced orientational order, whereas those of dendritic patterns have branches in preferred crystallographic directions. These can be further classified into fractal and compact patterns, which depend on the value of the Hausdorff dimension, but this will not be covered in our paper. We have previously found that the creeping patterns we observe in the case of NaCl with additives, show seaweed type growth (the crystals have no precise orientational order). [44]

The aim of this chapter is to describe the mechanism of how the chosen additives act on the sodium chloride crystals and the impact on their creeping patterns that come about. This will be done using an experimental approach, imaging how the crystallites grow from solution droplets in the presence of different additives. The influence of the additives is explained using a theoretical model.

2.2 Theoretical Considerations

In our semi-quantitative model we consider additives that adhere quite well to the growing crystal surface. This adhesion leads to two important effects: first, a lowering of the surface energy which allows easier nucleation and second, a blocking at the surface which leads to slower growth of specific crystals and increased supersaturation. This increase in supersaturation leads again to an increase in the 3D nucleation and kinetic roughening due to the decrease in surface binding energy. If homogeneous or secondary 3D nuclei are easily formed, enhanced branching of the growth features is expected and seaweed patterns are likely to develop. The difference in creeping growth of NaCl in the absence and presence of additive is schematized in Figure 1.

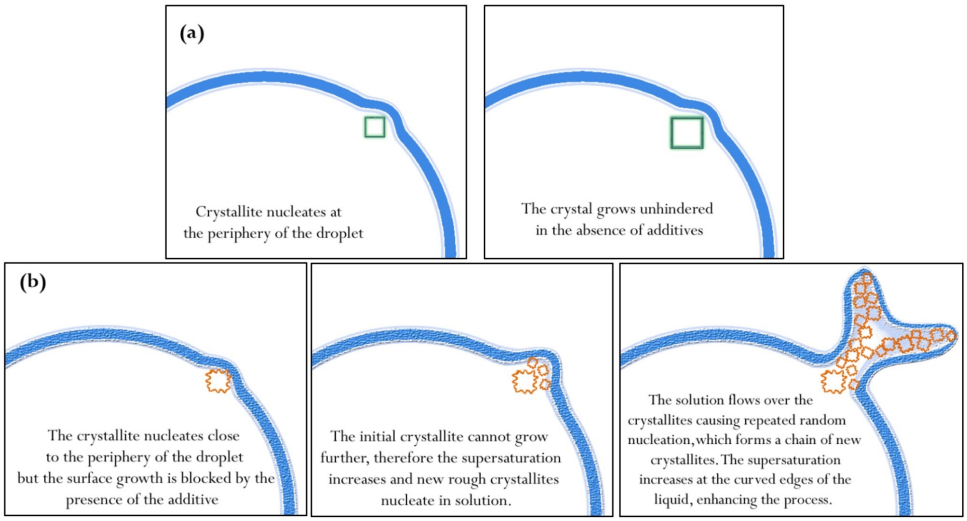

FIGURE 2.1: The difference in crystal growth of NaCl in the (a) absence and (b) presence of additive.

2.2.1 Surface free energy

To get a better understanding of the effect of supersaturation and additive content on the creeping process, we first estimate the influence of additive on surface free energy. The additive surface coverage, θ, is defined as the fraction of the crystal surface area covered by additive ($0 \leq \theta \leq 1$):

$$\theta = n_a \frac{F}{O}, \qquad (1)$$

with n_a, the number of additive molecules per surface site of area O, and F the surface area covered by one adsorbed additive molecule. Estimation of θ is done by using the simple Langmuir adsorption model. [49] [50] This model states that the fraction of surface area covered by additives, θ, is given by:

$$\theta = \frac{Kc}{1+Kc} \qquad (2)$$

with c the additive concentration in solution and $K = k_{ad}/k_{des}$, the ratio of adsorption probability and desorption probability of additive for a given surface area F. So, the fraction of free surface area is:

$$\theta^* = (1-\theta) = (1+Kc)^{-1} \qquad (3)$$

As was pointed out by Gibbs a (partial) surface coverage of additives leads to a lowering of the surface free energy, according to his adsorption isotherm. [40]

$$d\sigma = \Gamma d\mu_a, \qquad (4)$$

with σ the surface free energy, Γ surface concentration (number of additive molecules per surface area) and μ_a the thermodynamic potential of the additive in the solution,

$$\mu_a = {\mu_a}^0 + kTlnc, \qquad (5)$$

Here T is temperature and k is Boltzmann's constant. It is necessary that the adsorbed additives derange further addition of growth units at the surface. [51]

From Eq. 4 and

$$d\mu_a = kTd\ln(c) = kT\frac{dc}{c}, \qquad (6)$$

we obtain

$$\frac{d\sigma}{dc} = -\frac{\Gamma kT}{c}, \qquad (7)$$

Using $\Gamma = \frac{\theta}{F} = \frac{Kc}{(1+Kc)}\frac{1}{F}$, with F the surface area occupied by one adsorbed additive molecule, we get

$$d\sigma = -\frac{kT}{c}\frac{Kc}{(1+Kc)}\frac{1}{F}dc. \qquad (8)$$

Integration of Eq. 8 gives the decrease in surface free energy:

$$\Delta\sigma = -\frac{kT}{F}\ln(1+Kc) = \frac{kT}{F}\ln(1-\sigma). \qquad (9)$$

So, the surface free energy as a function of additive adsorption is:

$$\sigma = \sigma_0 + \frac{kT}{F}\ln(1-\sigma), \qquad (10)$$

with σ_0 the surface free energy of a "clean" surface, i.e. in contact with pure brine. Figure 2 displays the decrease of surface free energy of (100) NaCl in contact with saturated brine as a function of θ, starting from a clean (100) NaCl surface in brine, with $\sigma_0 = 38 * 10^{-3} J/m^2$ [52] and $F = 0.6 * 10^{-18} m^2$ (Table 1). This reduction in surface free energy with increasing additive coverage promotes morphological instability during crystal growth.

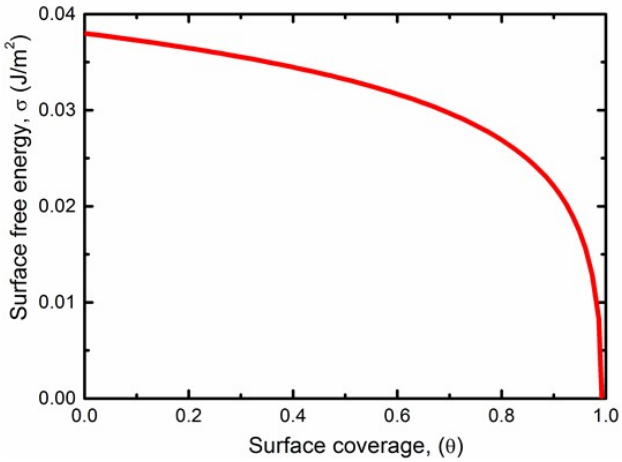

Figure 2.2: Surface free energy of (100) NaCl in contact with saturated brine as a function of additive surface coverage,σ.

2.2.2 Kinetic roughening, growth rate and supersaturation

As pointed out by Sears [51], the above not only holds for the crystal surface, but also for the free energy of the growth steps. The step free energy lowers by adsorption of additive and in combination with the high supersaturation during creeping this leads to kinetic roughening [15] as can be concluded from the non-facetted crystallites during our experiments.

The kinetically roughened crystal faces grow according to the Wilson-Frenkel mechanism [53] [54] [55], following:

$$R = A(1-\sigma)[exp(\Delta\mu/kT - \Delta\mu_0/kT) - 1], \qquad (11)$$

in which the growth rate is retarded because part of the surface is covered by additive, θ . We here assume a dead supersaturation zone [56], $\Delta\mu_0/kT$, where growth is

governed by 2D nucleation and blocking by incorporation of the additives.[57] Therefore, we approximate $R(\Delta\mu < \Delta\mu_0) = 0$. Further, A is only weakly dependent on surface free energy[58] and $\Delta\mu_0/kT$ tends to increase with additive coverage.

The rate limiting step in creeping is determined by solvent evaporation.[30] Here crystal growth follows the rate of solvent evaporation and is in first approximation independent of additive concentration. This implies that the driving force for crystal growth has to adapt to a given growth rate R_0, determined by solvent evaporation. Or, from Eq. 11 this gives:

$$\frac{\Delta\mu}{kT} = ln(\frac{R_0}{A(1-\theta)} + 1) + \Delta\mu_0/kT, \qquad (12)$$

So, for creeping an increased additive coverage results in a larger driving force for crystal growth. The combination of a higher driving force and a lower surface/step energy promotes the occurrence of kinetic roughening and thus morphological instability. Of course, a larger R_0, induced by lowering the solvent partial pressure during the creeping process also increases $\Delta\mu/kT$.

2.2.3 Competition between 3D nucleation and crystal growth

The formation rate of spherical 3D nuclei at/near the tips of the creeping branches is given by[59]:

$$J = C(1-\theta)\sigma^{1/2} exp(\Delta\mu\ kT - \Delta\mu_0\ kT) \exp[\frac{-B\sigma^3}{\Delta\mu^2}]. \qquad (13)$$

In this equation C is a kinetic constant and σ is given by Eq 10. Further,

$$B = f\frac{16\pi\Omega^2}{3kT}. \qquad (14)$$

with Ω is the volume of one growth unit and $f \leq 1$, being a correction term for heterogeneous 3D nucleation. As the second exponential term in Eq. 13 is determined by thermodynamics, rather than kinetics, here no correction for $\Delta\mu_0/kT$ is applied. It is clear from Eq. 13, that the rate of 3D nucleation rapidly increases for increasing supersaturation and decreasing surface free energy. To understand the effect of 3D nucleation on the creeping patterns, it is helpful to compare the 3D nucleation rate with the crystal growth rate. This gives an indication of the relative amount of microcrystallites and branching in the growth patterns.

In our model, we only consider homogeneous nucleation, i.e. $f = 1$, as in our seaweed creeping patterns the crystallite grains are not epitaxially related. In view of the high supersaturation involved during creeping growth, we also neglect the dead supersaturation zone, i.e. $\Delta\mu_0/kT \cong 0$.

It then follows from Equations 10, 11 and 13 that the ratio of 3D nucleation rate and crystallite growth, **R** is:

$$\mathbf{R} = J/R = \frac{C}{A}\frac{\exp(\Delta\mu/kT)}{\exp(\Delta\mu/kT)-1}(\sigma_0 + \frac{kT}{F}\ln(1-\sigma)^{1/2}\exp[-B\frac{(\sigma_0+\frac{kT}{F}ln(1-\theta))^3}{\Delta\mu^2}]. \quad (15)$$

and is displayed in figure 3 as a function of $\Delta\mu/kT$ for different θ values and in figure 4 as a function of θ for different $\Delta\mu$. As input the data given in Table 1 is used.

Parameter	**Value**
Volume growth unit, Ω	$22.43 * 10^{-30} m^3$ per ion
Temperature, T	300 K
Boltzmann's constant, k	$1.38 * 10^{-23} J/K$
Surface area of one additive unit, F	$0.6 * 10^{-18} m^2$ for $(Fe(CN)_6)$
Surface free energy clean (100) NaCl, σ_0	$38 * 10^{-3} J/m^2$ [15]
Kinetic constant: C/A	C/A is arbitrarily set to 1

Table 2.1: Summary of values for amount of creeping and for caking energy of each compound/additive

From the two graphs, it is clear that the 3D nucleation rate with respect to growth rate increases rapidly with supersaturation and additive coverage, the latter due to an increased additive concentration in the solution. This leads to an enhanced micro-crystallite formation and branching of the creeping patterns. The introduction of f < 1 or a finite value of $\Delta\mu_0/kT$, a higher σ_0 ($63\ mJ/m^2$) [60] or lower ($24.4\ mJ/m^2$) [61] changes the situation somewhat, but does not alter the general conclusions. It follows from Eqn. (11), that if $\Delta\mu < \Delta\mu_0$, no growth occurs and nuclei cannot expand. Therefore, Eqn. (15) only holds if $\Delta\mu$ exceeds $\Delta\mu_0$ to some extent and the possible existence of a dead zone should be considered in analysing the experiments.

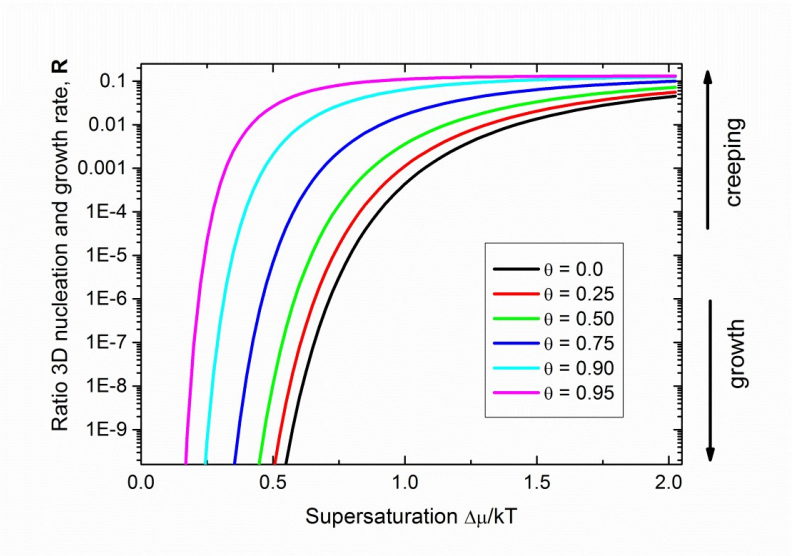

Figure 2.3: Ratio 3D nucleation rate and growth rate, **R**, as a function of supersaturation, $\Delta\mu/kT$, for six different surface coverages, θ.

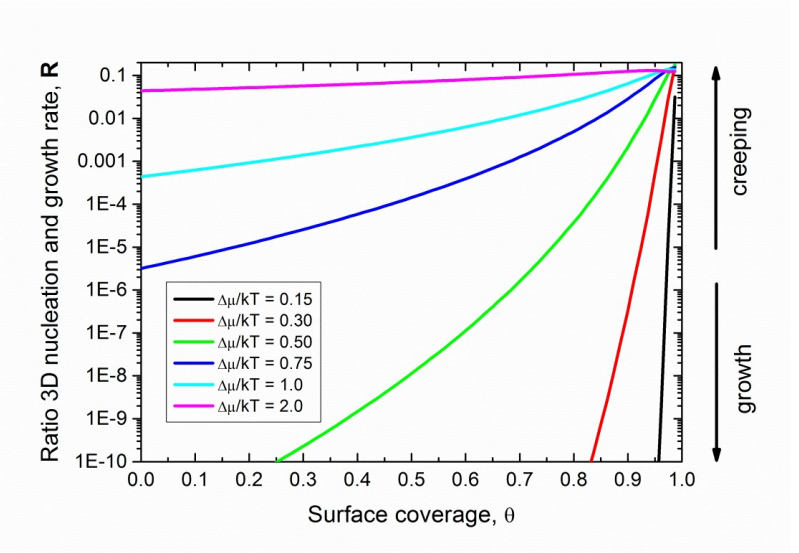

Figure 2.4: Ratio 3D nucleation rate and growth rate, **R**, as a function of surface coverage, θ, for six different supersaturations, $\Delta\mu/kT$.

2.3 Methods

The additives used in this investigation are a selection of three taken from our previous publication on the topic of creeping vs. anticaking [44], which exhibit markedly different NaCl creeping patterns (Table 2). The three additives all have very different molecular structures, but all have a large effect on the growth of NaCl on the (100) surface. All are effective anticaking agents, two of which are currently used in industry.

The first additive chosen is sodium ferrocyanide ($Na_4[Fe(CN)_6]$, in the following denoted as $Fe(CN)_6$), which is a widely used anticaking agent in the salt industry. It has been previously shown in the literature, that ferrocyanide causes severe creeping of NaCl. [29] [44]

The second additive is iron meso-tartrate (Fe-mTA), a complex containing Fe with meso, L and D tartrate ligands. The exact structure of this complex is as of yet unknown, but there is evidence that it contains 2 Fe atoms, with 2 tartrate ligands. [21] This complex is also currently in use in salt production at Akzo Nobel. This complex only causes a change in the crystal growth of NaCl at a specific pH, of approximately 4.2. [35]

The third additive chosen is a branched amide compound, nitrilotriacetamide (NTAA, $C_6H_{12}N_4O_3$). Nitrilotriacetamide has been previously reported in the literature to have an effect on the crystallisation of NaCl. [33] [36] [62]

Compound/ Additive	**Source purity**	**pH in brine solution**	**Concentration[a] (w/w)**	**Contact angle[b]**
NaCl (*Sanal P* ®)	>99%	-	-	9.7 °
$Fe(CN)_6$	99%	5.2	1%	9.4 °
$Fe(CN)_6$	99%	5.2	0.1%	10.3 °
Fe-mTA	*AN*	4.2	1%	7.1 °
Fe-mTA	*AN*	4.2	0.1%	9.0 °
NTAA	*AN*	5.0	1%	11.7 °
NTAA	*AN*	5.0	0.1%	7.2 °

Table 2.2: The additives and their characteristics in the different experiments. (*AN*: As per Akzo Nobel guidelines) [a]: in creeping experiment (w.r.t. solution), [b]: with glass substrate (±3°)

2.3.1 Creeping tests

The creeping tests performed in this investigation were all performed on glass microscope slides, previously washed with ethanol and dried with a dust free tissue, to minimise external nucleation effects. Saturated brine solution (solubility NaCl 359 gL^{-1} water at 25°C) was combined with the chosen additive, to give a solution containing concentrations of the additive in a range from 0.001-1% (w/w) with respect to the solution. A filtered 5 μL droplet of solution was placed on the microscope slide and placed into a climate chamber set at a fixed temperature of 20°C and relative humidity of 50%. The droplet was allowed to evaporate and the resulting creeping patterns were imaged using a Leica Wild M10 stereomicroscope and a FEI Scanning Electron Microscope. These experiments were performed using all concentrations of additive as shown in Table 2.

As the contact angle of the solution with the substrate can be important in the case of creeping, this was also measured for each solution using an optical set-up imagine the droplets viewed from the side by a CCD (values stated in Table 2). As there was little variation between the contact angles of each solution on the substrate, the effect was not considered during interpretation of the results. Also the experiments containing 0.001% (w/w) additive showed very little difference to the control, therefore these are not discussed in this paper. In addition, the pH of the individual solutions was measured and all experiments were performed in triplicate to ensure reproducibility.

2.3.2 In-situ Optical Microscopy

In order to visualise the evaporation of the droplets at higher magnification in-situ, samples were prepared as above but instead of being stored in a climate chamber, they were placed under a Leica DMRX optical microscope and allowed to evaporate at ambient temperature (on average 20°C, ∼50% relative humidity). The propagation of the droplet evaporation was imaged at a rate of 1 frame per second in transmission mode and a resulting movie was made using an amalgamation of the images. Singular images are displayed in the results section and movies of Figures 7 and 9 are included in the supplementary information of the published article. These experiments were performed with concentrations of 1% and 0.1% (w/w) additive in the brine solutions.

2.3.3 Scanning Electron Microscopy

In order to observe the crystal patterns at a higher magnification and a higher depth of field than feasible with optical microscopy, we used scanning electron microscopy

(SEM). The creeping patterns were fully dried in a climate chamber at 20°C and 50% R.H. and then sputtered with Au using a Cressington 108 auto sputter coater. The samples were imaged using a FEI Phenom Scanning Electron Microscope in back scattering mode at 5 kV.

2.4 Experimental Results and Discussion

From the theory section, we can summarise the following points on the effect that impurities have on the crystallisation of a material during creeping: (1) They lower the surface free energy, (2) They cause kinetic roughening, also because of the higher supersaturations involved, (3) They enhance heterogeneous/homogeneous 3D nucleation, (4) They promote branching. These conclusions will be verified by experiments in this section. Qualitative results can be obtained from this investigation; however, it is impossible to produce quantitative information as the surface coverage cannot be measured in situ for creeping and the supersaturation at the crystal-liquid interface is also difficult to determine in these situations.

As a reference sample, a saturated solution of NaCl was dropped onto a microscope slide using the above indicated method and allowed to dry at 20°C and 50% R.H. This pattern was observed using optical microscopy and SEM, as shown in Figure 5. It is evident that there is little to no roughness on the surface of the perfectly facetted cubic crystals. Here crystal growth proceeds by a layer by layer mechanism (no kinetic roughening) and the number of 3D nuclei formed is limited. There is also very little evidence of creeping.

To estimate the supersaturation at which the crystals first begin to nucleate from a saturated brine droplet with no additive, an evaporating droplet on a glass substrate was weighted in-situ using a precision balance. From the change in weight of the droplet when the first crystallites appeared as imaged using optical microscopy, we arrived at an approximate average figure of $\Delta\mu/kT \approx 0.06$. As the crystallites nucleated near the edges of the droplet, this value is likely larger.

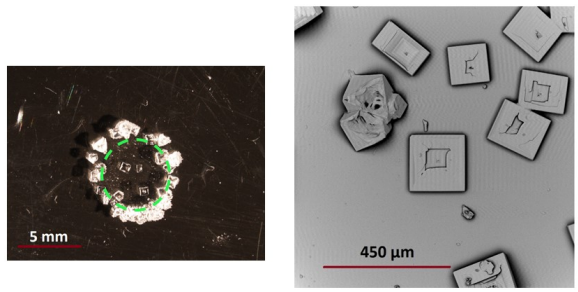

Figure 2.5: Left: Optical image of the pattern formed after the evaporation of a saturated brine solution droplet with no additive. Original droplet boundary is indicated on the image. Right: SEM image showing individual crystallites of a pattern similar to that displayed on the left.

2.4.1 Ferrocyanide ($Fe(CN)_6$) as an additive

A large difference exists between the creeping patterns of NaCl with decreasing amounts of $Fe(CN)_6$ additive in solution (Figure 6). There is a large amount of branched spread over the substrate when the solution contains 1% (w/w) $Fe(CN)_6$, which decreases towards 0.01% (w/w) $Fe(CN)_6$ and vanishes for 0.001% (w/w) $Fe(CN)_6$.

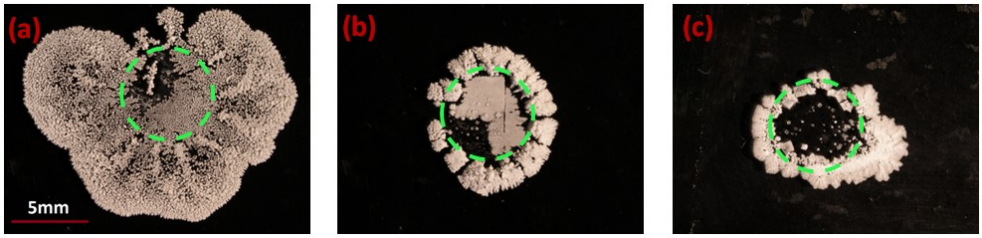

Figure 2.6: Creeping patterns from a saturated brine solution droplet containing (a) 1% (w/w) $Fe(CN)_6$, (b) 0.1% (w/w) $Fe(CN)_6$, (c) 0.01% (w/w) $Fe(CN)_6$. The original droplet boundary is indicated in each image.

Figure 7 shows the development of the NaCl creeping pattern with the addition of 1% (w/w) $Fe(CN)_6$. The crystallite growth begins at the edges of the droplet, where, as there is suitable wetting, a protrusion of the solution occurs and deposits a crystallite outside the boundary of the droplet. This crystallite acts as a frame for the solution to flow over and further crystallites are deposited in the extended solution boundary. There is no attachment between the crystallites, but they deposit one behind each other, and act as a "chain" for the continuing solution to spread over. There seems to be significant convection in the solution leading to an irregular deposition of the crystallites on the glass substrate. Likely this convection is due to the Marangoni effect, induced by concentration and temperature gradients in the droplet. It is also evident, as expected, that there is a large amount of 3D nucleation in comparison to that of the control. We postulate that this could be either homogeneous nucleation or heterogeneous nucleation from nano-fractured parts leaving the crystallites. In both cases, 3D nucleation is enhanced by the additive induced lowering of surface free energy and the high supersaturation during creeping because of blocking.

These chains then branch off from each other at a certain point, to form a seaweed pattern with no definite orientational order. This is as expected, as the crystallites are formed separately in the solution. The resulting creeping pattern is very open as there is wide spread of the branches.

The SEM images (Figure 8) show that the crystallites have strong morphological instability and are significantly roughened at the surface by the presence of the additive. In contrast to the pure NaCl solutions, no facetted morphology is observed. There is also evidence of spike-like growth pointing in the six {100} directions, indicating that the {100} facets of the crystals are significantly destabilised by $Fe(CN)_6$. Destabilisation of the cubic morphology is also evidenced by the occurrence of hopper-like growth, which is a manifestation of morphological as well (Figure 8b). Both non-facetted morphologies point to kinetical roughening due to low surface energy and high supersaturations which matches with our theoretical inferences.

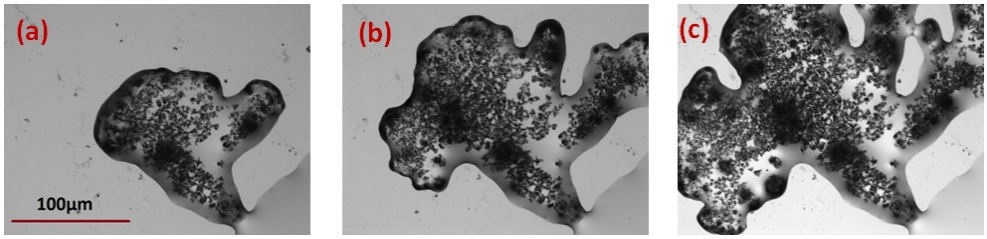

Figure 2.7: High magnification optical microscope in-situ images showing the propagation of the creeping pattern of brine with 1% (w/w) $Fe(CN)_6$. The time interval between successive pictures is 4 minutes.

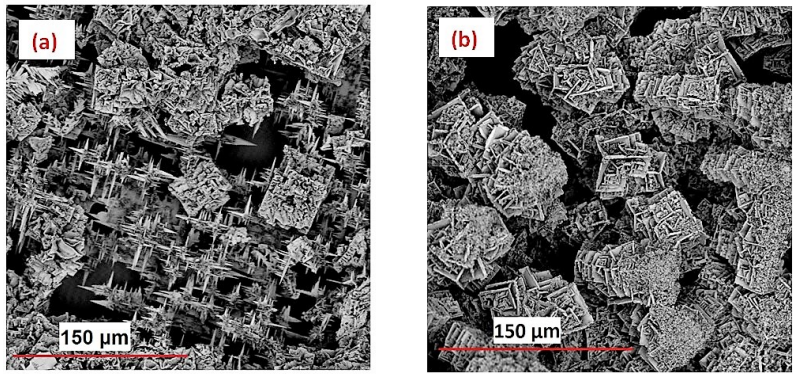

Figure 2.8: Scanning electron microscope images showing details of the creeping pattern from a saturated NaCl solution originally containing 1% (w/w) $Fe(CN)_6$.

Figure 9 shows the evolution of the creeping pattern of a saturated NaCl solution containing 0.1% (w/w) $Fe(CN)_6$. It was observed that the NaCl crystallites again

span outwards from the droplet boundary in a branched seaweed fashion, with no definite orientational order. Again, it is evident that the individual crystallites are weakly attached to one another and so arrange in a seaweed branched pattern. The individual crystallites exhibit a dendritic pattern, with spikes pointing towards the {100} directions (Fig. 9b).

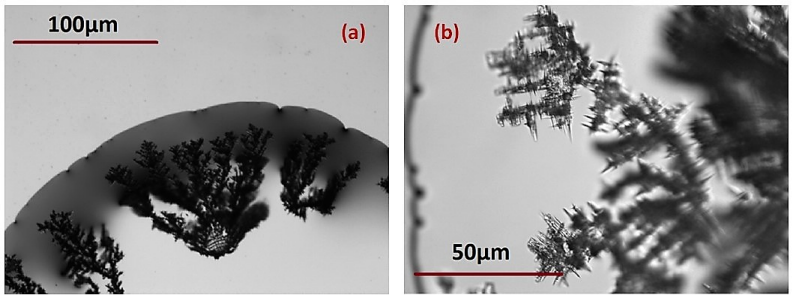

Figure 2.9: Optical microscope in-situ images of the creeping pattern of a saturated NaCl solution containing 0.1% (w/w) $Fe(CN)_6$.

With the decreasing amount of additive, there is less outward spread of the branches but with the same strong morphological instability as evident in the 1% (w/w) $Fe(CN)_6$ case. To obtain an idea of the supersaturation for the NaCl growth with 1% $Fe(CN)_6$ additive, a similar droplet evaporation experiment as for the pure NaCl solution was carried out. This gave an average supersaturation of $\Delta\mu/kT \approx 0.20$, which is beyond the value of $\Delta\mu/kT \approx 0.06$ for pure brine. This points to a large dead supersaturation zone, as was previously reported for the same NaCl-additive system in [17]. When growth sets on, branching immediately takes place as predicted by equation (15), regardless of $\Delta\mu/kT$. The dramatic change in nucleation rate and morphology indicates that the surface coverage of $Fe(CN)_6$ must be high. A high occupancy (∼52%) of $Fe(CN)_6$ of {100} NaCl was also observed by surface x-ray diffraction, although at different conditions.

2.4.2 Iron meso-tartrate (Fe-mTA) as additive

In a similar fashion to that observed for the creeping pattern of NaCl with $Fe(CN)_6$, there is a marked difference in the NaCl creeping patterns with decreasing amounts of Fe-mTA additive, as displayed in Figure 10. The spread of the branched patterns observed for that with 1% (w/w) Fe-mTA is not as wide as observed for $Fe(CN)_6$, but the cubic growth is very disrupted. For the lowest additive concentration of 0.01% (w/w), there is a tendency towards cubic growth.

Figure 2.10: Creeping patterns of a saturated brine solution containing (a) 1% (w/w) Fe-mTA, (b) 0.1% (w/w) Fe-mTA, (c) 0.01% (w/w) Fe-mTA. Original droplet boundary is indicated on each image.

For 1% and 0.1% (w/w) concentrations, the evolution of the creeping pattern begins at the peripheries of the droplet with branched patterns composed of singular crystals, which are morphologically unstable, and showing no evidence of cubic shape. This morphological instability is particularly evident in Figure 11a. More crystals nucleate until the entirety of the droplet edge is filled with crystallites. The solution then begins to flow outwards over the deposited crystals (Figure 11b). It is evident that the crystallites in the outward flowing solution are not attached to each other when they are formed and the solution flows over and around them until the liquid layer is low enough that the crystallites deposit onto the substrate in a chain to form the macroscopic seaweed branches of the creeping pattern. The individual microscopic crystallites are morphologically unstable with no clear shape to them.

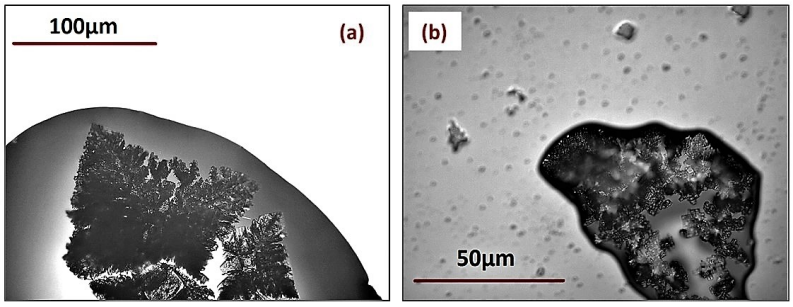

Figure 2.11: Optical microscope images of the evolution of the creeping pattern of a saturated NaCl solution containing 1% (w/w) Fe-mTA.

At a higher magnification of these branches, the SEM images show that there is a large amount of said morphological instability on the surface (Figure 12). It also indicates repeated 3D heterogeneous nucleation of numerous micro-crystallites. No {100}

spikes were observed growing in the 100 directions, as in the case of FCN. Figure 12b shows that morphological instability is still present at lower additive concentrations of 0.1% (w/w) Fe-mTA, with an extremely rough surface with no visible fully facetted crystallites. Instead, the surface is dominated by a chaotic growth pattern due to the lower surface energy and fast growth times. For both additive concentrations, there is also evidence of hopper growth, which is an indication of morphological instability as well. Our experimental findings in this case also link well with our theoretical work, as we have shown that Fe-mTA enhances the roughening of the crystal surfaces and the branching of the crystal creeping pattern, which is a result of the lowered surface energy and surface blocking. It is also evident from our results that there is a large increase in 3D nucleation, in comparison to that of the control.

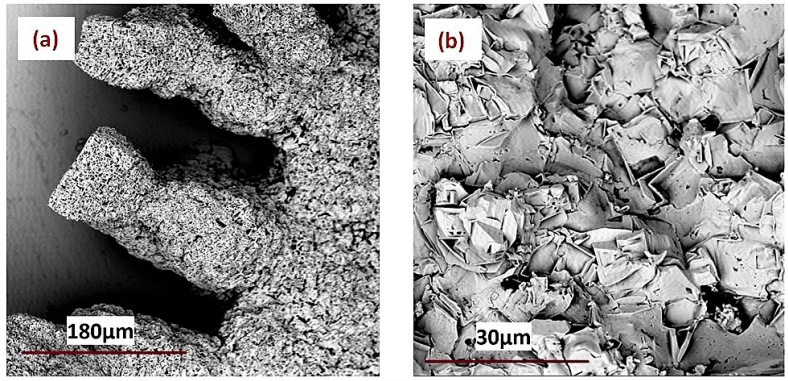

Figure 2.12: Scanning electron microscope images of the creeping pattern of a saturated NaCl solution containing (a) 1% (w/w) Fe-mTA and (b) 0.1% (w/w) Fe-mTA.

2.4.3 Nitrilotriacetamide (NTAA) as additive

In a similar fashion to the two previous examples, the decrease in additive concentration leads to a decrease in crystallite growth (Fig. 13). However, in the case of NTAA, the lowest concentration of 0.01% (w/w) still has a markedly non -cubic growth pattern. In all cases when using NTAA as the additive, there is little dendritic spread, resulting in a far more compact pattern than previously observed with $Fe(CN)_6$ and Fe-mTA. Therefore, this does not fully agree with our model lined out in this article.

In the case of the evaporation of a brine solution containing 1% (w/w) nitrilotriacetamide, the creeping pattern is markedly different to that observed when using 1% Fe(CN)6 and Fe-mTA. This can be seen in Figures 14 and 15. The growth of the

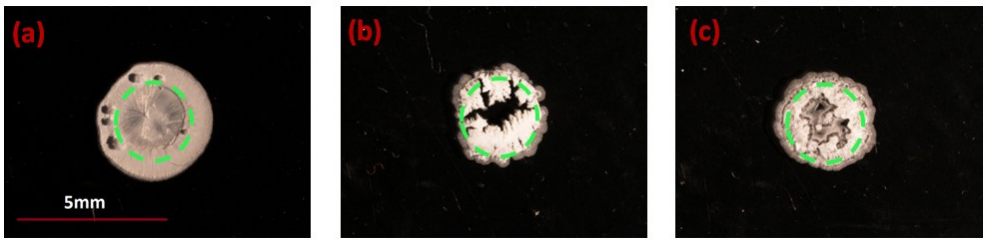

Figure 2.13: Creeping patterns of a saturated brine solution containing (a) 1% (w/w) NTAA, (b) 0.1% (w/w) NTAA, (c) 0.01% (w/w) NTAA.

crystallites begins at the periphery of the droplet but the outward spread of the initial crystallites is much more limited than that of the other two cases, leading to a more compact pattern. The salt crystals in this case are not in the expected cubic form, but instead display a needle shaped morphology. Powder X-Ray diffraction measurements have been performed to confirm that these needles are indeed made from NaCl and not the additive. The needles spread outwards over the glass substrate but also inwards into the centre of the droplet, leading to a complete coverage of the centre of the creeping pattern with layers of criss-cross NaCl needles. No branching of the needles is observed, which disagrees with the theory. Scanning electron microscopy shows that the entire surface of the creeping pattern consists of thin criss-cross needles of NaCl, of approximately 1-5μm in width (Figure 16a). The theory outlined in this paper does not explain the formation of this type of growth. The reason for the evolution of these needle crystals, which violate the m$\bar{3}$m point group symmetry of NaCl, is further outlined in Chapter 5. However, our results here do agree with the theoretical idea that the impurities cause largely increased 3D nucleation, which explains the formation of many small needles in this creeping pattern.

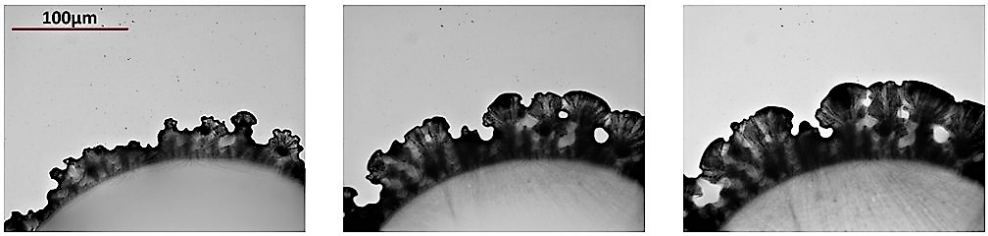

Figure 2.14: Optical microscope in-situ images of the creeping pattern of a saturated NaCl solution containing 1% (w/w) NTAA. The time interval between successive patterns is approximately 30 seconds.

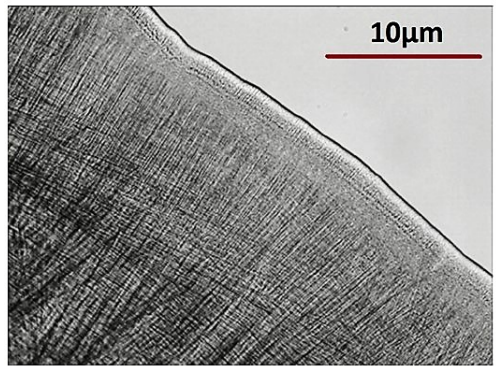

Figure 2.15: Higher magnification optical microscope in-situ image of the propagation of the creeping pattern from saturated brine with 1% (w/w) NTAA, showing needle growth.

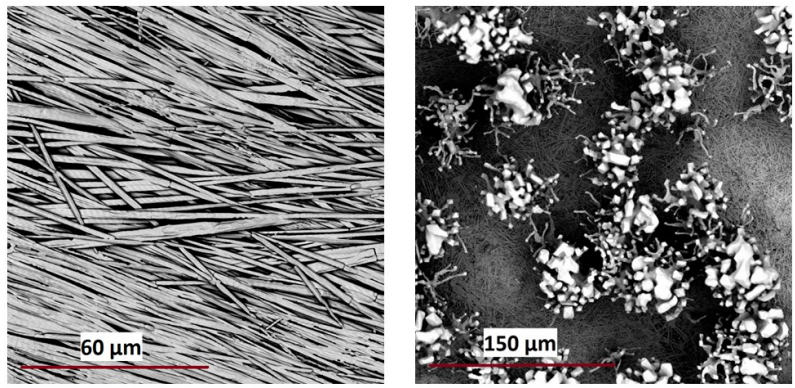

Figure 2.16: Scanning electron microscope image of the creeping pattern from a saturated NaCl solution containing 1% (w/w) NTAA. There is clear needle growth.

2.5 Conclusions

During this investigation, we have observed multiple changes in the morphology of sodium chloride creeping patterns which can be attributed to the introduction of various additives into a brine growth solution. We have also shown that the rate of 3D nucleation increases rapidly with increasing supersaturation and additive concentration. This leads to a branched crystal pattern consisting of numerous non-facetted microcrystals, which was observed for the cases of ferrocyanide and iron meso-tartrate

as additives. These observations have been explained using a semi-quantitative model, which postulated that the additive coverage on the surface of the sodium chloride crystals leads to a decrease in the surface free energy and therefore an increase in morphological instability and kinetic roughening.

We have found that when using nitrilotriacetamide as an additive, we do not observe the expected branching pattern, but instead a dense pattern consisting of ultra-thin NaCl needles. Therefore, the model does not fully explain the mechanism of this creeping pattern, which is a topic of further investigation.

Chapter 3

Polymer versus monomer action on the growth and habit modification of sodium chloride crystals

Eleanor R. Townsend, Willem J.P. van Enckevort, Jan A.M. Meijer, Elias Vlieg

Crystal Growth and Design, ***2015****, 15, 5375-5381*

Abstract

We have investigated the use of polymers and monomers as habit modifiers and anticaking agents for sodium chloride. We show that amide functional groups cause {111} faces to propagate on sodium chloride crystals and that polymer amides give a 1-2 orders of magnitude greater effect than the corresponding monomers on the habit modification of sodium chloride. We have also shown that the alcohol functional group does not have an effect on the surface or habit modification but that, when in a polymer form, leads to macrostep formation and acts as a nucleation inhibitor. The latter also holds true for other polymers that we have also tested. Finally, we found that no amino acids, apart from glycine, have an effect on the morphology of NaCl crystals.

3.1 Introduction

Sodium chloride is a very important industrial material, due to its uses in the chloral-kali industry, de-icing for winter road maintenance, as a vital part of our diet and as a food preservative. However, difficulties arise in industrial settings as sodium chloride has the tendency to cake, i.e., to form large agglomerates of material. [27]

It is therefore pertinent to develop methods of how to engineer the NaCl crystals so that this caking effect does not occur, which can be done by modifying the habit or blocking the growth. The first example of a habit modifier for sodium chloride, urea, was described by Romé d'Isle in 1783. [8] In this work, he reported a habit modification of the crystals from cubic to octahedral. This has led to the discovery of other habit modifiers for sodium chloride such as formamide and cadmium chloride. [63] In current salt production, the growth blocker sodium ferrocyanide (FCN) is used as an additive and has a very powerful effect on the surface. However, the use of this anticaking agent poses some problems. Large amounts of sodium chloride are used in the electrolysis process to produce chlorine gas and sodium hydroxide. This process is carried out through a cycle involving a series of membranes. The ferrocyanide compound decomposes during this process into free iron and free cyanide, with the iron forming iron hydroxide which degrades the membranes and the cyanide forming the explosive gas NCl_3. Therefore, it is of great interest to search for new habit modifier/growth inhibitors for sodium chloride which do not have these drawbacks.

Little research has been done on the use of polymers as modifiers for sodium chloride, which theoretically have the potential to have a strong effect on the crystals. Larger molecules have more attachment points and as adhesion increases largely with the number of attachment points, it is expected that polymers will be very strongly bound to the NaCl surface and therefore give a powerful modification effect. Also it is very important to have a strongly bound additive to minimize the possibility of leaching in the case of road de-icing.

Various small molecules (referred to from now on as monomers) have shown that they have an effect on the habit of sodium chloride; examples are urea, formamide and also glycine. Urea and formamide both promote the formation of the {111} face of NaCl, creating octahedral crystals, while glycine promotes the formation of {110} faces, creating dodecahedral crystals. However, large amounts of these materials are required to elicit a habit modification for sodium chloride. For example, 20-30 % (w/w) of formamide is necessary to obtain an octahedral sodium chloride crystal [64]

and 10-15% (w/v) glycine is required to elicit habit modification.[65] Other research has stated that an even higher concentration of glycine is required, up to 25% (w/v).[66] High concentrations of habit modifiers are not industrially viable due to the high costs associated. Theoretically then, polymers containing the same functional groups as these monomers could be able to give an effect at a much lower concentration.

In the literature, the only reported use of a polymer as an anticaking agent for sodium chloride is polyvinyl alcohol[67], which describes this polymer as being a better anticaking agent for sodium chloride than other more widely used modifiers. Consequently, it is applicable to repeat these experiments to determine their reproducibility and also to experiment using other polymers with different functional groups.

For this paper, different polymers (see Fig. 1) were utilised in a variety of experiments to determine their properties on the surface of sodium chloride. Larger scale solution crystallisation and small scale in-situ experiments were employed in conjunction with optical microscopy to determine the crystal shapes elicited by the sodium chloride and polymer solutions. Additionally, Atomic Force Microscopy (AFM)and Scanning Electron Microscopy (SEM) were used for *a posteriori* examination of the crystal surfaces. A Powder Flow Analysis technique was used to examine the caking properties of the crystals.

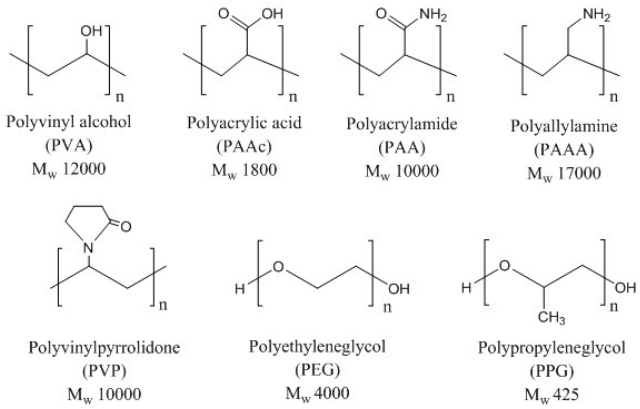

Figure 3.1: Polymers used in this investigation as potential modifiers of sodium chloride morphology and caking.

3.2 Methods

3.2.1 Crystal Growth

The effect of habit modifiers is known to depend on crystal growth rate. Therefore, two different sets of crystallisation experiments were performed: large scale solution crystallisation involving slow growth, and small scale in-situ experiments involving fast growth. In all experiments, the unit% (w/w) is used, which denotes g/100 g solution.

3.2.1.1 A: Large-scale solution crystallisation

A saturated solution of sodium chloride was prepared using 35.9 g Akzo Nobel SanalP®NaCl dissolved in 100 ml MilliQ water, then filtered using a 0.2 μm Whatman filter. 10 ml of the salt solution was mixed with a solution of the chosen additive; the amount added was dependent on the desired additive concentration of the mixed solution. The mixed solutions were placed into glass vials and evaporated in a Binder climate controlled chamber at 25°C and 50% relative humidity for 1-2 weeks. The resulting sodium chloride crystals were then removed from the solution, washed in saturated brine and dried for microscopic analysis. The resulting crystals had a length of 2-5 mm. All chemicals used were *pro analysi*. In the case of the PVA, the designated type used was a "short chain" molecule with a molecular weight of 12000 D. Longer chain variants were tested at the outset and it was determined that these gave no satisfactory results.

3.2.1.2 B: Small-scale in-situ crystallisation

Saturated sodium chloride and additive solutions were prepared as described in the preceding section in various concentrations. 5 μL droplets of these solutions were applied to a clean glass microscope slide and seeded with NaCl micro crystals. The droplets were then evaporated on a Linkam LTS420E temperature-controlled stage at 30°C for 5 minutes and observed *in situ* with optical microscopy using Linksys 32 software. Photographs were taken of the growing crystals at 5 second intervals using a CCD camera, in order to view the evolution of the crystal morphologies. The crystals grown were of an approximate length of 10 μm.

3.2.2 *A posteriori* characterisation

3.2.2.1 Atomic Force Microscopy (AFM)

5 x 5 mm crystals were cleaved from melt grown sodium chloride blocks purchased from Ted Pella, Inc. (Redding, CA, USA). Aqueous solutions of various concentrations

of ethanol, methanol, PVA and PAA in MilliQ water were made up and were applied in 10 μL droplets to the {100} surface of cleaved crystals or the {111} surfaces of solution-grown crystals. These crystals were allowed to dry for 48 hours in a Binder climate controlled chamber at 25°C and 50% relative humidity. In this period, the face of the NaCl crystal first dissolves in the droplet and then grows during subsequent evaporation. The AFM used in these experiments was a Digital Instruments Dimension 3100 and was applied to the {100}/{111} NaCl surface in contact mode with NT-MDT NSG 10 golden silicon probes. A scan rate of 1 Hz was used.

3.2.2.2 Scanning Electron Microscopy (SEM)

Large crystals were obtained from slow growth in solution and then removed from solution and dried using a paper tissue. These selected crystals were sputter-coated with gold using a Cressington 108A sputter coater and then the surface topography was viewed using a FEI Phenom-World scanning electron microscope.

3.2.2.3 Differential Interference Contrast Microscopy (DICM)

A Leica DM-RX-HC-POL optical DICM microscope was used to view selected crystals at different magnifications in transmission and reflection modes.

3.2.2.4 Powder Flow Analysis (PFA)

Tests were performed in quadruplicate using a Powder Flow Analyzer (type TA-XT21, Stable Micro Systems) to determine the caking strength of the sodium chloride when treated with polymer solutions. Both PVA and PAA were investigated. 50 g batches of Akzo Nobel Sanal P® salt were placed into separate plastic bags and treated with 2% moisture. The moisture consisted of a solution of a 0.1% (w/w) polyvinyl alcohol in MilliQ water. The treated salt batches were placed in separate plastic containers of 50 mm diameter and preconditioned by compressing with 1 kg weight and purging with dry air for 2 hours. The strength of the cake of the samples was then measured using a rheometer, which is a screw-like moving blade which enters the salt cake and continuously measures the vertical force imposed by the salt. The measurement unit is CE20, which is the relative caking energy in N.mm required to enter a cake of 20 mm, a standardized measurement employed by Akzo Nobel.[38] [68] This experiment was repeated for 0.2% and 1% (w/w) solutions of PVA and 0.5%, 1% and 5% (w/w) solutions of PAA and the results were compared to blank and ferrocyanide tests.

3.3 Results

3.3.1 Polyvinyl alcohol (PVA)

The beginning point of this investigation was to try to reproduce the results from , which claimed that PVA is a superior anticaking agent for sodium chloride. It also tied in well with our aim to investigate the properties of long chain molecules as modifiers for NaCl. Using PVA in a range of concentrations from 0.05% (w/w) to 1% (w/w), we found that cubic crystals formed when grown from solution. No other faces were detected on the crystals apart from {100}. The surfaces obtained were rough and showed numerous macrosteps when grown from large scale solutions (see Figure 2). Images obtained from salt crystals grown from clean solution showed no presence of macrosteps.

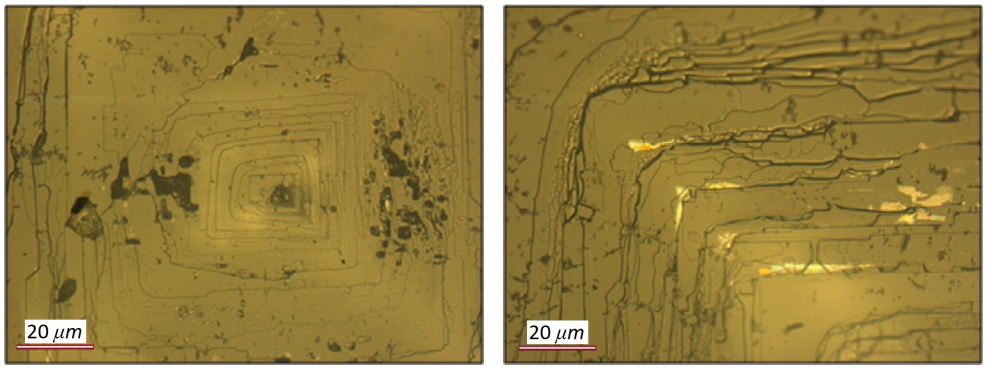

(a) (b)

Figure 3.2: Differential interference contrast microscopy images (reflection mode) of salt crystals grown from solution containing 1% (w/w) PVA. The steps originate from the edges of the crystal and propagate inwards.

The next logical step was to look at the crystals at a far higher magnification, in order to see if the crystallisation of the sodium chloride had been affected at the nanometre scale. AFM was used for this and the nanometre scale resolution images are displayed in Figure 3. On a 2.5 μm scale, agglomerations on the surface were present, which most likely consist of PVA chains. Assuming an average of 10 agglomerations per 2.5 μm^2 area, it follows that there are approximately 10^6 agglomerations per square mm. From a typical volume of 10^6 nm^3, derived from the average chain length of the PVA molecules, each agglomeration is estimated to contain approximately 10^4 chains of PVA. However, the surface of the sodium chloride between the agglomerations

remained extremely flat, only showing unit cell height steps of approximately 0.5 nm. We expected to observe a rougher surface from the spreading of polymers, however it is now evident that this is not the case. The unit cell step heights correspond well with the unit cell dimensions of sodium chloride, of which a=b=c=0.564 nm. These flat areas are representative of the regions between the macrosteps.

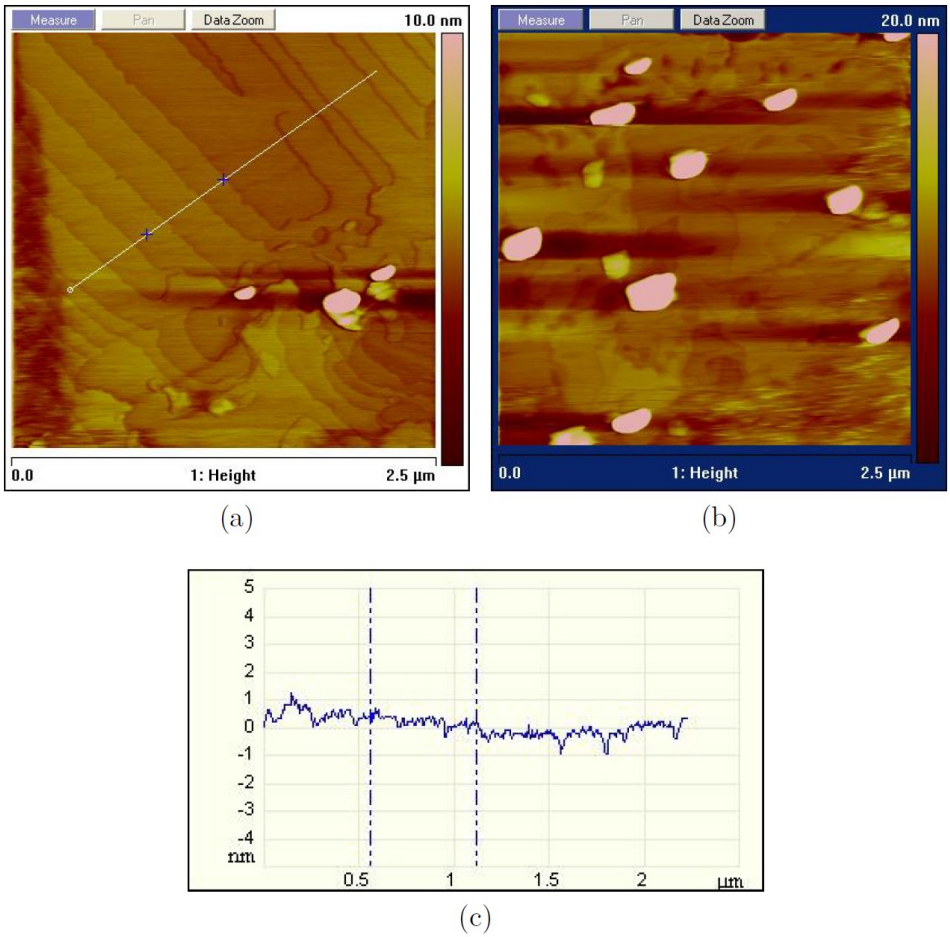

Figure 3.3: AFM images of cleaved salt crystals treated with 1.2 x 10^{-4}% (w/w) solution of PVA. Image (c) gives the step heights of the cross-section taken of image (a), which are ∼0.5-1 nm in height.

As the purpose of this investigation was to compare long chain polymer molecules with their respective monomers; the habit modification ability of those related to PVA

(i.e. ethanol and methanol) was then investigated. The crystals obtained from both large and small scale experiments all showed a cubic habit and had smooth surfaces (see fig. 4(a)) with height differences of approximately 5 nm (see Fig. 4b). No macrosteps were observed on the surfaces of these crystals.

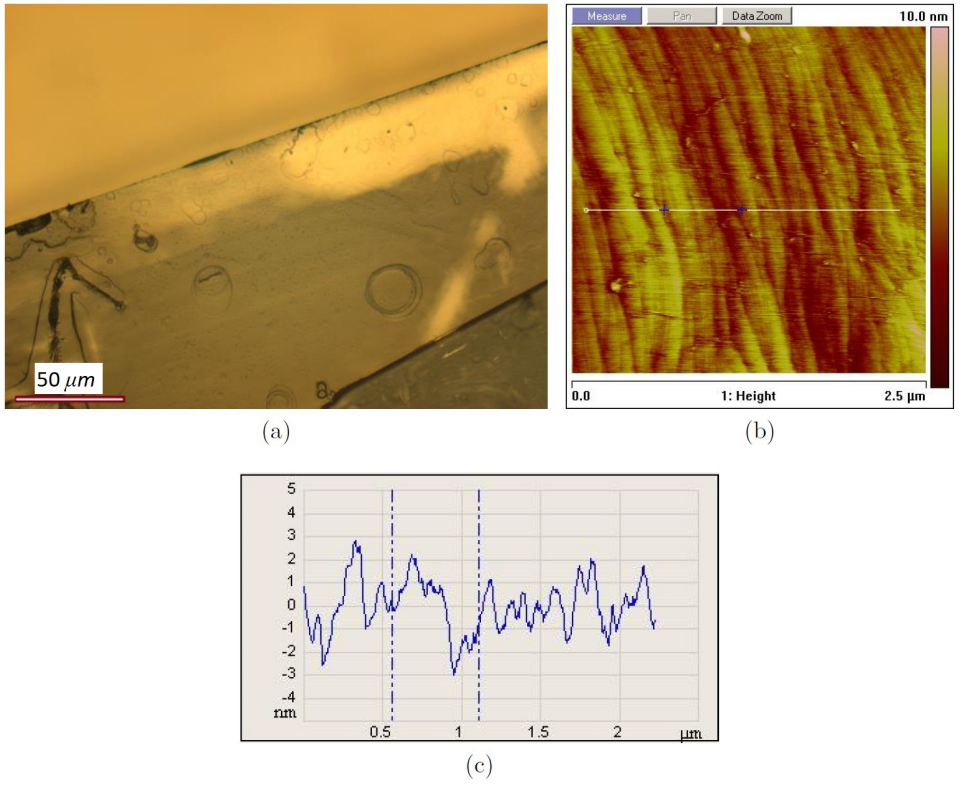

(a) (b)

(c)

Figure 3.4: (a) DICM micrograph of the surface of a crystal grown from large scale solution containing 1% (w/w) methanol. (b) AFM image of a cleaved crystal treated with 1% (w/w) solution of methanol. (c) Cross-section height graph showing height differences indicated over image (b).

Another of our propositions was that specific functional groups can give particular effects on the crystallisation of sodium chloride. As PVA contains an alcohol group, other polymers with oxygen containing functional groups (PEG, PPG, PVP, PAAc) were tested with large and small scale experiments. These were all in concentrations of 1% w/w. All the polymers produced only cubic crystals with no other faces present. Under optical microscopy, macrosteps were observed to be present on the surfaces of

these crystals.

The ideal outcome of this investigation would be to find a material that will affect the crystallisation of sodium chloride in so that it will have an anticaking effect. Therefore, the force required to break the caked sodium chloride was measured when treated with different concentrations of polyvinyl alcohol using PFA testing. For comparison, also the standard anticaking agent FCN was measured using the same conditions. Results are shown in Figure 5.

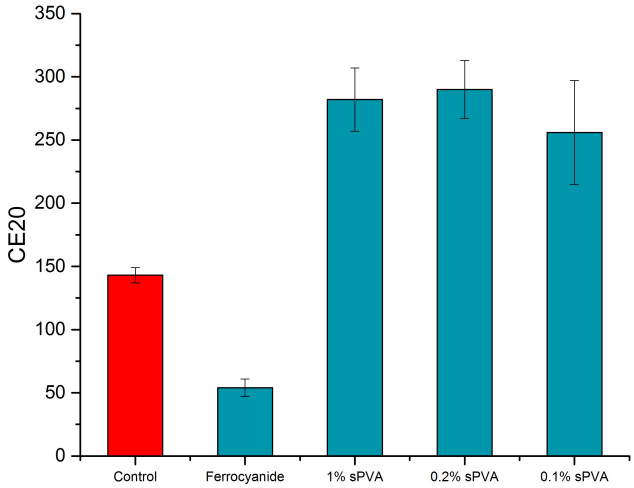

Figure 3.5: Caking energy values (CE20) for Sanal P® NaCl treated with PVA. FCN concentration fixed at 2.5x10^{-4}%.

From these experiments, it is evident that PVA appears to enhance the caking effect of the sodium chloride by a factor of two approximately. Therefore, the polyvinyl alcohol seems to act as a "pro-caking" agent on the sodium chloride, rather than having the desired anticaking effect as reported in [66] .

3.3.2 Polyacrylamide (PAA)

Next we used PAA, because this polymer contains an amide group, which is a known habit modifier for sodium chloride in monomer form. Also this compound is related to PVA in that both functional groups contain oxygen. On addition of this polymer to a sodium chloride solution, crystals with {111} faces were grown in both small and large

scale experiments. Solutions of 0.5% (w/w) PAA and above produced cubo-octahedral shaped crystals with larger {111} faces as opposed to {100} faces. Solutions of lower concentrations down to 0.05% (w/w) produced small amounts of {111} face development resulting in cubic crystals with tiny {111} facets. Figs. 6(a)-(d) show these face developments in small scale experiments.

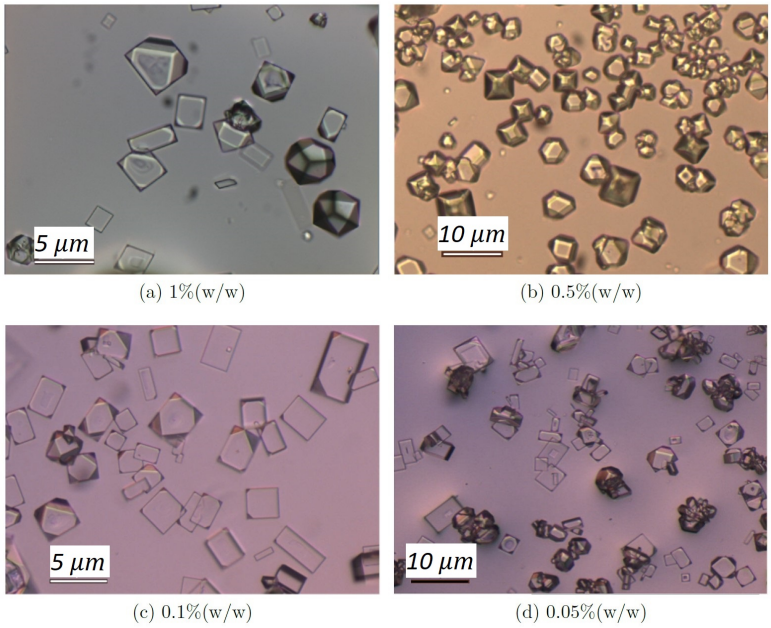

(a) 1%(w/w) (b) 0.5%(w/w)

(c) 0.1%(w/w) (d) 0.05%(w/w)

Figure 3.6: Small scale in-situ experiments with PAA additive

The {100} and {111} surfaces of crystals grown from large scale solution experiments in the presence of PAA were studied using SEM (Figs. 7 (a)(b)(e)(f)) and AFM (Figs. 7 (c)(g)). It was observed by SEM that the {100} surface is much flatter than the {111} surface. The {100} surface shows evidence of the shut off effect which occurs when a crystal is removed from solution and a thin-film of supersaturated solution remains on the surface and evaporates quickly giving rise to extra structures. [69] However, there is no ordered nucleation pattern. On the other hand, the {111} surface is more rough and displays trigonally shaped islands, which were not evident on the {100} surface. Using a stereographic projection for the {111} face of NaCl, it was found that the short edges of the trigonal islands on this face point towards the adjacent (100) faces of the crystal, i.e. the $<11\bar{2}>$ directions on (111). In order to obtain

a more detailed view of these surfaces, AFM was employed. On comparison of Fig. 7(c) with a surface treated with pure water (Fig. 7(d)), it can be deduced that the PAA polymer does not have a large effect on the {100} surface of NaCl on the smaller AFM nanometre scale. In both figures, steps are visible with small height difference. Fig. 7(g) shows, on the smaller AFM scale, that the {111} face of NaCl treated with PAA is much more rough than the corresponding {100} face. There is no evidence of step formation on the {111} surface.

As per the previous experiments, it is important to compare the PAA results to those of its corresponding monomer, formamide. Figure 8(a) shows crystals grown from a small scale experiment using brine containing 20% (w/w) formamide. The crystals show clearly developed {111} faces which is in accordance with the findings of Radenovic et al.[64] The surface of these NaCl crystals were further examined at a higher resolution to determine the crystallisation pattern on the surface. Figure 8(b) shows a SEM image of the {111} surface of a crystal grown from a large scale solution experiment in the presence of 25% (w/w) formamide. It was observed that there is no ordered pattern as in the case of the PAA treated salt.

In line with our idea that specific functional groups can give particular effects on the crystallisation of sodium chloride, additional polymers with one element of the amide group were used in experiments. The polymers PAAA and PAAc were used and only cubic crystals were formed with only {100} faces present. It was also observed that the large scale grown crystals, when treated with any polymer, were noticeably larger and less in number than in the case of the clean crystals.

PFA was then carried out on sodium chloride cakes treated with PAA in order to determine its efficacy as an anticaking agent. The results are shown in Figure 9.

No anticaking effect was observed from these results. The 0.1% and 0.5% PAA treated NaCl proved to have similar values to the control, whereas the higher concentrations of PAA proved to be procaking agents. Not included in this graph is the result for sodium chloride treated with 5% PAA, which proved to overload the machine and no reading could be taken. This indicates very heavy caking. It should be realised that in these experiments the crystals are primarily bonded by {100} faces rather than {111} faces. Using SEM imagery, it was confirmed that in these caking experiments, the crystals remain in cubic morphology with roughened surfaces.

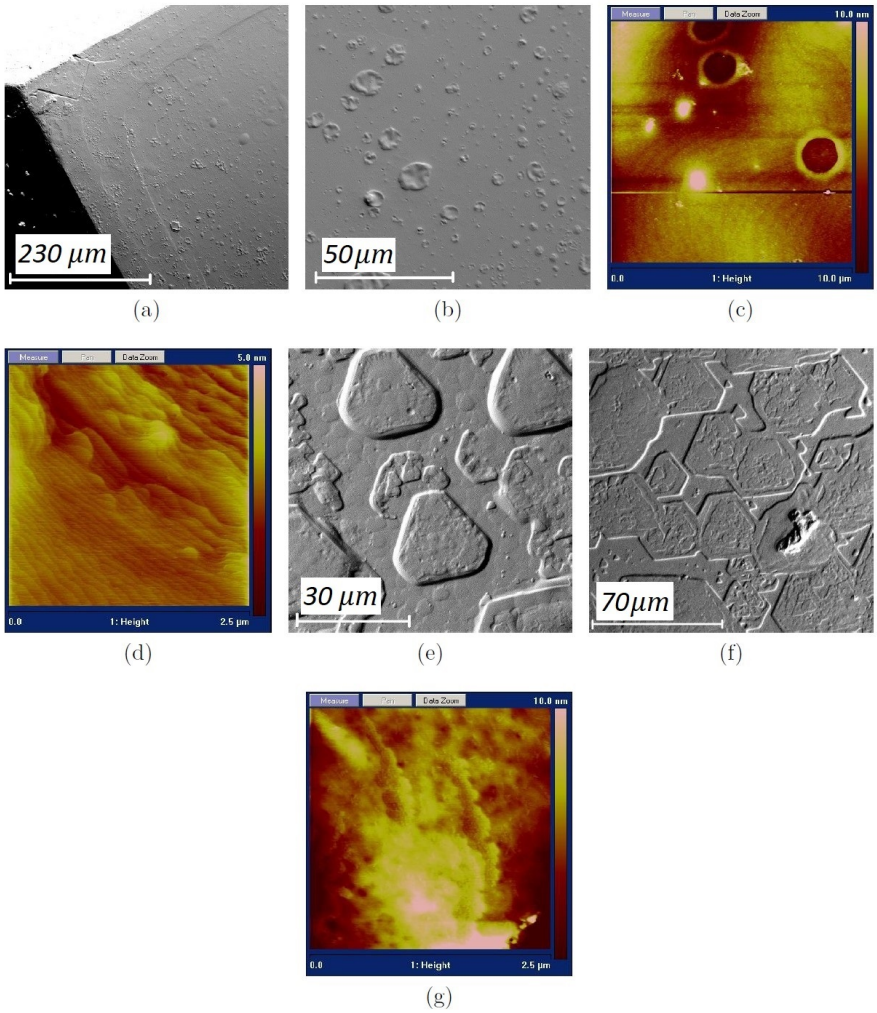

Figure 3.7: (a)(b) SEM images of {100} surface of NaCl crystals grown in the presence of 1% (w/w) PAA, (c) AFM image of {100} surface of NaCl crystal treated with 1% (w/w) PAA, (d) AFM image of {100} surface of cleaved NaCl crystal treated with water, (e)(f) SEM images of {111} surface of NaCl crystal grown in presence of 1% (w/w) PAA, (g) AFM image of {111} surface of NaCl crystal treated with 1% (w/w) PAA.

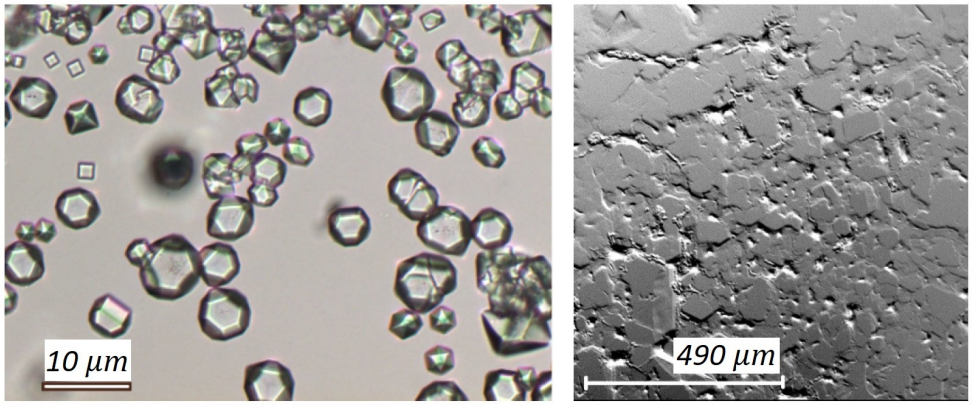

(a) (b)

Figure 3.8: (a) Small scale growth of NaCl crystals from solution containing 20% (w/w) formamide, (b) SEM image showing {111} surface of NaCl crystal grown in a large scale experiment in the presence of 20% (w/w) formamide.

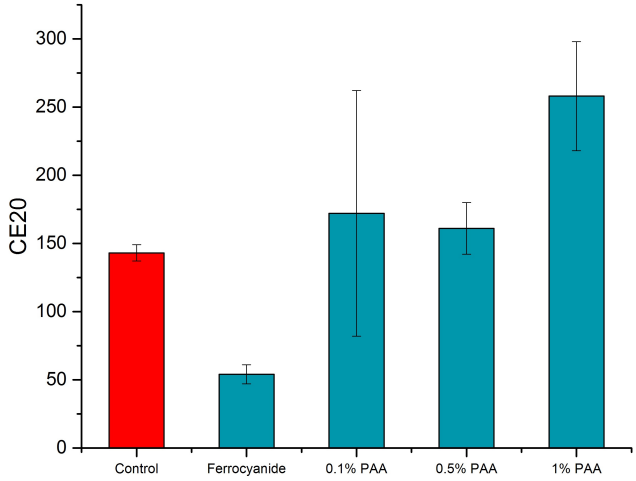

Figure 3.9: Caking energy values (CE20) for Sanal P® NaCl treated with PAA. FCN concentration is fixed at $2.5\text{x}10^{-4}$%.

3.3.3 Amino Acids and Proteins

As glycine has been previously reported to induce {110} face formation on sodium chloride crystals, it is interesting to investigate the abilities of other amino acids as modifiers for sodium chloride. They have similar end groups (namely oxygen and nitrogen) as the amide compounds, so it is possible a similar effect will be observed. Amino acids can be classed as monomers of a protein polymer and so a protein was also tested as a potential habit modifier for sodium chloride. As all amino acids have different solubilities in water, the first small scale experiments were performed using saturated NaCl solutions in MilliQ water with 1% (w/w) amino acid added. The selection of amino acids was chosen based on sufficient solubility in water: Asparagine, Aspartic Acid, Glutamic Acid, Histidine, Proline, Serine, Threonine, Arginine. All experiments showed development of cubic crystals with {100} faces only. Experiments with higher concentrated solutions of amino acids were then performed as literature states that effects are only observed with large amounts of additive. These small and large scale experiments were performed using 20% (w/w) solutions of DL-Proline, β-Alanine and monosodium glutamate. Again only cubic crystals were formed. In contrast to the work in [65], our case of β-Alanine showed no octahedral truncations on the cubic crystals.

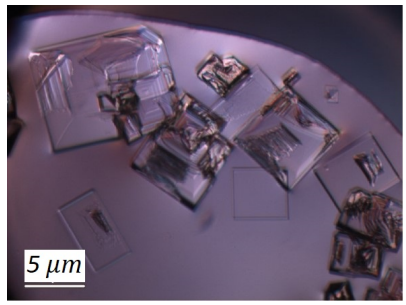

Figure 3.10: Small scale experiment with NaCl solution containing 20% (w/w) β-Alanine.

In order to compare the amino acid "monomer" results with their related polymers, small scale experiments were performed using lysozyme as the additive. The initial composition of the solutions consisted of 0.2% (w/w) lysozyme in undersaturated sodium chloride solutions. The solutions were required to be undersaturated, as when a saturated solution was used the lysozyme was found to precipitate immediately. Upon solution evaporation, these experiments yielded only cubic crystals with {100}

faces. No large scale experiments were performed because here a saturated sodium chloride solution was required. [70]

3.4 Discussion

3.4.1 Polyvinyl alcohol (PVA)

The sodium chloride crystals grown in the presence of PVA showed only {100} faces with the development of macrosteps. Macrosteps form by coalescence of laterally propagating surface steps originating from the periphery of the facets. [71] These macrosteps are likely caused by the presence of the polymer on the surface, as they are not present on the untreated sodium chloride crystals. Macrostep formation by the impurity adsorption is a well-known phenomenon. When the respective monomers methanol and ethanol were used as additives, the crystals all had extremely smooth {100} surfaces with no macrosteps present. This once more concludes that the polymer is the cause of the development of the macrosteps. It also concludes that an isolated alcohol functional group does not have an effect on the surface or habit modification of sodium chloride.
The agglomerations observed on the AFM images of these crystals are thought to consist of large entanglements of the PVA polymers. We first thought that the presence of these agglomerations could disrupt the caking between individual salt crystals. However, this idea was disproved when PFA was performed, as this determined that the PVA acts as a "pro-caking agent". The force required to break through the 0.1% (w/w) PVA treated salt was approximately twice as large as for the untreated salt. This was even larger for the salt samples treated with more concentrated PVA solutions. From these results it is clear that the polymer agglomerations act as an adhesive between the salt crystals, much like the commonly available polymer glues on the market today. The enhanced caking is likely caused by the fact that the chain length of the polyvinyl alcohol is so large that it is not lying on the surface but instead interacting with protruding chains from other salt grains. Therefore we can conclude that PVA is not an effective anticaking agent for sodium chloride and we have disproved the results in [66].

3.4.2 Polyacrylamide (PAA)

In the case of the NaCl crystals grown in the presence of PAA, it was observed that crystals with large {111} faces developed in all experiments at concentrations of 0.5% (w/w) and above. Development of {111} faces was already detected at concentrations

as low as 0.05% (w/w). It is clear that the amide functional group of this polymer plays a key role in the development of {111} faces on sodium chloride crystals. This finding is reinforced by previous research results which indicate that both urea and formamide produce octahedral sodium chloride crystals, albeit at much higher concentrations than the polymer. Both of these compounds contain amide functional groups in their structures.
In order to further support this conclusion, the experiments carried out on polymers with functional groups similar to amides but not exactly identical, yielded only cubic crystals without {111} faces. This leads to the conclusion that it must be the amide functional group that leads to {111} face formation on sodium chloride crystals. It can also be concluded that the polymer amide gives a one to two orders of magnitude stronger effect than the relative monomers. This is due to the fact that polymers are not singly bonded to the surface of the sodium chloride like the monomers, but rather have multiple bond sites, strengthening the interaction.
Comparison of the SEM imagery of the {111} faces of the crystals grown in the presence of formamide and polyacrylamide once more show that the {111} faces of the PAA treated crystals are more highly stabilised as compared to the formamide treated crystals. This conclusion is derived from the fact that clear trigonal shaped growths were observed on the PAA treated surface, but there was no distinct pattern evident on the formamide treated surface. The presence of the trigonally shaped growths on the PAA treated surface and the undefined features on the formamide treated surface are likely due to the shut off effect. It is also evident that, at the nanoscale, the {111} surface is far rougher than the {100} surface of the PAA treated salt. This could be due to a stronger interaction between the polymer and the {111} surface and so there is likely to be large amounts of polymer on this surface. This may mean that the PAA partially blocks the growth of the NaCl on the {111} face, therefore allowing the {100} faces to grow relatively faster, leading to a crystal with {111} facets. These findings are in contrast to the findings for PVA, as no agglomerations were observed on the surface of the PAA NaCl crystals. Consequently, we conclude that PVA has a poor wetting effect on the surface and therefore does not spread, which is in contrast to the PAA which has a better wetting effect.

3.4.3 Nucleation Inhibition

It was observed that the crystals grown from all polymer containing solutions were significantly larger and less in number than those grown from clean solution or from solutions containing only monomers. This indicates that the polymers act as nucleation inhibitors for sodium chloride.

3.4.4 Amino Acids and Proteins

In the case of the amino acid experiments, it was confirmed that adding 20% (w/w) glycine to the sodium chloride solution caused {110} faces to propagate on the resulting crystals. However, when other amino acids were used at concentrations of 1% (w/w) and 20% (w/w), only cubic crystals formed. The protein lysozyme, which was used in small scale experiments as a possible habit modifier, proved to have no effect as it has very low solubility in the NaCl solution. For this reason, no other protein experiments were attempted. The overall conclusion for this part of the investigation is that, apart from glycine, we found no evidence that amino acids or proteins produce any habit modification for sodium chloride.

3.5 Conclusions

In this investigation we studied the influence of different polymeric additives on the habit modification and caking of NaCl crystals grown from aqueous solution. We have shown that a polymer additive containing an amide functional group induces {111} face formation on NaCl crystals with a one to two orders of magnitude stronger effect than the corresponding monomer. This is a consequence of the enhanced bonding of the polymer compared with the monomer. However, if the polymer does not contain a suitable active functional group for habit modification, the effect is nil and the crystals remain cubic. It was further found that all polymeric additives led to macrostep formation and act as nucleation inhibitors. This leads to a low density of larger sized crystals. Two polymeric additives, namely polyvinyl alcohol and polyacrylamide were tested for their anticaking activity. The first polymer showed enhanced caking, whereas the second one showed no significant effect. We are currently investigating the use of oligomeric additives as potential growth or habit modifiers for sodium chloride.

Chapter 4

Additive induced formation of ultrathin sodium chloride needle crystals

Eleanor R. Townsend, Willem J.P. van Enckevort, Paul Tinnemans, Melian A. R. Blijlevens, Jan A.M. Meijer, Elias Vlieg

Crystal Growth and Design, accepted Dec. 2017

Abstract

A multitude of ultrathin crystal needles are formed during the evaporation of saturated aqueous NaCl solution droplets in the presence of amide containing additives. The needles are as small as 300 nm wide and 100-1000 μm in length. Heating experiments, X-ray diffraction and energy dispersive X-ray spectroscopy showed that the needles are cubic sodium chloride crystals with the needle length direction pointing towards [100]. This morphology, apparently violating the $4\bar{3}$m point group symmetry, has been explained using a model, based on tip formation by initial morphological instability followed by time dependent adsorption of additive molecules blocking the growth of the needle side faces. The latter also suppresses side branch formation, which normally occurs for dendrite growth.

4.1 Introduction

Much work has been done into the influence of additives on the habit of sodium chloride crystals. The earliest known example was published by Rome de l'Isle in 1783 [8], when he found that the addition of urea to a brine solution causes the development of {111} facets on the resultant crystals. Since then, there have been many additives found which have an effect on either the morphology or the growth of salt. For example, the addition of glycine to a brine solution has been shown to elicit <110> facets on the crystals [65] and formamide and several chromium and lead compounds have been shown to elicit {111} facets. [13] [14] [72] The stability of the polar{111} faces in the presence of formamide and Cd^{2+} has been explained by Radenovic et al. [64] [73], on the basis of surface X-ray diffraction measurements. The most widely utilised additive for NaCl currently is ferrocyanide, which causes a morphology change from cubic to dendritic, and has a positive effect on preventing caking of the material and is therefore very industrially relevant.

It has been mentioned as far back as in 1961 [36] that another additive, nitrilotriacetamide (NTAA), has an anticaking effect on sodium chloride at concentrations as low as $1x10^{-4}$ % (w/w). Its anticaking effectivity was also mentioned in the 1966 work by L. Phoenix [74] and the 1975 work by Sarig et al. [62] The latter investigation described in detail the observed habit modification of NaCl crystals in the presence of 50 ppm NTAA, presenting skeleton cubic morphology. A brief model was also presented, showing the expected binding points of the NTAA molecule on the NaCl {100} surface. The follow-up article to this investigation [33], showed that at higher concentrations of NTAA (100-500 ppm), the NaCl habit was further modified to display dendritic growth. Current uses of NTAA and its sister compounds, methylglycine diacetamide (MGDA) and glutamic acid diacetamide (GLDA) are as chelating agents, Dissolvine® in their sodium salt forms. NTAA has also been reported to reduce sodium chloride deposition in the drilling of oil wells. [75] [76] However, there is no current usage of NTAA or other branched amides in the salt anticaking industry.

The formation of sodium chloride needles was first mentioned in a 1932 note by Tauber and Kleiner [77] which stated that sodium chloride needles are formed when suspending an undersaturated solution in a colloidion bag (a membrane used to filter or concentrate substances using pressure) and allowing the solution to slowly evaporate. In 1933, Hinegartner [78] also observed sodium chloride needles but this time growing on a silica gel substrate. Sears [79] also observed the formation of needle crystallites (thus termed whiskers) from bulk crystals including NaCl, with a more in depth investigation being performed by Shichiri and collaborators. [80] [81] [82] Specifically, needle formation of NaCl in the presence of NTAA was mentioned by van Damme-van Weele in her 1965

thesis.[17] Also, using the technique of vapour growth, Noorduin observed an unusual formation of sodium chloride with extreme elongation in the {100} direction.[83]
In our previous work, we have described the technique of creeping, in which a droplet of solution containing brine and additive is allowed to evaporate and the resulting pattern is examined to determine the effectivity of the additive in the solution. In general, the greater the amount of creeping from the edges of the droplet, the more effective the anticaking agent is for sodium chloride. Using creeping, we have shown that the addition of large amounts (1% (w/w)) of nitrilotriacetamide and methylglycine diacetamide to a saturated brine solution, causes the formation of needle shaped sodium chloride crystals when allowed to evaporate on a glass substrate.[42] [44] A very compact evaporation pattern is observed, with many needles layered on top of each other. However, it is not known what is the mechanism behind the formation of these needle crystals. Using amide compounds of similar structure (Fig. 1), we aim to characterise this needle growth using an experimental approach, complemented with a theoretical model to describe our observations.

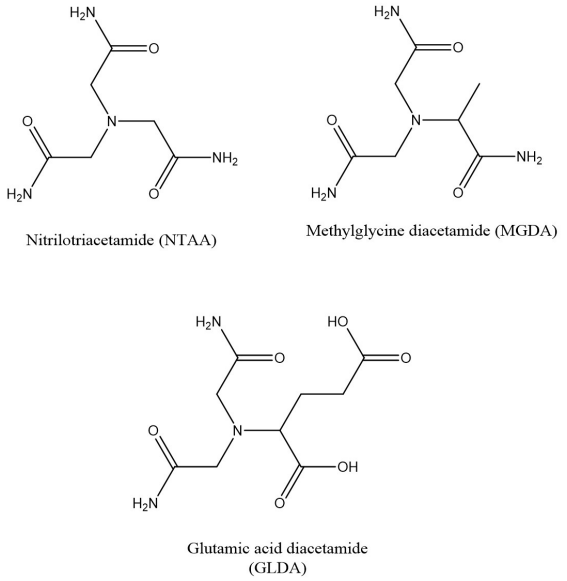

Figure 4.1: Structures of the amide compounds used in this investigation.

4.2 Methods

Nitrilotriacetamide has been widely reported in the literature in relation to sodium chloride, as described in the introduction. These observations were confirmed by our more recent work [42], which showed that as well as being an effective anticaking agent for NaCl, it also causes a habit modification of the crystals at high concentrations. The same effect has been observed for the sister molecule, methylglycine diacetamide. [44]

The third compound used in this investigation is the related compound, glutamic acid diacetamide. This is unreported in the literature in free amide form, but the sodium salt is used currently as a chelating agent.

The concentrations of the additives in solution used for each experiment were set at specific weight percentages with respect to the solution to ensure fair testing, with each additive containing brine solution being in the pH range of 5-6. The exception to this is the GLDA containing brine solution, which has a higher pH of 3.5, due to the presence of the two acid groups in the molecule. The concentrations used in the experiments were in a range between 0.1% (w/w) and 4% (w/w).

4.2.1 Creeping Tests

A solution was made using saturated brine and a certain percentage of the chosen additive at ambient temperature (20-25°C). The solution was filtered using a syringe fitted to a 0.45μm Pall GHP Acrodisc filter, and then dropped onto a glass microscope slide using a micro-pipette. These slides were cleaned beforehand using EtOH and dried using a dust-free tissue to minimise external nucleation effects. The amount of solution in each droplet varied from 5-10μL. The droplets were allowed to evaporate in a temperature and humidity controlled climate chamber at 20°C and 50% relative humidity. The resulting crystals were imaged using a Leica DMRX optical microscope, a FEI Phenom Scanning Electron microscope and a JEOL 6330 Field Emission Scanning Electron microscope. The optical microscope was also used to follow the creeping process in situ at ambient conditions ($\sim$20°C and $\sim$50% RH).

4.2.2 Scanning Electron Microscopy (SEM)

In order to view our samples at a sufficiently high magnification with a high depth of field, we used scanning electron microscopy (SEM). The creeping patterns were dried in a climate controlled chamber at 20°C and 50% relative humidity and then sputtered with Au-Pd using a Cressington 208HR sputter coater. The sample was left with a coating in the range of 0.5-3 nm in thickness. The samples were imaged in back

scattering mode at 5kV for the FEI SEM and in secondary electron mode at 12kV for the JEOL 6330.

4.2.3 Energy Dispersive X-ray Spectroscopy (EDX)

Mapping by EDX was used to determine the two-dimensional elemental composition of the sample surface. This was performed using a Zeiss Sigma 300 scanning electron microscope, coupled with a Bruker Energy-Dispersive X-ray Spectrometer.

4.2.4 Solution crystal growth and Single-crystal X-Ray Diffraction

The salt used in this investigation is Sanal P®, an AkzoNobel product of 99.99% purity and the additives used were obtained at a commercial grade from AkzoNobel, containing possible side products. Therefore, each compound was recrystallised out of solution by slow evaporation at a constant temperature and humidity (20°C and 50% R.H.). The resulting crystals were then analysed using single crystal X-ray diffraction to determine their compositions and structures. The crystal structures of MGDA and GLDA were previously unknown and are submitted to the Crystal Structural Database under codes *CCDC 1533349* and *CCDC 1533348* respectively. The NaCl needles obtained by the creeping experiments were examined by powder and single crystal X-ray diffraction. In powder X-ray diffraction experiments Cu$K\alpha$ radiation was used and in single crystal measurements, Mo radiation was used.

4.3 Experimental Results and Discussion

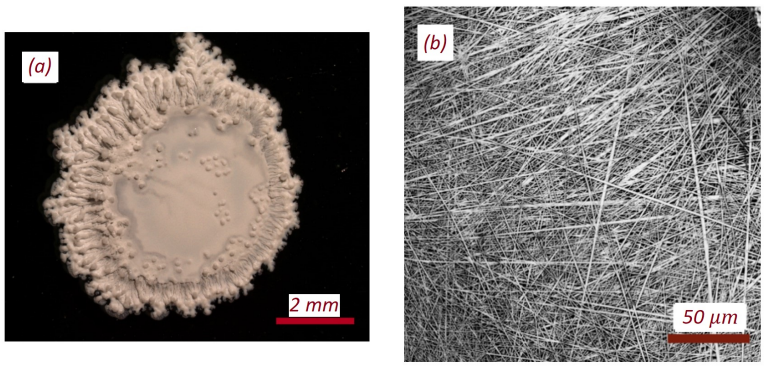

Figure 4.2: (a) An optical overview image of a dried droplet of saturated brine with 1% (w/w) NTAA, (b) the crystal pattern from the centre of the droplet observed at higher magnification using SEM.

At low magnification, on the addition of 1% (w/w) NTAA/MGDA/GLDA to a saturated brine solution, the resulting evaporation pattern consists of a dense formation of crystallites with no evidence of significant cubic crystal growth (see Figure 2a). From Figure 2b, it is evident that this formation is entirely filled with ultrathin needle-like crystallites with no definitive orientation. As described in our previous work, these needles form as a result of a lower surface free energy and an increased supersaturation, both of which promote extremely fast and numerous 3D nucleation. In-situ recording of the crystal growth process using optical microscopy at high magnification showed needle growth rates of approximately 10 μm/sec.

To estimate the supersaturation at which the crystals first begin to nucleate from a saturated brine droplet with 1% (w/w) NTAA as additive, an evaporating droplet on a glass substrate was weighted in-situ using a precision balance. From the change in weight of the droplet when the first crystallites appeared as imaged using optical microscopy, we arrived at an approximate average figure of $\Delta\mu/kT \approx 0.16$. This surpasses the value measured for pure brine[42], $\Delta\mu/kT \approx 0.06$ indicates a large supersaturation dead zone before nucleation occurs.

4.3.1 Composition of needles

Due to the relatively large amounts of additive used in these experiments, it was important to check the chemical composition of the needles, to determine if they

consist of sodium chloride, or the added amide compound. The melting point of NaCl is high as it is an ionic compound, with a value of 801°C. In comparison, the measured melting points for the additive compounds are much lower, being in the range of 160-200°C. These were determined using DSC measurements and are displayed in Table 1. The error presented is from the technical specifications of the DSC instrument (Mettler Toledo DSC 822e).

Compound name	**Melting Point** ($\pm 0.2°C$)
NTAA	$194.4°C$
MGDA	$176.1°C$
GLDA	$167.4°C$

Table 4.1: Additives used and their melting points

Using a temperature controlled cell, attached to an optical microscope, the sample was heated from 20°C to 400°C at a rate of 20°C/min. The sample was examined in-situ by this microscopy during heating and *a-posteriori* using SEM for evidence of decomposition of the crystallite microstructures. There was no evidence that the needle crystallites decomposed, apart from a slight black coating over the sample. This is a strong indication that the needles are indeed composed of NaCl and not the amide additive. It is likely that the discolouration on the top of the sample is due to the decomposition of the amide compounds which coat the needles. A post experiment SEM image is shown in Figure 3.

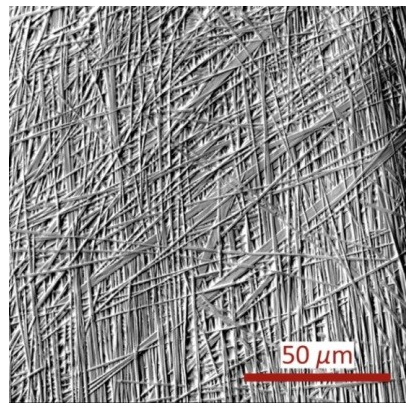

Figure 4.3: SEM image of needle pattern from a saturated solution of brine with 1% (w/w) NTAA additive, after heating to 400°C.

It was not possible to take a pre-experiment SEM image of this sample, due to the necessity of Au sputtering to make the sample conductive, but the crystallites can be favourably compared with other samples and we conclude that there was little change in the overall needle structure, which shows a pattern very similar to that without heat treatment (Figure 2b). In order to confirm our findings, Powder X-ray Diffraction (PXRD) measurements were taken of the samples (NaCl with 1% (w/w) amide additive) and compared with theoretical and measured patterns of pure NaCl and pure amide. These are shown in Figure 4. The powder pattern of NTAA was taken from the Crystal Structural Database (reference code: *VUSMOL*) and those of MGDA and GLDA were taken from the theoretical powder patterns calculated from the single crystal measurements described earlier.

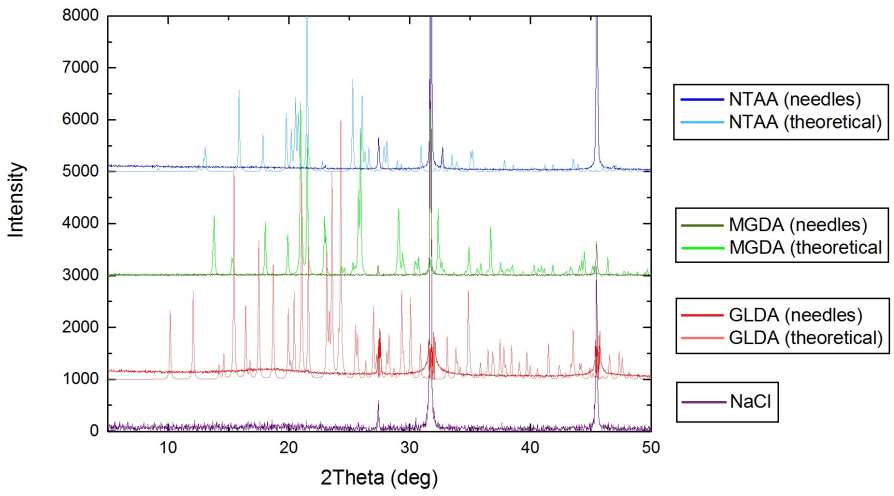

Figure 4.4: PXRD patterns comparing pure NaCl, pure amide and needle crystallites for NTAA, MGDA and GLDA. NaCl peaks are observed at 27°, 32° and 41°.

It is evident from these results that the diffraction peaks observed for the needles and the pure NaCl match whereas those for the pure amides do not. There is one extra peak noticeable in the PXRD for NTAA additive at 32°, and it is not known exactly what this corresponds to, but it is possible that it is a small amide peak. To obtain a final confirmation that the needles indeed consist of NaCl, an EDX measurement was performed showing that the crystals indeed consist of Na and Cl, see Figure 5. The measurement also showed the presence of Au as the sample had to be conductively

sputtered. As is also evident from the graph, there is very little nitrogen present and there is also only a very low level of carbon, which is present at 0.277 keV, concluding that the needles do not consist of amide. To obtain information on the crystallographic orientation of the needles, we selected a somewhat thicker needle from the NTAA sample and applied single crystal X-ray diffraction to it. This showed that the crystallographic directions of the top and side faces of the needle crystals are the {100} directions. This is illustrated in Figure 5.

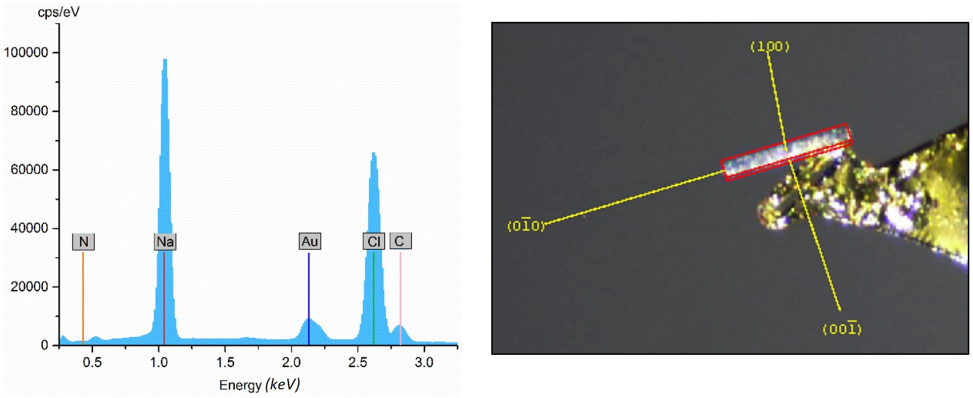

Figure 4.5: Left: EDX graph showing the expected and measured peaks for Na, Cl, N and Au. Right: Microscope image of single needle crystal with crystallographic directions indicated, as determined through single crystal x-ray diffraction. The dimensions of the crystal are 0.014 x 0.032 x 0.326 mm^3.

4.3.2 Properties of needles

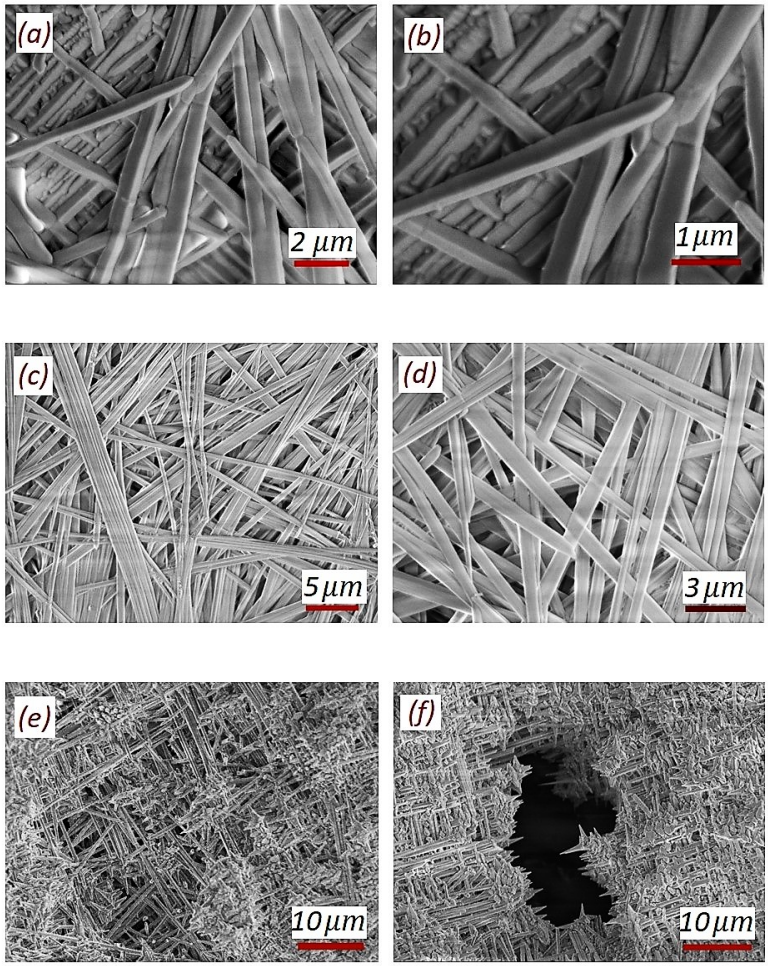

Figure 4.6: Detailed SEM views of needle shaped crystals obtained from a saturated brine solution containing (a)-(b) 1% (w/w) NTAA, (c)-(d) 1% (w/w) MGDA, (e)-(f) 1% (w/w) GLDA.

To obtain more detailed information on needle size and shape, high magnification observations using field emission SEM are performed. Some results are displayed in Figure 6. The needles show no preferred orientation and form a fibre-like network across the substrate, filling all available space. The needles are extremely thin, with

a width varying from 0.3-2 μm and a length ranging from $10^2 - 10^3 \mu m$. Except for the case of GLDA (Figure 6f), no evidence of side branching was found. There is also no evidence of any cubic crystal growth across the growth pattern. This is in contrast to the growth experiments in absence of additive, which only produce well-facetted cubes. Close inspection of the SEM images show that the needles have a rounded, non-facetted tip. Some needles have a ridge lengthways down the centre. The side facets of the needles have a tendency towards cubic morphology, but as growth in one direction is extremely fast, the final form is an extremely elongated cube. This confirms that the ultrathin needle axis direction is {100} as was also observed for the thicker needle in Figure 5.

4.3.3 Dependence of additive concentration on needle formation

A series of creeping experiments were carried out at concentrations lower and higher than that of 1% (w/w) to determine the necessary additive concentration to obtain needle crystallites.

It was observed at concentrations of 0.2% (w/w) and lower, that needle crystallites were no longer present in the creeping pattern, only a tendency toward cubic growth was found. SEM images of a series of creeping experiments with decreasing levels of additive are shown in Figure 7.

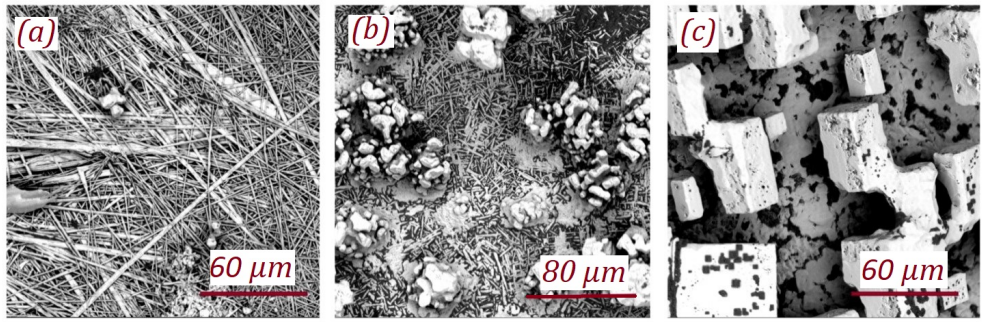

Figure 4.7: Detailed SEM views of needle shaped crystals obtained from a saturated brine solution containing (a) 0.75% (w/w) NTAA, (b) 0.5% (w/w) NTAA and (c) 0.25% (w/w) NTAA.

Similarly, at concentrations of 2% (w/w), the needle crystallites begin to disappear, making way for dendritic growth. At an additive concentration of 4% (w/w), there are no needle crystallites anymore. The NaCl crystals observed at these concentrations of additive have high levels of morphological instability with no clear {100} facets, as is shown in the SEM images of Figure 8. So, needles are only formed for additive concentrations ranging from 0.75 to ≈1.5% (w/w).

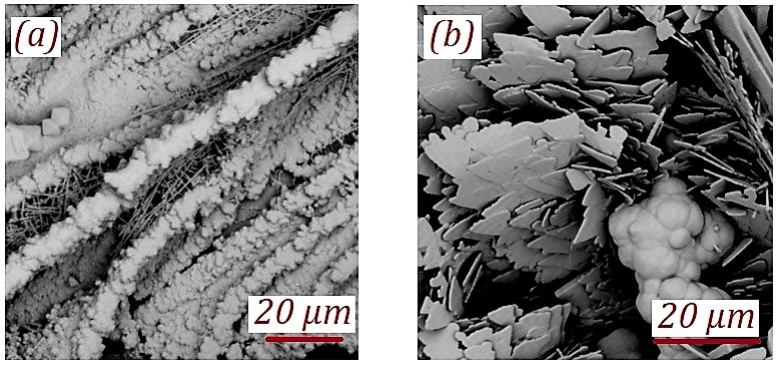

Figure 4.8: Detailed SEM views of NaCl crystals obtained from a saturated brine solution containing (a) 2% (w/w) NTAA, (b) 4% (w/w) NTAA.

4.4 Mechanism of needle formation

4.4.1 Principle

The formation of thin, elongated NaCl needles seems to violate the cubic $4\bar{3}$m point group symmetry of NaCl. The main question that arises is why does the (100) top face grow fast, while the symmetry equivalent $(010)/(0\bar{1}0)$ and $(001)/(00\bar{1})$ side faces of the cubic crystals do not grow at all. As we will argue below, we believe this is caused by tip formation induced by morphological instability followed by time dependent adsorption of the additives blocking the growth of the needle side faces. In our case the anisotropic growth of the needles is not explained by the presence of dislocations parallel to the needle axis and their absence directing towards the side faces, as the tips are not facetted, so spiral growth does not occur. Further, no re-entrant corner was observed at the needle tips, which excludes enhanced growth by the twin plane re-entrant edge (TPRE) mechanism.[84] [85] [86] Further, neither in-situ microscopic nor X-ray evidence was found for recrystallization from an unknown metastable form of NaCl to cubic *fcc* NaCl. Finally, morphological instability does not fully explain the development of the needles as follows from the fact that the needles often do not show a preferred direction of growth induced by a gradient in supersaturation, but are crisscrossed. Moreover, no branching was observed, which is typical for morphological instability. In our attempt to explain the formation of the needles, we were inspired by the experiments by Land et al.[87] and the theoretical model of Muira[88] for stepped surfaces and an earlier study by one of the authors for roughened faces.[57] Following Muira's model and the earlier work by Cabrera and Vermilyea[10] steps on a planar surfaces are retarded (I and II in Figure 10) by lowering the supersaturation and by increasing amounts of adsorbed additive until the advancement of steps is completely blocked. This happens above a critical additive surface coverage of:

$$\sigma_d \propto (\tfrac{1}{d^2}) \cong [\tfrac{(\Delta\mu/kT)h_{st}}{1.51\gamma\Omega}]^2. \qquad (1)$$

In which equation, d = average distance between adsorbed additives, $\Delta\mu/kT$ is supersaturation, h_{st} = step height, γ is step free energy and Ω the volume of one growth unit.[89] As now no further growth occurs, more impurities accumulate until the equilibrium concentration at zero growth rate, $\sigma_{eq,0} > \sigma d$ is attained (III in Figure 9). If the supersaturation is increased to such an extent that $\sigma d > \sigma_{eq,0}$, then growth restarts and growth steps pass the impurity fence "cleaning" the surface. On this surface freed from additives steps can propagate again, also for lower supersaturations (IV in Figure 9). A similar process occurs for roughened crystal faces as exemplified in [56]. On these thermally/kinetically roughened F-faces or S and K faces, growth is

no longer determined by step flow, but by a more or less random addition and removal of growth units.[90] In this case is determined by the surface free energy of the crystal - additive molecule boundary and supersaturation.[57] In both situations a hysteresis in the growth rate versus supersaturation curve can occur as shown in Figure 9.

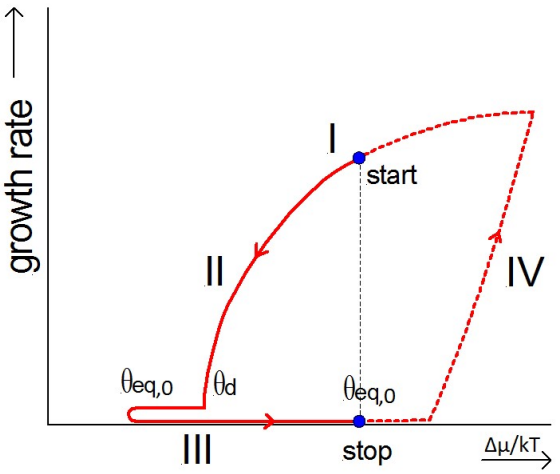

Figure 4.9: Hysteresis in the dependence of growth rate on supersaturation, induced by additive adsorption.

In our model we consider the 3D growth of needle crystals, the non-facetted tip surface of which is roughened by additive adsorption and fast growth. The needle side faces tend to be facetted, so here growth likely involves steps. Figure 10 shows the principle of the model, using the ideas presented in Figure 9. We consider three successive stages: **I**) Fast growth of the tip region as a consequence of morphological instability induced by high supersaturation and lowering of surface free energy, which is typical for additive induced creeping processes.[42] Here, growth is kinetically roughened and largely limited by mass transport. The higher growth rate leads to an enhanced incorporation of additives into the crystal lattice, which again results in a lower additive surface coverage as explained in the next section. In region **II**), the interfacial supersaturation decreases as a consequence of an expansion of the solute diffusion field, typical for mass transport limited growth of dendritic or needle crystals.[91] This leads to a decrease in growth rate; resulting in an increase in additive surface coverage which reinforces this decrease in growth rate. At a given moment we enter region **III**) where the critical surface coverage, σ_d, is reached and growth stops. Here more and more additives will be adsorbed at the surface until the equilibrium

concentration, $\sigma_{eq,0}$, is achieved. As a consequence of the halt of growth, no mass transport is needed and the interfacial supersaturation of growth units increases to the bulk value. However, in our case the bulk supersaturation is insufficient to break through the impurity fence, restarting growth. Growth remains blocked and stage IV in Figure 9 is never attained in our case. As growth in the region behind the tip is completely blocked, no side branching occurs and needles rather than dendrites are formed. For GLDA as an additive, an onset of dendritic growth can be perceived (Figure 6e+f).

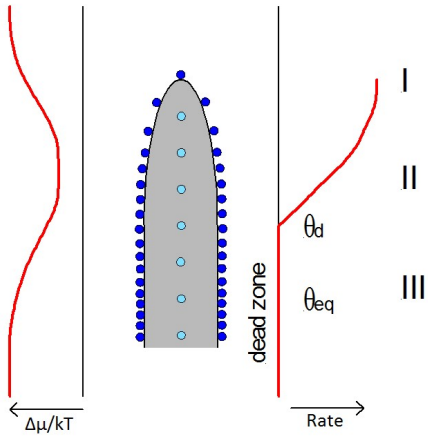

Figure 4.10: Mechanism of additive induced NaCl needle growth.

Inspired by the work of Land et al.[87], theoretical graphs of the growth rate with respect to the supersaturation are shown in Figure 11. These graphs help to understand the crystal growth phenomena that we observed for different additive concentrations in this investigation. As mentioned before and described in[87] [88] , additives cause a hysteresis in crystal growth. At low supersaturations, growth is blocked; at a specific supersaturation the "dead zone" of no-growth is overcome and crystal growth sets on. Increasing the supersaturation further and lowering it again leads to continued growth, also in the "dead zone" region, until it stops at a considerably lower supersaturation. The hysteresis interval with the "dual" growth rate shifts to higher supersaturation values for increased additive concentration, as displayed in Figure 11.

The impurity induced hysteresis in growth rate versus supersaturation explains the additives concentration dependence of needle formation. This is exemplified in Figure 11, which schematises the "twofold" growth rate versus supersaturation curves for different additive concentrations. The supersaturation interval used in the droplet

experiments is indicated in blue and pink, the latter for the region where needles are formed. For the lowest additive concentration (in our case 0.1% (w/w)), the growth of the needle side faces is not blocked and cubic crystals are formed. For medium additive concentrations (0.75-1.5% (w/w)) the needle tip grows, while the side faces are blocked. For the highest additive concentrations, exceeding 2% (w/w), also tip growth is blocked and featureless crystals rather than needles are formed. One should realise that supersaturation of the droplet experiments increases for increasing additive content to some extent, but this does not alter the general conclusions.

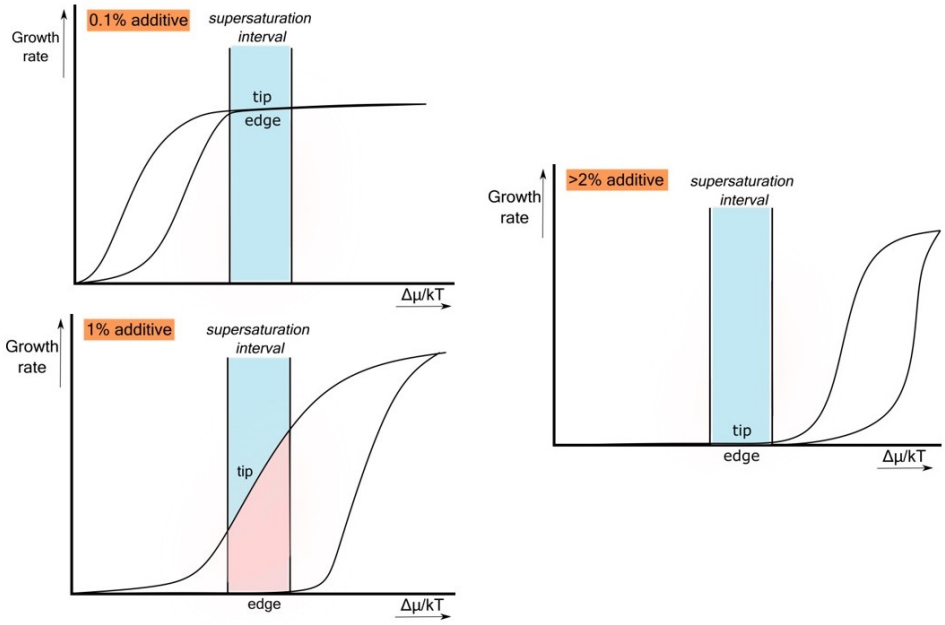

Figure 4.11: Growth rate curves describing the case of 0.1% (w/w), 1% (w/w) and >2% (w/w) additive. The supersaturation regime during the droplet evaporation is indicated in blue in the diagram, with the pink section indicating the presence of needle growth. In the cases of 0.1% (w/w) and >2% (w/w) additive, there is no needle growth, as the growth rates of the tip and edge are the same or almost zero at this specific supersaturation interval.

4.4.2 Additive surface coverage as a function of crystal growth rate in needle growth

As an approximation we consider a needle tip as a parabola $y(x) = ax^2$ advancing in the $-y$ direction at a constant rate ν_{tip}, as schematized in Figure 12. The ratio of needle growth perpendicular to its surface, dw, and the needle advancement in the $-y$ direction, dy, is:

$$\frac{dw}{dy} = \frac{\nu_{\perp} dt}{\nu_{tip} dt} = \frac{\nu_{\perp}}{\nu_{tip}} = \sin(\theta). \qquad (2)$$

as follows from Figure 13. As the parabola slope angle:

$$\phi = arctan\frac{dy(x)}{dx} = arctan(2ax) = arctan(2a^{1/2}y^{1/2}). \qquad (3)$$

and $\theta = 90° - \phi$, it follows that:

$$\nu_{\perp} = \nu_{tip} cos(\phi) = \nu_{tip} cos(arctan(2a^{1/2}y^{1/2})). \qquad (4)$$

It is clear that the perpendicular growth rapidly decreases further away from the needle tip (i.e. for increasing y).

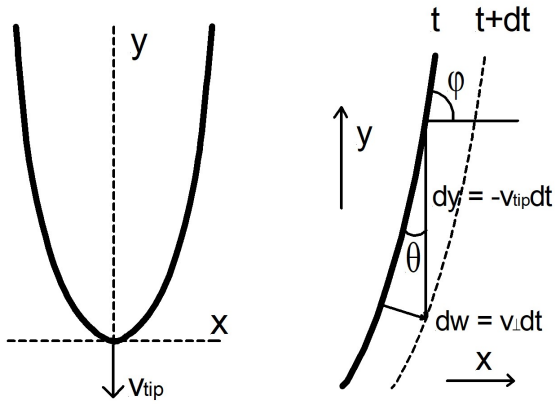

Figure 4.12: Perpendicular growth rate, $\nu_{\perp}$, as a function of the distance, y, from a parabolic needle tip.

To keep matters simple, we presume equilibrium surface coverage of the additives during needle growth. Following the Langmuir's adsorption isotherm this equilibrium surface coverage is given by:

$$\theta_{eq} = \frac{k_a c}{k_a c + k_d}. \qquad (5)$$

With k_a the adsorption rate per surface site. The other term:

$$k_d = k_d^0 + bR^n. \qquad (6)$$

is the rate constant of removal of adsorbed additive units per surface site. In this, k_d^0) is the rate constant of desorption of additive molecules and bR^n is the rate constant of incorporation of additives into the crystal lattice, which we presume to be an exponential function of the growth rate, or $(\nu_\perp)^n$, Further, b is a constant. From the growth rate dependence of θ_{eq},

$$\theta_{eq} = \frac{k_a c}{k_a c + k_d^0} + b\nu_\perp^n. \qquad (7)$$

it follows that the additive coverage on the growing needle faces increases with distance y from the needle tip according to:

$$\theta_{eq}(y) = \frac{k_a c}{k_a c + k_d^0 + [b\nu_{tip} cos(arctan(2a^{1/2}y^{1/2}))]^n}. \qquad (8)$$

For $y = 0$:

$$\theta_{eq}(0) = \frac{k_a c}{k_a c + k_d^0 + b\nu_{tip}^n}. \qquad (9)$$

the surface coverage is low and many additives are incorporated in the lattice. For $y = \infty$ or if $\nu_\perp = 0$

$$\theta_{eq}(\infty) = \theta_{eq,0} = \frac{k_a c}{k_a c + k_d^0}. \qquad (10)$$

We can see that θ_{eq} increases for increasing y until it reaches the value of θ_d and growth stops, i.e. $\nu_\perp = 0$. Then, more additives accumulate at the surface until the situation given by Equation 10, i.e. a surface coverage of $\theta_{eq,0}$, is reached. Then, growth is irreversibly blocked for the supersaturations applied in our case. Partial incorporation of additives is essential in our model, as the value of $\theta_{eq}(\infty)$ is attained readily if $b = 0$, blocking growth completely and no crystals will be formed.

4.5 Conclusions

During this investigation, we have observed that when concentrations of $\approx 1\%$ (w/w) nitrilotriacetamide, methylglycine diacetamide and glutamic acid diacetamide are added to a saturated brine solution and allowed to evaporate, a dense layer of ultrathin crystal needles, $0.3 - 2\mu m$ wide, is formed.

We concluded experimentally that these needles are formed from cubic NaCl, with no evidence of large amounts of amide in the composition. We also determined that the crystallographic direction of the needles is $\{100\}$. Overall however, there is no preferred direction in which the needles grow on the substrate, leading to a chaotic "criss-cross" pattern.

From high magnification SEM observation, we concluded that the needle shape of these crystals is not due to parallel dislocations or twinning. We interpreted the NaCl needle growth by tip formation induced by morphological instability at the earliest stage followed by additive adsorption on the needle side faces, preventing thickness growth and side branch formation. Needle formation in this work is a unique combination of initial morphological instability and subsequent additive blocking of crystal growth.

Chapter 5

Amides as anticaking agents for sodium chloride: is a triple branched variant necessary?

Eleanor R. Townsend, Willem J.P. van Enckevort, Jan A.M. Meijer, Elias Vlieg

CrystEngComm, accepted Dec. 2017

Abstract

Amides are well known for their potential as anticaking agents for sodium chloride. We have investigated what is the ideal structure for an amide based anticaking agent and what features lead to effective anticaking. Through a series of experiments, we have found that a triple-branched structure, with the three branches radiating from the same nitrogen centre, is the only effective compound for preventing caking for sodium chloride. We conclude that this is likely due to bonding between the atoms of the amide functional group and the ions of sodium chloride, with an extra bond from the central nitrogen giving a strong attachment to the surface, thus leading to blocking of growth. We have also outlined a list of four categories, of which a compound must obey all of in order to act as an effective anticaking agent.

5.1 Introduction

An anticaking agent for a crystalline compound can be identified by its specific properties, in that it is able to bind effectively to the facets of the crystals and prevents the propagation of steps across the surface at a molecular level, thus blocking growth. The interaction between the species and the surface (of, for example, NaCl) is thus vital to have the desired anticaking effect. It is well known that amide containing compounds have a strong interaction with the NaCl surface. For example, urea was reported by Rome de l'Isle in 1783 [8] as having an effect on the growth of NaCl. He demonstrated that using 30% (w/w) urea in a brine solution caused octahedral NaCl crystals to grow from solution. In 2010, Smith [92] suggested a mechanism for this process, that urea is being preferentially excluded from {100} facets, leading to the characteristic octahedral form of the crystals. A habit modification effect has also been reported for crystals grown in the presence of 20% and more (w/w) formamide [63], of which a mechanism has also been discussed by Radenovic et al. [37] Also, as far back as in 1961 [36], it has been reported in the literature about the effectivity of a triple branched, amide containing compound, nitrilotriacetamide (NTAA), as an anticaking agent for sodium chloride. It has been shown that this compound has effects on the surface growth at concentrations as low as $1x10^{-4}$ % (w/w). [62] [74] We have previously shown that NTAA also acts as a habit modifier for NaCl in high concentrations. The crystals grow instead of in the expected cubic form, as ultrathin needles. [42] [93]

However, what we have discovered is that habit modification is no guarantee for a clear anticaking effect. While NTAA shows a strong anticaking effect, neither urea nor formamide have been reported to have an effect on the anticaking of sodium chloride crystals. From this we can deduce that an increasing number of amide groups on a molecule leads to a stronger interaction with the NaCl surface. Conversely, there is some evidence to dispute this theory, in that we have shown that the polymer variant of these compounds, polyacrylamide, which has chain length of up to twenty units, also does not have an anticaking effect. [32] This shows it seems that a happy medium must be struck between the size of a molecule and the amount of amide groups present to have an effective growth blocking effect and thus make a good anticaking agent.

The aim of this paper is to therefore explore in more detail, what makes a good amide-based anticaking agent. We have characterised the effect in crystal growth and nucleation and the anticaking effects of a series of amides, both short and long, and with different levels of branching.

5.2 Methods

In addition to the known anticaking agent nitrilotriacetamide (NTAA); urea, 2-[(carbamoylmethyl)amino]acetamide (2-CMAA), two polyacrylamide molecules of differing sizes and two other triple branched molecules, methyl glycine diacetamide (MGDA) and glutamic acid diacetamide (GLDA), were examined. The structures of these molecules are outlined in Figure 1.

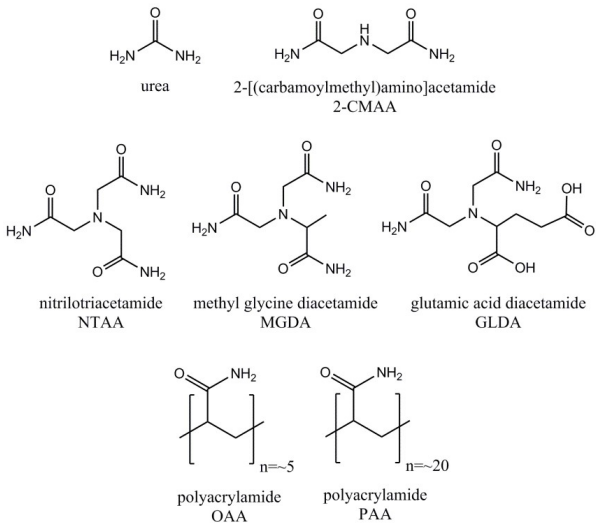

Figure 5.1: Chemical structures of chosen amide containing additives.

Urea and PAA were both obtained from Sigma Aldrich. Urea was provided in powder form with a purity of ≥98% and PAA was obtained in a 50% (w/w) aqueous solution. 2-CMAA, NTAA, MGDA, GLDA and OAA were all synthesised and obtained through AkzoNobel as they are not commercially available. NTAA, MGDA and GLDA are currently used in their sodium salt forms as chelating agents by AkzoNobel Industrial Chemicals under the trademark name Dissolvine®. It is also known that the pH of an additive can have a large effect on its anticaking abilities [20], and so it was monitored closely during our experiments. The "natural" pH values of each additive in brine solution are listed in Table 1.

Additive	pH
Urea	6.9
2-CMAA	7.4
NTAA	5.6
OAA	6.4
PAA	6.0
MGDA	5.1
GLDA	3.5

Table 5.1: pH values of 1% (w/w) additive in concentrated brine solution

5.2.1 Creeping tests

In our previous work [44], we have shown that creeping can be used as a simple initial method to test for potential anticaking effects on sodium chloride crystals. A solution was made using saturated brine and 1% (w/w) of the chosen additive at ambient temperature (20-25°C). The solution was filtered using a syringe fitted to a $0.45\mu m$ Pall GHP Acrodisc filter, and then dropped onto a glass microscope slide using a micro-pipette. These slides were previously cleaned using EtOH and dried using a dust-free tissue to minimise external nucleation effects. The amount of solution in each droplet varied from 5-10μL. The droplets were allowed to evaporate in a temperature and humidity controlled climate chamber at 20°C and 50% relative humidity. The resulting crystals were imaged using a Leica DMRX optical microscope.

5.2.2 Supersaturation experiments

It is well known that growth blocking additives delay the nucleation of crystals in solution, leading to sudden and extremely fast nucleation at higher supersaturations. Therefore, the determination of the supersaturation at which 3D nucleation commences appears to be a powerful method for detecting the blocking activity of additives and subsequent anticaking activity.

These tests were performed by weighing a siliconised glass slide, which had been pre-cleaned using ethanol to remove any dust which could promote nucleation. In contrast to the creeping experiments, the siliconised glass slide proved necessary in this experiment, as it has less wetting than a normal glass slide and therefore, the droplets had a higher contact angle and did not evaporate so quickly. The contact angle of all droplets were all very similar. The slide was placed on a precision balance and single 20μL droplet of brine (with or without additive) was dropped on top.

The initial weight was recorded and the sample was closely observed until nucleation and subsequent initial crystal growth could just be discerned with the naked eye. At times, the edges of the droplet were observed using a magnifying glass to detect any tiny crystallite growth. The weight at nucleation was recorded and the average supersaturation was calculated through the weight difference at the beginning and the end of the experiment. As nucleation is a stochastic process, the experiments were performed in triplicate to obtain an average value for the approximate supersaturation.

5.2.3 Powder Flow Analysis

Caking tests were performed following a standardized measurement employed by AkzoNobel.[38] The measurements were performed in quadruplicate using a Powder Flow Analyzer rheometer to determine the caking strength of the sodium chloride when treated with additive solutions. 50 g batches of high-purity Akzo Nobel Sanal P® salt were placed into separate plastic bags and treated with 2% (w/w) moisture. The moisture consisted of a solution of a chosen concentration of additive in MilliQ water. Using this dilution factor, a 1% (w/w) solution yields an additive concentration of 0.02% (w/w) with respect to the salt. In the cases of varying pH of additive solution, the pH was set before the experiment using either a dilute solution of HCl or NaOH. The treated salt batches were then placed in separate plastic containers of 50 mm diameter and preconditioned by compressing with 1 kg weight and purging with dry air for 2 hours. The strength of the cake of the samples was then measured using the rheometer (type TA-XT21, Stable Micro Systems), which is a screw-like moving blade which enters the salt cake and continuously measures the vertical force imposed by the salt. The measurement unit is CE20, which is the relative caking energy in N.mm required to enter a cake of 20 mm. All results were compared to a standard blank test, without additive. These experiments were carried out at ambient temperature. The error of the measurements was calculated using a standard deviation calculation over the four measurement values. The limit of the machine occurs when a force of 55N is exceeded.

5.3 Results and Discussion

5.3.1 Creeping Tests

In order to initially determine whether the chosen additives had any effect on the growth of NaCl, creeping tests were performed. These tests were performed at a concentration of 1% (w/w) and at a pH value as determined by the acidity of the compound. Therefore, this varied over the experiments, but was always in the range of pH 3-7. This technique was chosen as it is extremely fast and effective when employed as a qualitative screening method for caking activity.[44] The results are shown in Figure 2.

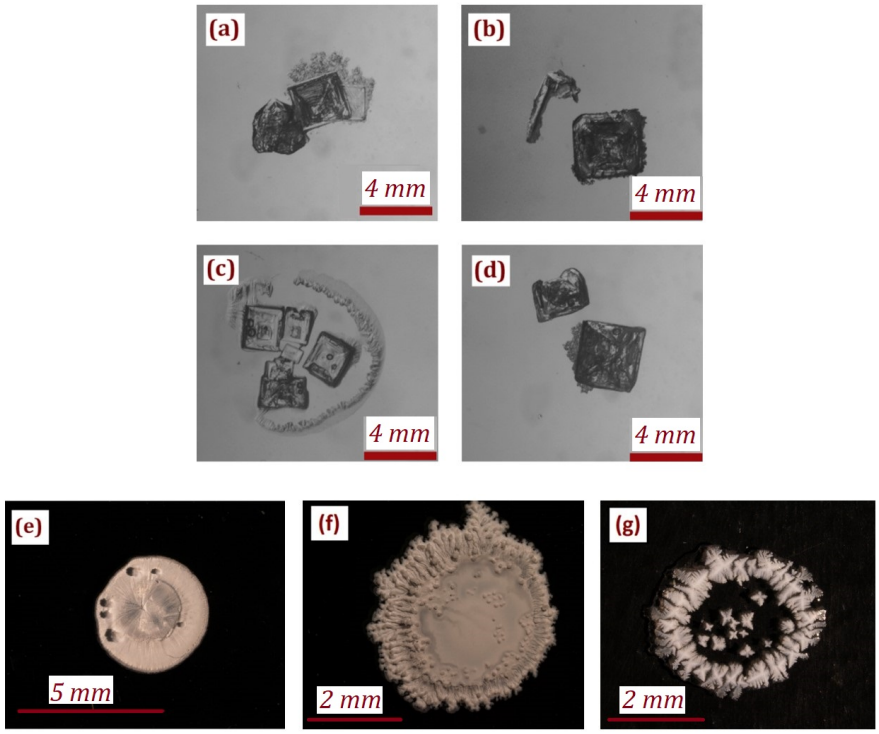

Figure 5.2: Crystal growth patterns from saturated brine solution containing: (a) 1% (w/w) urea, (b) 1% (w/w) 2-CMAA, (c) 1% (w/w) OAA, (d) 1% (w/w) PAA, (e) 1% (w/w) NTAA, (f) 1% (w/w) MGDA and (g) 1% (w/w) GLDA.

From these results, we can conclude that the only additives, at this concentration,

which have any effect on the growth of NaCl are NTAA, MGDA and GLDA. In the cases of urea, 2-CMAA, OAA and PAA as additives in the brine solution, the resulting creeping patterns consisted of crystals only of cubic morphology. This result was expected in the case of urea, as it has been reported that a concentration of >20% (w/w) in solution is required to have any habit modification effect.[8] In the case of PAA, some discernible octahedral type growth was expected as it has been previously reported[32], however it is likely that the crystals formed extremely quickly due to the small amount of growth solution (5-10μL) and the {111} facets are reported to only develop at low supersaturations, involving slow growth.[32] In contrast to Figure 2(a)-(d), it can be seen in Figure 2(e) that NTAA causes the formation of an extremely dense opaque crystal pattern, with no apparent cubic crystal growth. Microscopically, this crystal growth pattern consists of numerous crystals in a needle-like morphology.[93] MGDA and GLDA exhibit more traditional branched creeping patterns (Figs. 2(f)-(g)).

5.3.2 Supersaturation experiments

For NaCl-additive systems, the effect that additives have on the nucleation of NaCl crystals in solutions is significant.[17] These experiments were carried out to determine whether an additive which has an effect on the growth also has a significant nucleation hindering effect. The control brine solution containing no additive gave a calculated approximate supersaturation value at nucleation of 6%.[42] On addition of the range of additives to the saturated brine solution, it was clear that in all cases, the approximate supersaturation values at which nucleation occurs is significantly increased. The values are shown in Table 2.

Additive	**Approximate $\Delta\mu/kT$ (%)**
None (pure brine)[42]	6 (±0.4)
Urea	16.5 (±4)
2-CMAA	15.5 (±3)
NTAA[93]	17 (±1)
OAA	21.5 (±5)
PAA	48 (±6)
MGDA	22 (±3)
GLDA	13 (±2)

Table 5.2: Approximate supersaturation values at the point of nucleation for additives at 1% (w/w) concentration in a saturated brine solution

In comparison to the control value of 6%, the measured supersaturations are all approximately three times larger, except for that of PAA, which has a much higher value. From Chapter 3, we know that PAA is a habit modifier, but is not an anticaking agent. This leads us to the conclusion that nucleation inhibition is an important criterion for making a good anticaking agent, but it is not the only one which needs to be fulfilled in order to find an effective additive.

5.3.3 Powder Flow Analysis- Variation of pH and concentration

Creeping tests and supersaturation tests are extremely useful initial techniques, but it is important to quantify our findings to be able to properly conclude the extent of anticaking effects. In order to do this, the caking energy exhibited by sodium chloride treated with various amide based additives was measured using the technique of Powder Flow analysis. The results are shown in Figure 3 for different pH values and different additive concentrations. The level at which normal salt cakes, i.e. treatment with water containing no additive is indicated on the graph with a dotted line. Any value above this line indicates that an additive acts as a pro-caking agent.

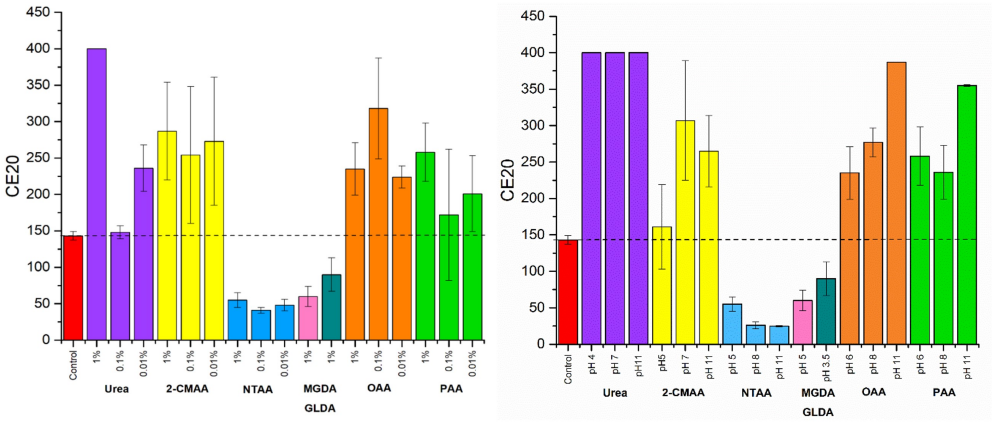

Figure 5.3: Powder flow experiments comparing amides of different sizes. Left: as a function of additive concentration at "natural" pH value; Right: as a function of pH, with the concentration remaining at 0.02% (w/w) w.r.t salt.

From these results, the overall finding is that the additives which have an anticaking effect on sodium chloride are NTAA, MGDA and GLDA. The other four additives; urea, 2-CMAA, OAA and PAA all give average caking energies which surpass that found for the control measurement of 143 ± 6 CE20. These overall findings mirror

what we have found in the Creeping Experiments section. It is evident from the results that pH does not have a large effect on the effectivity of each anticaking agent. However, it seems that there is a slight tendency towards the lower pH values for the majority of additives except NTAA. As regards to the variation in concentration, there is also not a clear correlation between the amount of anticaking and the level of additive down to a minimum concentration of 0.01% (w/w) w.r.t the solution, which equates to fifty times less, w.r.t. salt. Due to the similarities between NTAA and MGDA/GLDA and the time-consuming nature of PFA experiments, only one experiment was performed for MGDA and GLDA, at a concentration of 1% (w/w) w.r.t solution and at the natural pH. It is also noticeable from the results that the CE20 value for GLDA is higher than those of NTAA and MGDA; this is likely to be attributed to the fewer amide groups on this molecule, which have been replaced by acid groups. For NTAA, it was found that extreme pH differences in the additive solution did not have a large effect on the anticaking properties. This is likely due to the stability of amides in solution, in that they are not particularly acidic or basic (the conjugate acid of an amide has a pKa value of 9.5). As PFA experiments are time-consuming, only three pH values were measured, but all showed values far below that of the control and in the same order of magnitude as each other. This indicates that the NTAA complex and its interaction with the NaCl surface is stable at a wide range of pH values. Especially for the case of urea as an additive, it was shown that all measured pH values and concentrations showed only values higher than the control and thus showed a pro-caking effect, i.e. "glued" the crystals together. Urea is a known habit modifier for NaCl, but does not show a growth blocking effect. The reason for the enhanced caking effect is not clear, a possible explanation is the formation of a thin layer of urea connecting adjacent crystallites. The thickness of the urea layer between adjacent crystals in the cake is estimated to be between 0.3 and 30 nm for the 0.1% and 1% solutions. Urea is a widely used industrial product in the fertiliser industry and many studies have been undertaken to attempt to lessen the amount of caking between urea crystals.[94] [95] Therefore it is likely that the urea actually contributes to the caking of NaCl. At 0.1% (w/w) additive concentration, urea gave a CE20 value very similar to that of the control. The difference between this and those at the higher and lower concentrations can possibly be attributed to the salt samples being slightly wet, which aids in breaking the cake. In this, it should be realised that the solubility of urea in water is extremely high (119 g/100 g H_2O).

5.3.4 What makes a good anticaking agent?

We can conclude that there are a set of criteria which must be fulfilled for an additive to be deemed an effective anticaking agent. These criteria are outlined in Figure 4 and made explicit in Table 2. It should be realised that only creeping is not sufficient, as some pure compounds show creeping as well.

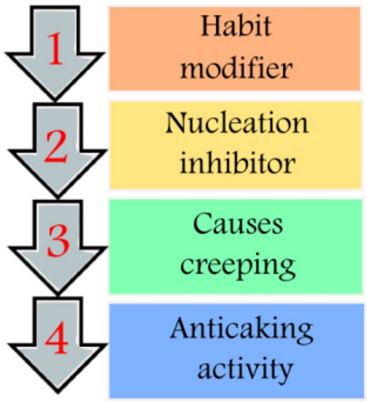

Figure 5.4: A flow chart depicting the necessary criteria for an effective anticaking agent.

Additive	Habit modifier?	Nucleation Inhibitor?	Causes creeping?	Anticaking activity?
Urea	✔[8]	✔	✗	✗
2-CMAA	✗	✔	✗	✗
NTAA	✔	✔	✔	✔
MGDA	✔	✔	✔	✔
GLDA	✔	✔	✔	✔
OAA	✗	✔	✗	✗
PAA	✔[32]	✔	✗	✗

Table 5.3: Relating the properties of the tested additives to the anticaking agent criteria

From this table it is clear that the only additives which fulfil all necessary criteria to act as anticaking agents for NaCl are NTAA, MGDA and GLDA. This agrees with our experiments, and it points to a specific feature of three branched amide molecules that

induces an anticaking effect which is impossible for those compounds with a differing structure.

It seems that some type of "happy medium" exists between the amount of amide groups on the molecule and its size. Habit modification of the NaCl by the additives from {100} to {111} and a delayed nucleation are not enough to have an anticaking effect. Although the additive binds some extent to the surface, it does not block the surface strongly enough to produce the "weaker" crystals with needle like or dendritic habits needed to have the desired creeping effect, which is indicative for a roughened and blocked surface during anticaking treatment.[18] [38] Insufficient bonding was observed for both the smallest compound, urea, and the largest polymer, PAA. This also shows that there is no correlation between the anticaking effectivity of a molecule and its chain length and subsequent amount of amide groups. This points to the idea that the unique structure of the triple branched amides is vital to the explanation for their effectivities.

We hypothesise that there are two possible mechanisms with which the triple branched amides can bond to the NaCl. The first is inspired by the Sarig model[62] for the binding of NTAA *onto* NaCl {100}. This model suggests that the partially negatively charged oxygens of the amide groups are bonded to the sodium ions of the substrate, assisted by a weaker bonding of the amine to the chlorine ion. The compound therefore anchors itself to the substrate with three contact points at the ends of each branch radiating from the central nitrogen and a final contact point from the central nitrogen. The second model is inspired by the model from Bode et al.[18] in which the additive anchors itself into the surface at one point, by replacing some of the surface atoms of the substrate.

From an estimation of bond lengths, the Bode mechanism is unlikely, as the length of the amide branch (approximately 4.5 Å) is much larger than the distance between the surface Na and the Cl below (2.81 Å) if they are removed. It is thus unlikely that an amide functional group would be incorporated into the crystal lattice as observed for ferrocyanide and $PbCl_2$.[96]

Thus, the most likely model seems to centre on the idea that the triple-branched amide lays on the surface of the NaCl, bonded by three amide group branches and a central nitrogen atom, as described by Sarig. However, it can be said that it is likely not the matching of the three-fold symmetry of the amide molecules with the threefold symmetry of NaCl {111}, as only {100} growth is involved in anticaking experiments. Density Functional Theory (DFT) was employed to calculate the charge distribution over the NTAA molecule and its 2-branched counterpart 2-CMAA to determine if there are any large differences over the molecules which can explain the tendency of

one to bind over the other. However, this did not give any meaningful results, it was found that the charge distribution over both molecules was very similar. So it is the addition of an extra amide group (or the acid groups in GLDA) reinforcing bonding to the NaCl surface, which is decisive. Inspired by the work of Pastero et al.[63], it is possible that the additives are ordered in layers. The three-fold branching of the triamide allows the formation of highly distorted 2D connected network patterns interlinked by $C{=}O\cdots H_2N$ hydrogen bonds. This grouping leads to strong bonding, both vertically to Na^+ and Cl^- and horizontally by hydrogen bonds. However, a more in-depth molecular modelling study is necessary to confirm this suggestion or to find an alternative as to why the triple branched amides are so effective for blocking the growth of NaCl, in contrast to the other amide compounds.

5.4 Conclusions

The overall conclusion that we can draw from this investigation, is that the three branched amide compounds nitrilotriacetamide, methyl glycine diacetamide and glutamic acid diacetamide all act as anticaking agents for NaCl, whereas single and double branched and polymer analogues do not have the same effect. This indicates that there is a clear correlation between the amount of amide branches radiating from one centre and the anticaking ability of a compound.

In contrast to the growth blocking tri-amides, the other non-blocking compounds show an enhanced caking effect on NaCl. A possible explanation is the formation of a thin layer of additive between adjacent NaCl crystallites, acting as an adhesive.

We have also determined that an effective anticaking agent must obey all of the criteria in a four-step process: habit modification, nucleation inhibition, ability to induce creeping, leading to anticaking activity. If it fails in any of these categories, then it is ineffective as a growth blocker.

Chapter 6

The structure of $PbCl_2$ on the {100} surface of NaCl and its consequences for crystal growth

Eleanor R. Townsend, Sander J. T. Brugman, Melian A. R. Blijlevens, Wester de Poel, Mireille M. H. Smets, Willem J.P. van Enckevort, Jan A.M. Meijer, Elias Vlieg

in preparation

Abstract

The role that additives play in the growth of sodium chloride is a topic which has been widely researched but not always fully understood at an atomic level. Lead chloride ($PbCl_2$) is one such additive which has been reported to have growth inhibition effects on NaCl {100} and {111}, however no definitive evidence has been reported which details the mechanism of this interaction. In this investigation, we used the technique of surface x-ray diffraction to determine the interaction between $PbCl_2$ and NaCl {100} and structure at the surface. We find that Pb^{2+} replaces a surface Na^+ ion, while a Cl^- ion is located on top of the Pb^{2+}. This leads to a charge mismatch in the bulk crystal, which, as energetically unfavourable, leads to a growth blocking effect. While this is a similar mechanism as in the anticaking agent ferrocyanide, the effect of $PbCl_2$ is much weaker. Moreover, $PbCl_2$ has an even stronger effect on NaCl {111}.

6.1 Introduction

Sodium chloride has now for many years been a model compound of choice for investigation into the effects of additives on crystallisation, along with its sister compound potassium chloride, due to its relatively simple crystal structure and abundance in nature. In 1932, Kading[97] reported that lead ions can have a marked effect on the crystallisation of many alkali halide salts, including NaCl and KCl, of which discovery led to many more investigations into the effect of Pb^{2+} on NaCl and KCl. Bunn and Emmett[98] suggest that Pb^{2+} causes both a decrease in step height and growth inhibition of a growing NaCl crystal, a finding which is echoed by Botsaris et al.[99] and Glasner and Skurnik[100] in their 1966 and 1967 articles respectively. Both articles agree that Pb^{2+} ions retard the nucleation and subsequent growth of KCl, however there is a disagreement between the two on the mechanism of this interaction. This growth blocking was also observed by Sears, who described the hindering of KCl growth from a supersaturated solution containing 1% $PbCl_2$.[101]

As a consequence of the growth blocking, lead ions are also known to affect the habit of alkali halide crystals.[102] This was first reported by Bienfait et al.[15] who showed, through the use of a growth morphodrom, that Pb^{2+} significantly lowers the supersaturation needed to change the external form from {100} to {111} in NaCl. The same was found for other ions, such as $Mn^{2+}$and Cd^{2+}. A similar observation was seen by Li et al.[103], who also described a growth morphodrom, except this time for KCl in the presence of Pb^{2+}. They described the changes in crystal habit and surface microtopographs observable dependent on the supersaturation and respective Pb^{2+} concentration, showing the eventual elucidation of {111} facets under varying additive concentrations and supersaturations.

It is thus interesting to understand the mechanism of how the Pb^{2+} interacts with the {100} and {111} surfaces of NaCl. Booth[104] suggested that in the case of NaCl, Pb^{2+} is incorporated along the {100} facets but not the {111}. The explanation using a variety of models was discussed by Botsaris et al.[99] but no definitive experimental proof was reported. More recently, Radenovic et al.[105] showed definitively the structure of the {111} NaCl crystal surface in contact with a brine solution containing $CdCl_2$ using surface x-ray diffraction (SXRD). They showed that the adsorption layer consisted of a mixed monolayer of Cd^{2+} and water with occupancies of 0.25 and 0.75 respectively, in contact with the top Cl^- layer on the {111} surface. As $CdCl_2$ was reported by Bienfait et al.[15] as having a similar effect on the NaCl habit as $PbCl_2$ (i.e. change from {100} to {111} observable facets), we can assume that $PbCl_2$ would

show the same mechanism. However, this does not explain the role of Pb^{2+} when it is put into contact in solution with an already formed {100} surface.

The aim of this paper is to determine the mechanism of attachment of $PbCl_2$ to the {100} surface of sodium chloride at an atomic scale. The technique of surface x-ray diffraction (SXRD) is used for this. We intend through this investigation to gain valuable insight into the mechanism of action of transition metal halides on this substrate and to create a model which describes accurately this process.

6.2 Methods

TThe cubic NaCl crystals used in this experiment were grown from a saturated sodium chloride solution, which had been filtered using 0.45 μm Whatman filters. The approximate size of the crystal used in the final experiment was 6 x 6 x 3 mm^3. Evaporation was minimised by crystallising in an Erlenmeyer flask, with the opening covered with Parafilm containing a small hole. This set-up also prevented contamination of the growth solution with dust or other foreign particles. After removal from the growth solution, the NaCl crystals were dried using a dust-free tissue and stored in a temperature and humidity controlled climate chamber to prevent roughening. The resulting crystals were nearly optically defect free.

In previous experiments, SXRD has been used successfully with NaCl as a substrate, both on the {100} and {111} facets. Arsic et al.[106] determined the ordering of the water layers on the {100} surface, which was then followed by the previously mentioned work by Radenovic at al., in which the influence of cadmium on the {111} surface was investigated. More recently, SXRD was also used to determine the mechanism of the anticaking activity of ferrocyanide on the {100} NaCl surface.[18] With SXRD, the diffracted intensity is measured along so-called crystal truncation rods (CTR).[107] These rods consist of out-of-plane tails of diffracted intensity connecting bulk Bragg peaks[25] and are sensitive to the interface structure.

The SXRD experiments for this investigation were performed at the MS-X04SA beamline[108] at the Swiss Light Source (SLS) in the Paul Scherrer Institute in Villingen, Switzerland. The radiation used had a photon energy of 20 keV, corresponding to a wavelength of 0.62 Å, and a beam size of 60 x 1000 μm^2. The measurements were taken using a vertical (2+2) type diffractometer with a PILATUS area detector at an incidence angle of 0.6°. Complementary experiments were performed prior to this at the Diamond Light Source in Didcot, U.K. In this paper we only show the more extensive results from the SLS, but the data from the Diamond Light Source were very similar, proving the reproducibility of the experiments.

We measured data sets for NaCl {100} treated with a solution of $PbCl_2$. The solution consisted of a slightly undersaturated solution of brine containing varying amounts of $PbCl_2$, which was subsequently filtered using a 0.2μm Whatman filter. The data which we obtained and analysed in this paper was gathered using a solution saturated with $PbCl_2$, which equates to a concentration of 4.4 g/L in pure water. This value was obtained using the solubility constant K_{sp} of 1.7 x 10^{-5} for $[Pb^{2+}][Cl^{-}]^2$. How-

ever, the equilibrium is shifted dramatically with the addition of NaCl to the $PbCl_2$ solution, as NaCl is extremely soluble in water ($K_{sp} = 36$). The high concentration of Na^+ and Cl^- from the dissolved NaCl, forces the equilibrium $Pb^{2+} + (Cl^-)^2 \Leftrightarrow PbCl_2$ towards the right. This means that the concentration of Pb^{2+} dissolved in the solution is actually very low, approximately 2.8 x 10^{-11} molecules Pb^{2+} / μL. The remainder of the $PbCl_2$ is thus likely precipitated as minute particles which are either removed by the filtration step/tissue method or sit on the surface as the $PbCl_2$ crystals.

5 μL solution was applied to the crystal surface using the following method: a dust free tissue was pulled tightly across the crystal surface, a droplet applied to this and allowed to soak in for a few seconds before removal. This method was employed to minimise the height of the liquid layer present on the crystal surface and prevent roughening of the surface. The crystal was then immediately placed into the set-up, which consisted of an isolated cell at room temperature, in which the relative humidity was regulated at 75%. This humidity was regulated by the presence of a saturated solution of NaCl in the environment. By using this method, we found that roughness was minimised on the NaCl surface and also there was no presence of a thick liquid layer which would impede our measurements. However, as this is just at the deliquescence point of NaCl, there is definitely a water layer present.

Other measurements which were performed used a range of $PbCl_2$ concentrations were also analysed for the discussion of this article, however we have come to the conclusion that it is likely that the Pb^{2+} concentration in these solutions is still extremely low.

In order to fully derive the surface structure, a data set of different CTR's is necessary. The momentum transfer $\vec{Q}$ is dependent on the the diffraction indices hkl and the reciprocal lattices vectors $\vec{b_i}$:

$$\vec{Q} = h\vec{b_1} + k\vec{b_2} + l\vec{b_3}. \qquad (1)$$

We orient the unit cell such that the direction perpendicular to the surface is denoted by l, and h and k denote directions that are parallel to the a and b axes respectively. Therefore we are technically studying the (001) surface of NaCl. Model calculations and fitting was performed using the program ROD.[109] The contribution of the data points close to the Bragg peak were weighted to give a 30% larger error bar, in order to increase the weight of the surface sensitive data points.

6.3 Results

6.3.1 The Model

The data set consists of 401 non-equivalent reflections, relating to the (00), (11), (13), (20) and (22) rods. The full data set that was measured also included the rods $(1\bar{1})$, $(1\bar{3})$, (02) and $(2\bar{2})$, which was then averaged to give the final data set which had an agreement factor of 12%. The data are shown later in the article as blue dots, together with the calculated profile for an ideal NaCl (001) surface (red curves). It is clear that the data deviates strongly from this, and also from the data on NaCl (001) in water.[109] From this we conclude that the $PbCl_2$ must have a well-defined location at the surface. There are two simple configurations in which the $PbCl_2$ could be located at the surface: either embedded in the top NaCl layer, or on top of this. These two different models are hereby named "*embed*" and "*surface*".

The first model, *embed*, was inspired by the models from Arsic[106] and Bode[18]. Bode placed ferrocyanide ions into the surface, positioned with the iron atom at the sodium ion location and five cyanide ligands replacing the chlorines surrounding the sodium atom and one cyanide ligand sticking out perpendicular to the surface. In *embed*, the first surface layer consists of chlorine and sodium atoms, with some sodium positions being substituted with a lead atom. This gives to a surface structure shown in Figure 1a. In order to balance the extra positive charge of the lead atom, we placed a chlorine atom directly above the positions where lead was present. The rest of the empty positions on the second layer are occupied with oxygen atoms. In the case of these models, oxygen is used to describe the locations of water molecules, as hydrogen is invisible in these SXRD measurements, due to its low electron density.

The second model, *surface*, is inspired by the findings of Radenovic[105] on the {111} surface, where the ions are in contact with the upper layer of the NaCl surface, but do not replace atoms as in the *embed* model. In this model, lead atoms are ordered above the chlorine positions of the first NaCl bulk layer. The charge of the lead is compensated with two chlorine atoms in the same layer, the rest of which is then filled with oxygen atoms representing water molecules. This model is explained diagrammatically in Figure 1b.

In both models we consider two types of oxygen units directly on top of the NaCl surface. Atom O1a is placed directly on a Cl^- ion and O1b is placed above a Na^+ ion. In addition, two extra water layers described as oxygen atoms, O2 and O3 are

not defined in the models displayed in Figure 1, but are incorporated in a liquid layer parameter in order to accurately describe the water layering as observed earlier.[106]

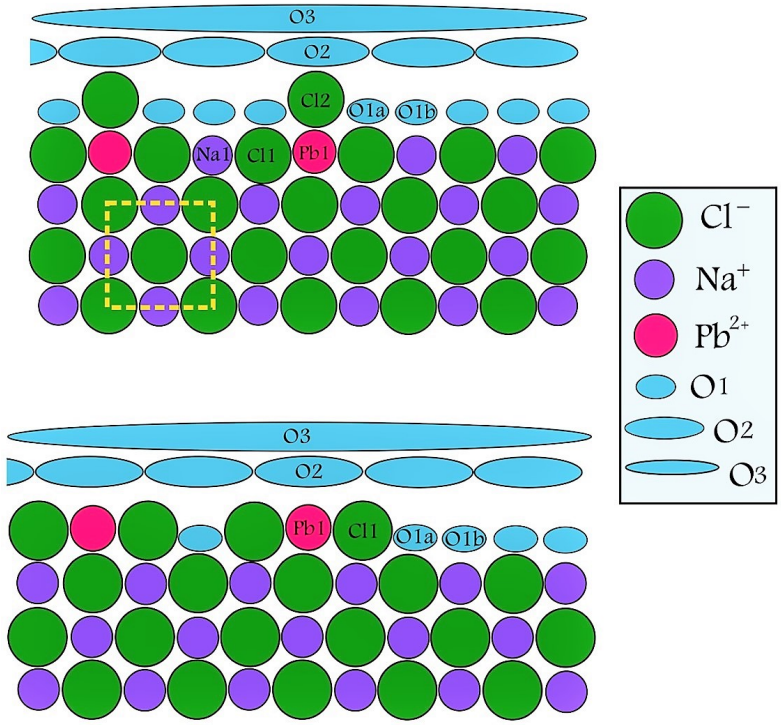

Figure 6.1: Side views of the models used to fit the data: Above: embed, Below: surface. The conventional fcc unit cell is indicated in yellow on the diagram ($a = b = c = 5.62$Å$, \alpha = 90°$).

6.3.2 Fitting to the models

In order to determine the optimum fit, the data set was fitted using a χ^2 minimisation routine in which the position and occupancies of the various atoms in the models are varied. Due to the similarities in ionic radius between Pb^{2+} (119 pm[110]) and Na^{+}(102 pm[110]), we do not expect that a large surface reconstruction is necessary to incorporate the Pb ion into the NaCl lattice structure. In addition, no evidence for long range ordered surface reconstruction, manifesting as extra, higher order peaks in the x-ray diffraction rod patterns, was found. Therefore, we will only consider a

normal 1 x 1 unit cell, as indicated in Figure 1. Some relaxations on the surface are expected and these were incorporated into the models.

The fits were built upon the upper layers of bulk sodium chloride, as shown in Figure 1. Fit parameters were used for the labelled atoms in the vertical positions only, as we expect the horizontal positions to largely retain the expected bulk positions. Δz is defined with respect to the bulk positions of Na^+ and Cl^- ions. Furthermore, Debye-Waller parameters were fitted, to allow for disorder in both the in-plane and out-of-plane directions. These values help to indicate low levels of relaxation in the horizontal and vertical directions, if present. It was not necessary to incorporate a roughness parameter into our model, this indicates that we had a very high-quality surface before and during the experiment.

6.3.2.1 Model 1: Embed

The data fitted to the model embed is shown in Figure 2, with the corresponding parameters shown in Table 1. The agreement is excellent, with a final reduced χ^2 value of 1.17.

	Occupancy	Δz **(Å)**	$\mathbf{DW}_{\parallel}$(Å^2)	$\mathbf{DW}_{\perp}$ (Å^2)
O 1b	1.3 ±0.2	-0.393 ±0.11	11 ±4	92 ±5
O 1a	0.909 *	0.394 ±0.06	20 ±4	6.3 ±1.2
Cl 2	0.091 *	0.36 ±0.06	24 ±45	50 ±6
Pb 1	0.091 ±0.001	0.36 ±0.06	6 ±1	2.1 ±0.7
Cl 1	1	-0.013 ±0.005	1.3 ±0.2	5.7 ±0.6
Na 1	0.909 *	≡ 0	≡ 1.7	≡ 0

Table 6.1: Summary of best fit parameters for the data set using model *embed*. Δz values are described with respect to bulk NaCl positions.

The Δz and DW factors were fixed for Na 1 as we expect no deviation from its original position. Also, some occupancies were constrained in relation to each other, as they are dependent on each other to achieve the expected full coverage of the NaCl surface and charge neutrality. These are indicated in Table 1 with an asterix. We assume therefore:

$$\text{Occ (Pb 1)} = \text{Occ (Cl 2)}$$

Occ (Na 1) = 1 - Occ (Pb 1)
Occ (O 1a) = Occ (Na 1)

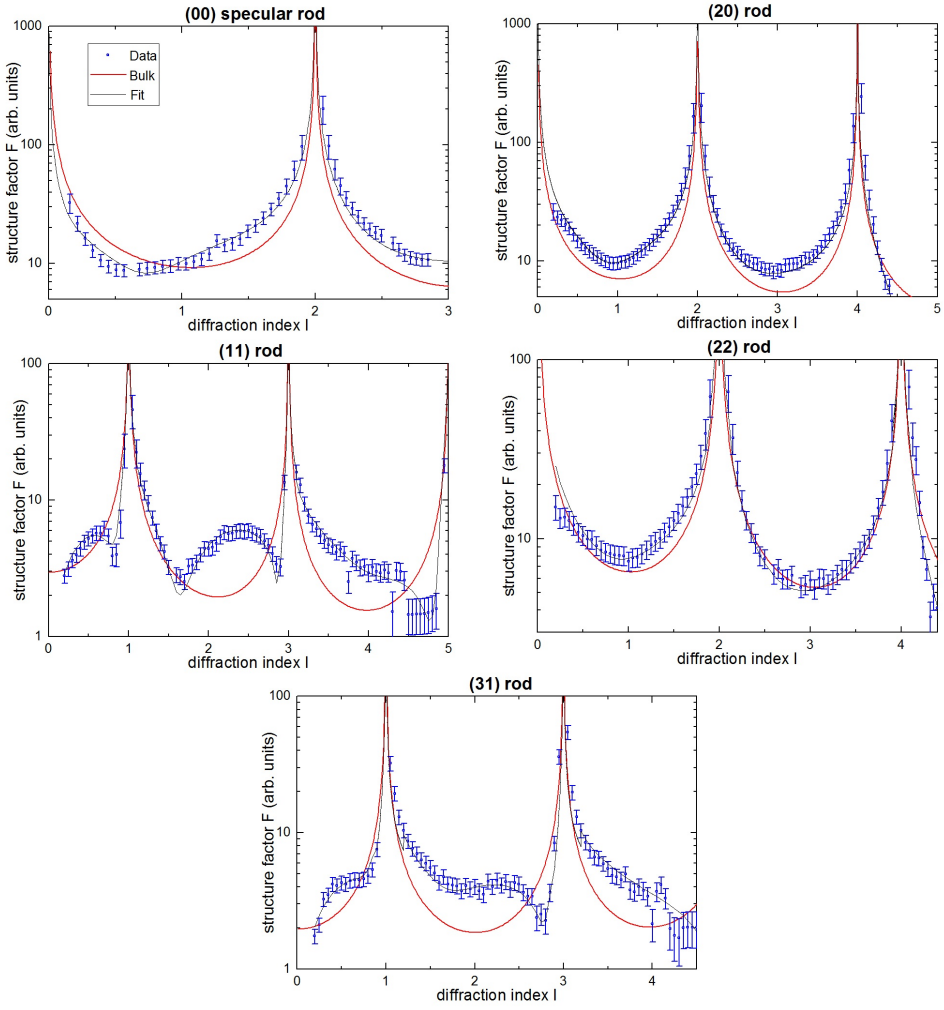

Figure 6.2: The rods of NaCl (100) fitted to the model *embed*. Blue: measurements with error intervals, black: fit, red: calculated values for ideal (001) surface.

From the refined model, we can calculate the z- projected electron density for the (00) and (11) CTR's, as shown in Fig. 3. The specular rod (00) is only sensitive to order in the out-of-plane direction, but this is not the case for other rods, which also have an in-plane component. As we also see a peak at 10.8 Å for both the (00) and (11) projection, this shows that we also have significant in-plane ordering of the upper water layer, i.e Cl 2 and the water layers O 1a and O 1b, as well as out-of-plane. This plot also shows us that above 12.5 Å in the upper layer of our model i.e. the water layers O 2 and O 3, there is very little order.

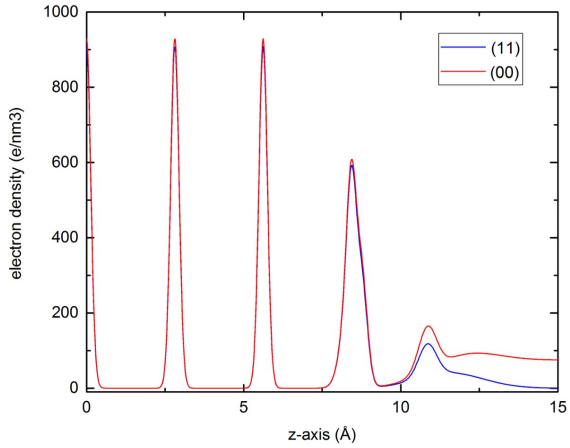

Figure 6.3: The projected z-density as seen for the (00) and (11) rods, calculated from model *embed*.

6.3.2.2 Model 2: Surface

The data fitted to the model *surface* is shown in Figure 4, with the corresponding parameters shown in Table 2. The final reduced χ^2 value for this fit was 2.74.

	Occupancy	Δz **(Å)**	$\mathbf{DW}_{\parallel}$(Å^2)	$\mathbf{DW}_{\perp}$ (Å^2)
O 1b	0.59*	8.54 ±0.06	0.2 ±2	0.4 ±4
O 1a	0.795 *	-5.39 ±0.06	15 ±4	0.2 ±3
Cl 1	0.41 *	-0.225 ±0.039	0.3 ±2	3 ±2
Pb 1	0.205 ±0.018	0.62 ±0.06	8 ±2	10 ±2

Table 6.2: Summary of best fit parameters for the data set using model *surface*. Δz values are described with respect to bulk NaCl positions.

In the case of this model, constraints were also made in relation to the occupancies of the various sites on the surface. Again, these are indicated in Table 2 with an asterix.

Here:

$$\text{Occ (Cl 1)} = 2[\text{Occ (Pb 1)}]$$
$$\text{Occ (O 1a)} = 1 - \text{Occ (Pb 1)}$$
$$\text{Occ (O 1b)} = 1 - 2[\text{Occ (Pb 1)}]$$

If extra layers are added, the fit of the *surface* model can be improved, but the fitting parameters are then essentially trying to mimic the *embed* model.

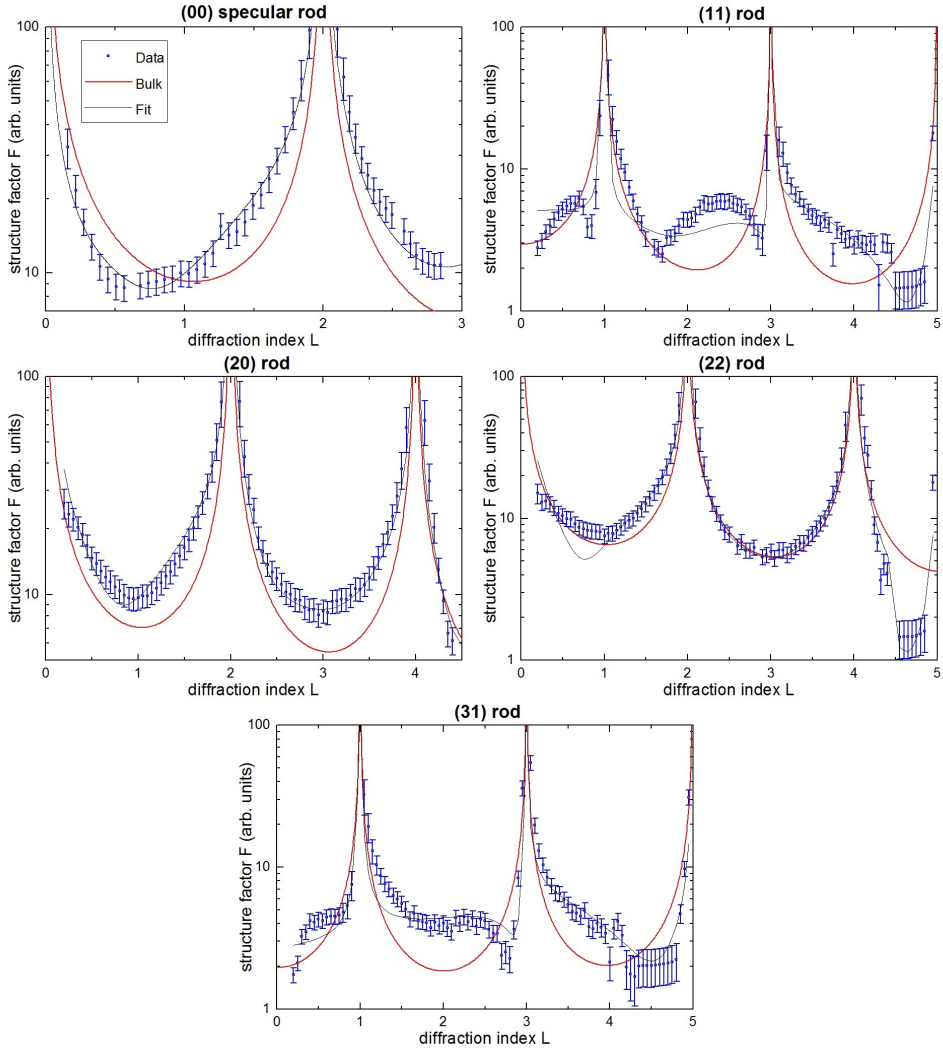

Figure 6.4: The rods of NaCl (100) fitted to the model *surface*. Blue: measurements with error intervals, black: fit, red: calculated values for ideal (001) surface.

6.4 Discussion

Comparing the results from the fitting of both models, it is clear that the *embed* model gives a superior fit to that of the *surface* model. This follows from comparing the data and fits in Figures 2 and 4 as well as from the much lower χ^2 value of the fit in the *embed* model. The largest discrepancies in the surface fit are observable in the (11) and (31) rods. We can therefore conclude that on the NaCl {100} surface in the presence of a saturated solution of $PbCl_2$, Pb^{2+} ions replace Na ions at certain positions; at a slightly higher position (0.36Å) that reflects the larger size of Pb. Above each Pb^{2+} ion on the surface is a chlorine ion, which allows for charge neutralisation of the Pb^{2+} atom, with the remaining surface covered with an ordered layer of water. From the z-density calculation, we can see that the water layers above the first water layer are hardly ordered (Figure 3).

Our results here show an occupancy of 9% for the Pb^{2+} ion. This occupancy is relatively low, but considering the very low amount of Pb^{2+} ions in the applied solution (4.4 g/L), it is to be expected. As we have used a solution which is almost entirely saturated with $PbCl_2$ in equilibrium with NaCl, we postulate that approximately 9% occupancy represents the equilibrium condition for this interface and therefore no more Pb^{2+} can be adsorbed. This was confirmed by the analysis of two previous experiments, one using a solution with an initial $PbCl_2$ concentration of 1.5 g/L and one using a solution with an initial $PbCl_2$ concentration of 0.2 g/L. The latter experiment was performed at Diamond Light Source. Upon analysis of these data, we confirmed that also here the *embed* model gave an excellent fit. The observed occupancies for these experiments were 8% and 5% respectively. Therefore we can definitively say that 9% is the maximum occupancy for Pb^{2+} ions on this surface.

The excess of Pb^{2+} can be confirmed by the presence of $PbCl_2$ crystallites on the surface, these were observed at certain points on the specular rod by the presence of strong diffraction ring patterns. $PbCl_2$ crystallites were also observed by optical microscopy by Li et al.[103] It is likely that the relaxation needed on the surface to incorporate the Pb^{2+} ion is relatively large (its radius is 14% larger than the smaller Na^+ ion), and is too disruptive to the surface for it to be feasible to occupy more than 10% of surface sites. However, it should be realised that a 9% occupancy corresponds with an average distance between adjacent Pb^{2+} ions of only 3.3 unit cell lengths, which is quite close. Our SXRD measurements did not show that the Pb^{2+} positions had long range order, but short range order is still possible. This could be confirmed using atomic resolution atomic force microscopy.

Here we have determined that Pb^{2+} is embedded in the {100} surface. We can also safely assume that the mechanism for the attachment of Pb^{2+} to the NaCl {111} surface mirrors that found by Radenovic at al.[105] for $CdCl_2$, in which they state that a mixed 1:3 monolayer of Cd^{2+} and water is in direct contact with the top Cl^- layers of the {111} surface below. We are thus in the unique situation that we have an atomic scale picture of the interface of NaCl in the presence of Pb^{2+} for both the {100} surface and the {111} surface. Based on this, one would initially expect the embedded Pb^{2+} on the {100} surface to have a stronger blocking effect that the floating Pb^{2+} on the {111} surface.

It has long been established however, that while there is a retardation effect of the {100} surface[101] [104] , the effect on the {111} is even stronger[15] [103] [104] and thus the presence of Pb^{2+} ions in the growth solution lead to a change in growth morphology from {100} to {111} facets. Pb^{2+} thus blocks the growth steps on the {111} facets more strongly than on the {100} facets. The Pb^{2+} that is floating on the {111} terraces many be strongly bound at step edges but again, a local probe like atomic force microscopy is needed to confirm this.

The fact that the embedded Pb^{2+} is not a good step blocker is surprising, given the similarity with ferrocyanide, a well-known anticaking agent for NaCl that blocks growth steps on the {100} surface very effectively. Bode et al.[18] found that the ferrocyanide ion $[Fe(CN)_6]^{4-}$, replaces a $[NaCl_5]^{4-}$ cluster at the surface, rather similar to the replacement of Na^+ by $[PbCl]^+$ in our case. In both cases, the geometric match is excellent. However in order for the crystal to continue growing, i.e. to incorporate the ferrocyanide ion into the bulk, a Na^+ vacancy must be created in order to balance the charges between$[Fe(CN)_6]^{4-}$ and$[NaCl_6]^{5-}$. This is energetically unfavourable and therefore causes growth to be blocked. A similar mechanism occurs for $PbCl_2$ but wth one large exception. Unlike the large and strongly bound ferrocyanide, the single Pb^{2+} ion does not necessarily have to be incorporated, but can alternatively desorb. The difference in desorption behavious is thus likely the reason why ferrocyanide is an outstanding anticaking agent for NaCl, while $PbCl_2$ is not.

In addition, the Pb^{2+} has a lower concentration than ferrocyanide (9% versus 50%), but this is probably less important for the step blocking.

6.5 Conclusions

In this investigation, we have applied surface x-ray diffraction to study the sorption of Pb^{2+} ions on sodium chloride crystals. Using this technique, we were able to deduce a mechanism for how the Pb^{2+} ion adsorbs to the {100} facet of sodium chloride, which involves the replacement of a Na^{+} ion with a Pb^{2+} ion, partially blocking the growth through an ion charge mismatch in the bulk. The blocking on the {100} facet, however, is much weaker than on the {111} facet and thus the growth morphology of NaCl changes from {100} to {111} for increasing Pb^{2+} concentrations.

Other routes explored

Four years of research leads to a multitude of positive results, which can be published and used to further the knowledge of the specific scientific topic. However, what is not always discussed are the failures. These are the unsuccessful initiatives and ideas that lead to negative or null results, but can bring about important conclusions that ultimately contribute to the success of the project.

This chapter aims to summarise and discuss the failures that were encountered during this project, as on the road to further success on this topic, it is important to know in which direction to look and which directions have thus far not yielded any results.

At the commencement of this project, three broad research questions were outlined which were deemed to be the best way forward in furthering our knowledge about anti-caking properties of sodium chloride. The first was aiming to determine the anticaking mechanism of iron meso-tartrate (Fe m-TA) on NaCl. This would involve efforts to crystallise the iron meso-tartrate compound to elucidate the actual crystal structure, which could then lead to answers from a surface study using surface x-ray diffraction of exactly how the compound is arranged on the {100} surface of NaCl and how it has a strong growth modification effect.

Multiple attempts to crystallise Fe m-TA were undertaken, using a variety of methods including gel crystallisation, anti-solvent crystallisation (including hanging drop experiments) and slow evaporation crystallisation. Also efforts were put into counter anion replacement in the complex, from Na^+ to K^+, Rb^+ and Cs^+, with the aim of

creating a "heavier" complex which is more likely to precipitate out of solution. These attempts were all unsuccessful, leading to either the precipitation of an amorphous material or a semi crystalline material, which was analysed using EDX and found to consist of an undesired bitartrate complex. From these results, it can be concluded that Fe m-TA is a complex which seems to only exist in solution in a specific pH range. Previously, other techniques have been utilised such as x-ray absorption spectroscopy (specifically EXAFS) [111] and electron paramagnetic resonance (EPR) [21] to attempt to gain further information, but with limited success. Attempts to model the Fe m-TA complex also proved too challenging to attain any precise results at present, the lack of definitive structure led to too many possibilities to condense into a viable model.

Nonetheless, a surface x-ray diffraction study was undertaken to try to gain some useful information about the surface structure of NaCl in contact with Fe m-TA. NaCl {100} surfaces were placed into contact with a saturated solution of NaCl containing a specific amount of Fe m-TA to ensure full coverage of the surface. After much experimentation, it was found that the best conditions for the experiment were to keep the crystal in an enclosed environment with a saturated salt solution surrounding it to keep the relative humidity of the atmosphere at 75%. This technique was effective for the control tests, but when Fe m-TA was introduced into the contact solution, no diffraction signal could be gained from the surface. It is likely that the sensitivity of the complex played a role in this, as the extremely powerful x-ray beams necessary to perform these experiments caused it to degrade. Moreover, the surfaces treated with Fe-mTA were always found to be too rough for the acquisition of good quality X-ray diffraction data. This could be due to the step-blocking effect of Fe-mTA itself of its degradation products.

Another possible research path suggested at the beginning of the project was to investigate possible anticaking agents for sodium chloride dihydrate. Sodium chloride dihydrate is an alternate form of sodium chloride which only exists below 0°C and has a vastly different crystal structure to the anhydrous sodium chloride, monoclinic $P2_1/c$ instead of $Fm\bar{3}m$. As salt can also be used as de-icing agent on roads in winter temperatures, i.e. below 0°C, is it a relevant endeavour to try to find an anticaking agent which works for both the anhydrous and dihydrate forms of NaCl.

We performed many different experiments, to observe the nucleation of dihydrate in brine solution and to determine whether the addition of additives to the growth solution have any effect on the number or morphology of crystals. A wide variety

of additives were used, including polymers, sugars, metal complexes and previously reported anticaking agents for anhydrous salt. This investigation proved to be extremely challenging and it was evident that the additives we used did not have a notable effect on the nucleation and growth of sodium chloride dihydrate. From the observed differences between the effects of these additives on NaCl and the dihydrate, we can conclude that it is very challenging to find an additive that will have a strong anticaking effect on both compounds.

The final research point outlined in the beginning of the project was successful and forms the content of the rest of this thesis.

Summary

Sodium chloride is a crystalline material which has the tendency to cake when exposed to conditions of high humidity, leading to impaired physical properties. Additives can be employed to prevent this effect from occurring, these are thus named anticaking agents. Anticaking agents are compounds applied in minimal amounts to the bulk sodium chloride product which cause growth blocking at an atomic level. This growth blocking inhibits the formation of bridges between the individual crystallites, thus preventing caking. In this work, we investigate the effects of both known and previously unknown additives on sodium chloride, consequently leading to a deeper understanding of how the additives interact with the surface and leading us towards our ultimate goal of determining what makes the perfect anticaking agent for sodium chloride.

Chapter Two introduces a new technique which we have employed throughout our subsequent investigations as a powerful screening method. This technique is named "creeping" and follows the same mechanism as that of anticaking, i.e. atomic scale growth blocking. In this chapter, we investigated the relationship between the amount of creeping observed for sodium chloride droplets containing various levels of additive and the corresponding anticaking activity of the additive, thus concluding that this technique was viable as a screening technique, as well as being extremely simple and fast.

Following from Chapter Two, in the third chapter we combined experimental observations with theoretical considerations to discuss fully the mechanism of additive induced creeping in sodium chloride. We found that a number of factors contribute to this phenomenon, the additives causing both an increase in 3D nucleation and a

decrease in surface energy. This surface energy decrease leads to increased morphological instability and surface roughening, which when coupled with the increase in 3D nucleation, leads to the characteristic creeping patterns we observe.

Chapter Four investigates the growth effect and anticaking potential of polymers on sodium chloride, drawing comparisons to their respective monomers. We found that polymers have a strong effect on the surface of sodium chloride, promoting macrostep formation and causing nucleation inhibition. Polymers with an amide functional group were shown to have a much greater effect on the growth of the sodium chloride crystals than the respective amide containing monomer, roughly one to two orders of magnitude larger. However, the polymers tested here were all found to produce a "pro-caking" effect on the sodium chloride crystals and thus were not found to be effective anticaking agents.

The fifth chapter explores the effect that specific amide containing additives have on sodium chloride growth, namely the formation of ultrathin needle crystals. This additive induced crystal morphology has been previously unreported for sodium chloride; we have coupled experimental work with theoretical inferences in order to fully explain this unique phenomenon. The needle crystals were fully characterised using a range of techniques such as x-ray diffraction, energy dispersive x-ray spectroscopy and scanning electron microscopy and shown to consist of cubic NaCl which grow in the {100} direction. We suggest that this is due to morphological instability at the earliest stage of nucleation, leading to enhanced additive adsorption on the sides of the needles and subsequent additive incorporation.

Chapter Six investigates the capabilities of the amide functional group in an anticaking agent and why a triple branched variant is necessary to have the desired anticaking effect. Through creeping tests, supersaturation experiments and powder flow analysis we confirmed that in order to have an anticaking effect, a compound containing three amide branches radiating from one nitrogen centre is necessary. We also showed that effective anticaking agents must obey a set of criteria, if they fail in any one of these categories then they are ineffective.

Finally, in Chapter Seven, we discuss the mechanism of the adsorption of lead chloride to the sodium chloride {100} surface. Lead chloride is a previously reported habit modifier and growth blocker for sodium chloride but up until now, the exact mechanism at an atomic scale was unknown. Using surface x-ray diffraction, we found that

lead adsorbs to the NaCl surface replacing a sodium ion, which cannot be incorporated into the bulk as there is a charge mismatch of which it is energetically unfavourable to compensate for. This thus slows the growth of NaCl {100}. Lead chloride has therefore clear similarities with the best-known anticaking agent ferrocyanide, but is found to be much less efficient.

Samenvatting

Natriumchloride (ook wel keukenzout genoemd) is een kristallijn materiaal dat de neiging heeft om vast te koeken (caking) als het blootgesteld wordt aan een vochtige omgeving. Dit leidt tot een aantal ongewenste eigenschappen, zoals klonteren en een slechte strooibaarheid, waardoor de verwerking van dit materiaal moeilijk wordt. Men kan additieven toevoegen om dit vastkoeken te voorkomen; deze toevoegingen noemt men "anticaking agents". Deze additieven worden in heel kleine hoeveelheden aan het zoutproduct toegevoegd en remmen de groei van de kristallen af door aanhechting aan het oppervlak. Deze blokkade voorkomt de vorming van kristalbruggen tussen naast elkaar gelegen kristallieten in een batch en dus het samenkoeken hiervan. In dit proefschrift onderzoeken we de effecten van zowel bekende als onbekende additieven op de groei van natriumchloride, om te begrijpen hoe deze additieven wisselwerken met het kristaloppervlak. Dit helpt ons om de eigenschappen van een perfect anticakingmiddel te vinden en deze kennis toe te passen in de industriele praktijk.

In hoofdstuk twee introduceren we een nieuwe testmethode waarmee we mogelijke kandidaten voor een geschikt anticakingmiddel voor keukenzout kunnen selecteren. Deze techniek hebben we gebruikt in ons verdere onderzoek. De methode wordt "creeping" genoemd: het horizontaal uitgroeien van kristallen vanaf de rand van een verdampende oplossing op een vaste ondergrond. In aanwezigheid van geschikte additieven zien we bij dit proces veel overeenkomsten met de processen die ook bij anticaking een rol spelen, namelijk het blokkeren van de groei van de kristallen en het ruwer worden van hun oppervlak. In dit hoofdstuk onderzoeken we het verband tussen de hoeveelheid en het soort additief en de daarbij behorende anticakingwerking. Het blijkt dat deze simpele en snelle screening methode heel goed werkt.

Na hoofdstuk twee combineren we in het derde hoofdstuk de resultaten van verschillende creeping experimenten met een theoretische beschouwing om zodoende de invloed van additieven op het creeping proces van natriumchloride beter te begrijpen. We vonden dat een aantal verschillende factoren bijdraagt tot dit fenomeen: de additieven verlagen de oppervlakte-energie van de kristallen en doen de kiemvorming toenemen, mede als gevolg van een hoge oververzadiging. De verlaging van de oppervlakte-energie leidt tot een toegenomen morfologische instabiliteit en oppervlakteverruwing, welke gekoppeld met de versnelde kiemvorming resulteert in heel karakteristieke creeping patronen.

In hoofdstuk vier kijken we naar het effect van polymeren op de groei en anticaking van de zoutkristallen; dit wordt vergeleken met dat van de overeenkomstige monomeren. We vonden dat de polymeren het oppervlak van de natriumchloride kristallen sterk beinvloeden, leidend tot hogere groeitreden en afremming van kiemvorming. Polymeren met een amide functionele groep hebben een veel grotere invloed op de groei van de kristallen dan de overeenkomstige monomeervarianten. Het effect van de polymeren is ruwweg een a twee ordes van grootte sterker. Echter, alle hier onderzochte polymeren resulteerden in een toegenomen caking van de NaCl kristallen en zijn dus geen geschikte anticakingmiddelen.

In het vijfde hoofdstuk onderzoeken we het effect dat additieven met specifieke amidegroepen hebben op de groei van NaCl kristallen, leidend tot de vorming van ultradunne naaldvormige kristallen. Deze afwijkende kristalvorm veroorzaakt door een additief was tot nu toe geheel onbekend voor het normaliter kubusvormige keukenzout. We hebben experimenteel werk gecombineerd met theoretische beschouwingen om dit bijzondere fenomeen te verklaren. De naaldkristallen werden minutieus onderzocht met verschillende technieken, zoals rontgendiffractie, energie dispersieve rÃűntgen spectroscopie en scanning elektronenmicroscopie. Hieruit bleek dat de naalden uit puur NaCl bestaan en altijd groeien in de {100} kristalrichting. De vorming van de naalden wordt toegeschreven aan een morfologische instabiliteit in het allereerste begin van hun groei, gevolgd door adsorptie van de additieven op hun zijvlakken, waardoor ze niet in de dikte groeien.

In hoofdstuk zes besteden we aandacht aan het aantal en de ordening van de verschillende amide functionele groepen in het de additiefmolecule. Door middel van creepingproeven, bepaling van de kiemvormingssnelheid en het meten van de caking-

sterkte, bleek dat alleen verbindingen bestaande uit drie amidetakken verbonden met een centraal stikstofatoom een anticaking effect hebben. In dit deel toonden we ook aan dat een effectief middel tegen het vastkoeken van kristallen moet voldoen aan een drietal criteria. Als het aan een van deze criteria niet voldoet, dan is het additief niet geschikt als anticaking middel.

Tenslotte kijken we in hoofdstuk zeven naar hoe loodchloride zich aanhecht op het NaCl {100} oppervlak. Loodchloride is in eerdere literatuur genoemd als een additief dat de vorm van het kristal beinvloedt ("habit modifier") en bovendien de groei vertraagt, maar tot nu toe is het exacte mechanisme hoe dat op atomaire schaal werkt onbekend. Met behulp van oppervlakte rontgendiffractie ontdekten we dat lood adsorbeert op het {100} oppervlak, waarbij een natriumatoom aan het oppervlak wordt vervangen. Hierdoor ontstaat een niet passende verhouding van elektrische lading die bij verdere groei moeilijk is te compenseren. Dit verklaart de tragere groei van {100} NaCl in aanwezigheid van kleine hoeveelheden lood.

Bibliography

[1] Kepler, J. *De Nive Sexangula*; d, 1611.

[2] Ball, P. *Nature* **2011**, *481*, 455.

[3] Lovette, M. A.; Browning, A. R.; Griffin, D. W.; Sizemore, J. P.; Snyder, R. C.; Doherty, M. F. *Ind. Eng. Chem. Res.* **2008**, *47*, 9812.

[4] Brockel, U.; Wahl, M.; Kirsch, R.; Feise, H. *Chem. Eng. Technol.* **2006**, *29*, 691.

[5] Rumpf, H. *Chemie Ing. Technol.* **1958**, *30*, 144.

[6] Chen, M.; Wu, S.; Xu, S.; Yu, B.; Shilbayeh, M.; Liu, Y.; Zhu, X.; Wang, J.; Gong, J. *Powder Technology* **2017**, *in press.*

[7] Buckley, H. E. *Crystal Growth*; John Wiley and Sons Inc., 1951.

[8] de l'Isle, J. B. L. R. *Cristallographie ou description de formes propres a tous les corps du regne mineral, dans l'etat de combinaison saline, pierreuse ou metalliques, 2nd Ed., Vol. 4*; d, 1783.

[9] Weissbuch, I.; Addadi, L.; Lahav, M.; Leiserowitz, L. *Science* **1991**, *253*, 637.

[10] Cabrera, N.; Vermilyea, D. A. *Growth and Perfection of crystals*; d, 1958.

[11] Chernov, A. A. *Sov. Phys. Usp.* **1961**, *4*, 116.

[12] Chernov, A. A. *Growth of Crystals* **1962**, *3*, 31.

[13] Retgers, J. W. *Z. Physik. Chem.* **1892**, *9*, 267.

[14] Royer, L. *Compt. rend.* **1934**, *198*, 585.

[15] Bienfait, M.; Boistelle, R.; Kern, R. *Adsorption et Croissance Cristalline*; Centre National de la Recherche Scientifique, Paris, 1965.

[16] Boistelle, R. d. Ph.D. thesis, Universite de Nancy, 1966.

[17] van Damme-van Weele, M. A. d. Ph.D. thesis, TU Twente, 1965.

[18] Bode, A. A. C.; Vonk, V.; van den Bruele, F. J.; Kok, D. J.; Kerkenaar, A. M.; Mantilla, M. F.; Jiang, S.; Meijer, J. A. M.; van Enckevort, W. J. P.; Vlieg, E. *Cryst. Growth. Des.* **2012**, *12*, 1919.

[19] Boon, H. F. 2000.

[20] Geertman, R. M. 2006.

[21] Bode, A. A. C.; Grannemann, S. J. C.; Feiters, M. C.; Jiang, S.; Meijer, J. A. M.; van Enckevort, W. J. P.; Vlieg, E. *Dalton Trans.* **2016**, *45*, 6650.

[22] Feidenhans'l, R. *Surf. Sci. Rep.* **1989**, *10*, 105.

[23] Robinson, I. K.; Tweet, D. J. *Rep. on Prog. Phys.* **1992**, *55*, 599.

[24] Binnig, G.; Quate, C. F.; Gerber, C. *Rep. on Phys, Prog.* **1992**, *56*, 930.

[25] Vlieg, E. *Surface Science* **2002**, *500*, 458.

[26] Vlieg, E. *Surface and Interface Science, Vol. 1: Concepts and Methods*; Wiley, 2012.

[27] Kaufmann, D. *Sodium Chloride: The Production and Propoerties of Salt and Brine*; Reinhold Publishing Corporation, 1960.

[28] Bode, A. A. C.; Jiang, S.; Meijer, J. A. M.; van Enckevort, W. J. P.; Vlieg, E. *Cryst. Growth Des.* **2012**, *12*, 5889.

[29] Rodrigues-Navarro, C.; Linares-Fernandez, L.; Doehne, E.; Sebastian, E. *J. Cryst. Growth* **2002**, *243*, 503.

[30] van Enckevort, W. J. P.; Los, J. H. *Cryst. Growth Des.* **2012**, *12*, 1838.

[31] Shahidzadeh, N.; Schut, M. F. L.; Desarnaud, J.; Prat, M.; Bonn, D. *Sci. Rep.* **2015**, *5*, 10335.

[32] Townsend, E.; van Enckevort, W. J. P.; Meijer, J.; Vlieg, E. *Cryst. Growth Des.* **2015**, *15*, 5375.

[33] Sarig, S.; Tartakovsky, F. *J. Cryst. Growth* **1975**, *28*, 300.

[34] Hazlehurst, T. H.; Martin, H. C.; Brewer, G. *J. Phys. Chem.* **1935**, *40*, 439.

[35] Boon, H. F. 1970.

[36] Bromby, N. G.; Coningsby, A.; Scott, T. R. 1961.

[37] Radenovic, N.; van Enckevort, W. J. P.; Vlieg, E. *J. Cryst. Growth* **2004**, *263*, 544.

[38] Bode, A. A. C.; Verschuren, M.; Jansen, M.; Jiang, S.; Meijer, J. A. M.; van Enckevort, W. J. P.; Vlieg, E. *Powder Technology* **2015**, *277*, 262.

[39] Emelyanenko, V. N.; Verevkin, S. P.; Varfolomeev, M. A.; Turovtsev, V. V.; Orlov, Y. D. *J. Chem. Eng. Data* **2011**, *56*, 4183.

[40] Gibbs, J. W. *The Scientific Papers of J. Williard Gibbs*; Longmans Green, 1906; Vol. 1.

[41] Gardeniers, J. G. E.; Mooren, M. M. W.; de Croon, M. H. J. M.; Giling, L. J. *J. Cryst. Growth* **1990**, *102*, 333.

[42] Townsend, E.; v. Enckevort, W. J. P.; Meijer, J.; Vlieg, E. *Cryst. Growth Des.* **2017**, *17*, 3107.

[43] Washburn, E. R. *J. Phys. Chem.* **1926**, *31*, 1246.

[44] Townsend, E. R.; Swennenhuis, F.; van Enckevort, W. J. P.; Meijer, J. A. M.; Vlieg, E. *CrystEngComm* **2016**, *18*, 6176.

[45] Scherer, G. W. *Chem. Concr. Res.* **1999**, *29*, 1347.

[46] Rijniers, L. A.; Huinink, H. P.; Pel, L.; Kopinga, K. *Phys. Rev. Lett.* **2005**, *94*, 75503.

[47] Doehne, E. *Geol. Soc. Spec. Publ.* **2003**, *205*, 51.

[48] Brener, E.; Muller-Krumbhaar, H. *D. Europhys. Lett.* **1992**, *17*, 535.

[49] Langmuir, I. *J. Am. Chem. Soc.* **1918**, *40*, 1361.

[50] Atkins, P.; de Paula, J. *Atkins' Physical Chemistry*; Oxford, 2006; Vol. 8.

[51] Sears, G. W. *J. Chem. Phys.* **1958**, *29*, 1045.

[52] Sangwal, K. *J. Cryst. Growth* **1989**, *97*, 393.

[53] Frenkel, W. *Phys. Z. Sowjet Union* **1932**, *1*, 498.

[54] Wilson, H. A. *Philos. Mag.* **1900**, *50*, 238.

[55] van der Eerden, J. P. *Crystal Growth Mechanisms: Handbook of Crystal Growth*; Elsevier, 1993; Vol. 1a.

[56] Sangwal, K. *Additives and Crystallisation Processes: From Fundamentals to Applications*; Wiley, 2007.

[57] van Enckevort, W. J. P.; van den Berg, A. C. J. F. *J. Cryst. Growth* **1998**, *183*, 441.

[58] de Haan, S. W. H.; Meeusen, V. J. A.; Veltman, B. P.; Bennema, P.; van Leeuwen, C.; Gilmer, G. H. *J. Cryst. Growth* **1974**, *24-25*, 491.

[59] Kashchiev, D.; van Rosmalen, G. M. *Cryst. Res. Technol.* **2003**, *38*, 555.

[60] Mersmann, A. J. *J. Cryst. Growth* **1990**, *102*, 841.

[61] Bahadur, R.; Russell, L. M.; Alavi, S. *J. Phys. Chem. B* **2007**, *111*, 11989.

[62] Sarig, S.; Glasner, A.; Epstein, J. A. *J. Cryst. Growth* **1975**, *28*, 295.

[63] Pastero, L.; Aquilano, D.; Moret, M. *Cryst. Growth Des.* **2012**, *12*, 2306.

[64] Radenovic, N.; van Enckevort, W. J. P.; Verwer, P.; Vlieg, E. *Surf. Sci.* **2003**, *523*, 307.

[65] Fenimore, C.; Thrailkill, A. *J. Am. Chem. Soc.* **1949**, *71*, 2741.

[66] Ballabh, A.; Trevedi, D.; Dastidar, P.; Ghosh, P.; Pramanik, A.; Kumar, V. *Cryst. Growth Des.* **2006**, *6*, 591.

[67] Heiss, J. F.; Kolasinski, R.; Sclar, C. B. 1966.

[68] Bakkenes, H.; Bergvoet, R. A. G. M.; Meijer, J. A. M.; Steensma, M. 2010.

[69] van den Bruele, F. J.; Marks, K. M.; Harmsen, B.; Alfring, A. L.; Sprong, H.; van Enckevort, W. J. P.; Vlieg, E. *Cryst. Growth Des.* **2012**, *12*, 2265.

[70] Vlachos, D. G.; Jensen, K. F. *Surf. Sci.* **1992**, *262*, 359.

[71] Alderton, G.; Ward, W. H.; Fevold, H. L. *J. Bio. Chem.* **1945**, *157*, 43.

[72] Gille, F.; Spangenburg, K. *Z. Krist. Miner. Petrograd A* **1927**, *65*, 204.

[73] Radenovic, N.; Kaminski, D.; van Enckevort, W. J. P.; Graswinckel, S.; Shah, I.; in 't Veld, M.; Algra, R.; Vlieg, E. *J. Chem. Phys.* **2006**, *124*, 164706.

[74] Phoenix, L. *Brit. Chem. Eng.* **1966**, *11*, 34.

[75] Boone, D.; Ralston, P. H. 1970.

[76] Kelland, M. A. *Production Chemicals for the Oil and Gas Industry*; CRC Press, 2009.

[77] Tauber, H.; Kleiner, I. *J. Am. Chem. Soc.* **1932**, *54*, 2392.

[78] Hinegartner, W. S. *J. Am. Chem. Soc.* **1933**, *55*, 1461.

[79] Sears, G. W. *J. Chem. Phys.* **1957**, *26*, 1549.

[80] Shichiri, T.; Kato, N. *Acta Metallurgica* **1965**, *13*, 785.

[81] Shichiri, T.; Kato, N. *J. Cryst. Growth* **1968**, *3/4*, 384.

[82] Shichiri, T. *J. Cryst. Growth* **1974**, *24/25*, 350.

[83] Noorduin, W. private communication.

[84] Wagner, R. S. *Acta Metall.* **1960**, *1*, 57.

[85] Hamilton, D. R.; Seidensticker, R. G. *J. Appl. Phys.* **1960**, *31*, 1165.

[86] van Enckevort, W. J. P.; Graef, M. W. M. *J. Electrochem. Soc.* **1981**, *128*, 154.

[87] Land, T.; Martin, T. L.; Potapenko, S.; Palmore, G. T.; de Yoreo, J. *Nature* **1999**, *399*, 442.

[88] Muira, H. *Cryst. Growth Des.* **2016**, *16*, 2033.

[89] Potapenko, S. Y. *J. Cryst. Growth* **1993**, *133*, 147.

[90] Bennema, P. *Growth and Morphology of Crystals: Handbook of Crystal Growth*; Elsevier, 1993; Vol. 1.

[91] Glicksman, M. E.; Marsh, S. P. *The Dendrite: Handbook of Crystal Growth*; Elsevier, 1993; Vol. 1b.

[92] Smith, P. E. *Fluid Phase Equilibria* **2010**, *290*, 36.

[93] Townsend, E.; Blijlevens, M. A. R.; van Enckevort, W.; Meijer, J.; Vlieg, E. *Cryst. Growth. Des.* **2017**, *accepted*.

[94] B. P. Johan, N. J. T., L. Hammer 1965.

[95] Rutland, D. W. *Fertiliser research* **1991**, *30*, 99.

[96] Townsend, E. R.; Brugman, S. J. T.; Blijlevens, M. A. R.; van Enckevort, W. J. P.; Meijer, J. A. M.; Vlieg, E. *Langmuir* **2017**, *in progress*.

[97] Kading, H. *Z. Physik. Chem.* **1932**, *162*, 174.

[98] Bunn, C. W.; Emmett, H. *Discuss. Faraday Soc.* **1949**, *5*, 119.

[99] Botsaris, G.; Mason, E. A.; Reid, R. C. *J. Chem. Phys.* **1966**, *45*, 1893.

[100] Glasner, A.; Skurnik, S. *J. Chem. Phys.* **1967**, *47*, 3687.

[101] Sears, G. W. *J. Chem. Phys.* **1958**, *29*, 979.

[102] Glasner, A. *Israel J. Chemistry* **1969**, *7*, 633.

[103] Li, L.; Tsukamoto, K.; Sunagawa, I. *J. Cryst. Growth* **1990**, *99*, 150.

[104] Booth, A. H. *Trans. Faraday Soc.* **1951**, *47*, 640.

[105] Radenovic, N.; van Enckevort, W. J. P.; Kaminski, D.; Heijna, M.; Vlieg, E. *Surface Science* **2005**, *599*, 196.

[106] Arsic, J.; Kaminski, D.; Radenovic, N.; Poodt, P.; Graswinckel, W.; Cuppen, H.; Vlieg, E. *J. Chem. Phys.* **2004**, *120*, 9720.

[107] Robinson, I. K. *Phys. Rev. B* **1986**, *33*, 3830.

[108] Willmott, P. R. et al. *Journal of Synchrotron Radiation* **2013**, *20*, 667–682.

[109] Vlieg, E. *J. Appl. Cryst.* **2000**, *33*, 401.

[110] Wells, A. F. *Structural Inorganic Chemistry*; Clarendon Press, 1984; Vol. 5.

[111] AkzoNobel, private communication.

Acknowledgments

At the culmination of this four year period, it is clear that I am indebted to a number of people who have contributed, either directly or indirectly, to the process of writing this thesis and for that, I would like to convey my gratitude in the words below.

Firstly, I would like to express my sincere thanks to **Professor Elias Vlieg** for acting as my promotor and mentor throughout this four year journey. Elias, thank you for choosing me as your Ph.D. candidate and for helping me to develop as a researcher under your guidance. You have taught me how to think critically, be more confident in my own work and how to be direct (Dutch honesty!). You also gave me the opportunity to present my work in front of international audiences in Italy and Japan and to travel with you on various trips to France, Switzerland and the UK, which I am very grateful for. I was very happy to be in your department for the past four years.

Secondly, I would like to thank **Dr. Willem van Enckevort**, as my co-promotor, for being there every step of the way along the way to finishing this thesis. Thank you Willem for your daily supervision, your creativity and enthusiasm; you could always think of an idea if we were stuck and this has led to development of some articles that I am very proud of. I really appreciated how much time you had for me, I could count on you to correct my work at lightning speed and always were available for a discussion with me or my students whenever we needed it. You have also greatly contributed to my knowledge about Venlo, Limburg, wine, the birds of the Netherlands and astronomy, so for that, I thank you too!

To **Dr. Ir. Jan Meijer**, my second co-promotor, I would like to thank you for the

support throughout these four years and for the many fruitful (and funny) discussions we had during our visits to Akzo Nobel in Deventer. The partnership between Akzo and Radboud gave me a valuable insight into industry and how research is conducted non-academically. I have never met someone who knows so much about salt (!), and so your valuable input made this investigation much easier for me. **Shanfeng Jiang, Anamaria Soare, Paul Verwer** and the rest of the group from Akzo, I would like to thank you all also for the help you gave me and all of the meetings we had over these four years.

In Nijmegen, the friendly and relaxed environment in the VSC group made it a very welcoming group to join and even though a lot of people come and go, there are some I would especially like to thank.

Erik, I really don't think that the department would be able to run without your technical support, organising everything from machine repair to chemical ordering. Also, your creativity led us to some interesting ideas for experiments and you were always available to help if needed. I really liked that we had mutual music interests and I learned a lot from you, especially about Dutch things such as the Efteling and what is actually inside a kroket!

Wiesiek and Paul, thanks to you both for your help at various times during the past years. Wiesiek, you especially helped me with the SXRD set-up, which led to a successful experiment and thank you also for the nice conversations. Paul, ("good moaning!") apart from being a x-ray diffraction extraordinaire, we bonded over our mutual love of food!

Hugo and Rene de G: although you were not directly involved in my project, I very much enjoyed working alongside you both. Hugo, your dry humour never failed to make me laugh and your questions about the etymology of the English language never failed to baffle me.

Elizabeth, you were the first person I met when I came for my interview and you made me feel very relaxed and welcomed. Thank you for your support and organisation of everything surrounding my project.

I was also very lucky to have such kind Ph.D. colleagues to work alongside, some who have now already gone onto new things. **Rene, Laura, Stelian, Alaa, Rita,**

Joost; thank you to you all for the welcome and the good times we had working together. **Eline**, thank you for being both a caring colleague and friend and a gezellig huisgenootje!

To those who are still around: **Wester and Ton**, thank you for being primary babysitters for my plants, and for all the dinners and movie nights we had together. Wester, thank you for my panda painting and for all the dirty jokes I now know because of you. Ton, I will miss the insults and the Geography Sporcling Friday afternoons. **Sander**, dank voor de vriendschap over de jaren, ik heb heel veel plezier gehad op onze reizen naar de pretparken van Nederland en Belgie, en de Ardennen (samen met Smetsie en Tonnetje). Ook, heel veel bedankt voor de hulp met SXRD, het was zeer gewaardeerd en ik heb van onze reizen naar Frankrijk, UK en Zwitserland genoten; de nachtdienst was niet zo moeilijk omdat we foute muziek en step races hadden! **Mireille**, it was lovely to have you as a colleague and friend during my time in the Netherlands, you are a very talented researcher and it was great to work alongside you. I really enjoyed all our travels together, from London, to Granada, to Nagoya and inside the Netherlands and also thank you for all the Maltesers! Finally, merci beaucoup to **Adrien**, thank you for being a caring friend and for the computer help.

To my new colleagues from the past year: **Jan Joris, Paolo and Giuseppe**, thanks for the good times we had together in the short period we knew each other!

Particular thanks also to the Master and Bachelor students who decided to work with me on my project, your work contributed to this thesis and for that I am very grateful! **Lian**, thank you for all your hard work through both your Bachelor and Master projects; your bright personality made it a pleasure to work with you. **Floris**, thank you to you also for your hard work which contributed to a chapter in this thesis and a publication. **Marc**, even though your project was not directly related to mine, I enjoyed supervising you through your Master research project. **Ilonka and Rozemarijn** (putting you guys together as you came as a pair!), thank you for your contributions, and Ilonka especially thanks for your continued effort, even though the project did not exactly end up how we had hoped. Finally, **Michaela**, my last Bachelor student, we worked together at the very end of my study and I hope that the excellent work you did will continue for something in the future. To all the other students who came and went through the VSC department, thanks for all the fun times, such as the Thursday afternoon borrels, quizzes, beer tastings and delicious AIO/studenten/Paul etentjes with the ever more elaborate themes!

I was also extremely lucky to have the support of many new and old friends, who have encouraged me and helped me during my time here.

To the Spanish(ish) group: **Ester, Lau, Merce, Roque, Dario, Riccardo, Julio, Blanca, Ale, Ivan** and everyone else; thank you all for the great times we had together here. I am really very happy that I met you all and thank you for being such a big part of my life here in Nijmegen, it was very nice to share the experience with you and I really hope that it will not end here. **Dan**, I am very grateful for our friendship, thank you for always making me laugh and asking me hard questions about atoms. To the rest of my UK friends: **Laura, David and Phil B**, thanks for all the good times we had together! **Celine**, I am glad to have met you at the ECCG and I really liked our trips together afterwards.

Also to **everyone from home**, (too many to name, I'm sorry, but you know who you are!), thanks for the continued friendship across the sea and for all the great visits I've been lucky enough to have!

To the very talented **Floor**, thank you for the design of my thesis cover!

To my two paranimfs, **Ester and Annelie**. It is not often that you meet people who are so similar to you, and I am extremely glad that I found it in you both. You are both extremely talented and dedicated scientists and also you have both been supportive and caring friends to me. Thank you for agreeing to be my paranimfs!

Especially, **Pim**, ik hoop dat je weet dat ik heel blij ben dat ik je heb ontmoet.

Finally, to my family. **Mum, Dad and Alice**, without you, there is no way that I could have finished this Ph.D.. Thank you for your understanding and unconditional support and I really hope that you are as proud of me as I am of myself for finishing this.

List of Publications

- E. R. Townsend, W. J. P. van Enckevort, J. A. M. Meijer, E. Vlieg; "Polymer versus monomer action on the growth and habit modification of sodium chloride crystals", *Crystal Growth and Design*, **2015**, *15*, 5375-5381.

- E. R. Townsend, F. Swennenhuis, W. J. P. van Enckevort, J. A. M. Meijer, E. Vlieg; "Creeping: An efficient way to determine the anticaking ability of additives for sodium chloride", *CrystEngComm*, **2016**, *18*, 6176-6183.

- E. R. Townsend, W. J. P. van Enckevort, J. A. M. Meijer, E. Vlieg; "The mechanism of additive enhanced creeping of sodium chloride crystals", *Crystal Growth and Design*, **2017**, *17*, 3107-3115.

- E. R. Townsend, W. J. P. van Enckevort, P. Tinnemans, M. A. R. Blijlevens, J. A. M. Meijer, E. Vlieg; "Additive induced formation of ultrathin sodium chloride needle crystals", *Crystal Growth and Design*, **2017**, *accepted*.

- E. R. Townsend, W. J. P. van Enckevort, J. A. M. Meijer, E. Vlieg; "Amides as anticaking agents for sodium chloride: is a triple branched variant necessary?", *CrystEngComm*, **2017**, *accepted*.

- E.R. Townsend, S.J.T. Brugman, M.A.R. Blijlevens, W.de Poel, M.M.H. Smets, W.J.P. van Enckevort, J.A.M. Meijer, E. Vlieg; "The structure of $PbCl_2$ on the {100} surface of NaCl and its consequences for crystal growth", **2018**, *in preparation*.

- S. J. T. Brugman, E. R. Townsend, M. M. H. Smets, P. Accordini, E. Vlieg; "Concentration-dependent adsorption of CsI at the muscovite-electrolyte interface", **2018**, *in preparation.*

- W. de Poel, S. L. Vaessen, J. Drnec, A. H.J. Engwerda, E. R. Townsend, S. Pintea, A. E. F. de Jong, M. Jankowski, F. Carla, R. Felici, J.A.A.W. Elemans, W.J.P. van Enckevort, A. E. Rowan, E. Vlieg; "Metal ion-exchange on the muscovite mica surface", *Surface Science*, **2017**, *665*, 56-61.

Curriculum vitæ

Name:	Eleanor Rose Townsend
Date of Birth:	23 April, 1991
Place of Birth:	Ipswich, United Kingdom

2003-2009	**Secondary Education**, Colaiste Choilm, Ireland
2009-2013	**BSc. Chemistry and Forensic Science**, University College Cork
2013-2017	**Ph.D. Solid State Chemistry**, RU, Nijmegen, The Netherlands

BSc. Thesis	*"Chirality and co-crystals"*
Ph.D Thesis	*"Insights into the role of additives as anticaking agents for sodium chloride"*